TECHNISCHE UNIVERSITÄT WIEN

Master Thesis

Synthesis of photocatalytic polymer systems for the reduction of carbon dioxide

Ausgeführt am
Institut für Angewandte Synthesechemie

unter der Leitung von
Univ. Prof. Dipl.-Ing. Dr. techn. Katharina Schröder

eingereicht an der Technischen Universität Wien
am 14.09.2022
von

Bletë Hulaj, BSc.

[redacted]

Die approbierte gedruckte Originalversion dieser Diplomarbeit ist an der TU Wien Bibliothek verfügbar
The approved original version of this thesis is available in print at TU Wien Bibliothek.
TU WIEN Bibliothek Your knowledge hub

Die approbierte gedruckte Originalversion dieser Diplomarbeit ist an der TU Wien Bibliothek verfügbar
The approved original version of this thesis is available in print at TU Wien Bibliothek.

Acknowledgments

I want to thank everyone, who supported me during my diploma thesis and my university studies in general.

A big thank you to Univ. Prof. Dr. Katharina Schröder for giving me the opportunity to extend my knowledge by working in her research group and supporting me, when needed. Thank you, as well, for all the opportunities to come that I can enjoy thanks to my time in this research group.

Another big thank you has to go to Projektass. Lisa Eisele for supervising me during my diploma thesis and supporting me continuously.

Of course, I want to also thank the whole research group, old members and new, for providing a pleasant work atmosphere.

A special thank you to my friends and family for always being there for me, motivating me to continue my studies, and celebrating achievements together.

Die approbierte gedruckte Originalversion dieser Diplomarbeit ist an der TU Wien Bibliothek verfügbar
The approved original version of this thesis is available in print at TU Wien Bibliothek.
TU WIEN Bibliothek Your knowledge hub

Abstract

Photocatalytic systems consisting of a photosensitizer and a photocatalyst, such as Ru and Re-based catalysts, show high selectivity for carbon monoxide (CO) formation, allowing for visible-light photocatalyzed reduction of carbon dioxide (CO_2). Ionic liquids (IL) have considerable potential as cooperative media since they can solubilize large concentrations of CO_2, and are also able to activate CO_2.[1] Materials that combine both photocatalyst and IL are, thus, highly desirable for a photocatalytic CO_2 reduction to generate CO under benign conditions.

Consequently, in this work different IL-photocatalyst polymers were developed by combining the IL 1-butyl-3-vinylimidazolium chloride and photocatalytically active Re- and Ru-complexes *via* radical co-polymerization, utilizing varying ratios of photocatalytic materials with vinyl functionalized ligand systems. The desired materials were obtained in high yields, and the composition of the synthesized materials was confirmed through analysis.

Die approbierte gedruckte Originalversion dieser Diplomarbeit ist an der TU Wien Bibliothek verfügbar
The approved original version of this thesis is available in print at TU Wien Bibliothek.
TU WIEN Bibliothek Your knowledge hub

Kurzfassung

Photokatalytische Systeme aus einem Photokatalysator und einem Photosensibilisator, wie z.B. Re und Ru-basierte Komplexe, ermöglichen die photokatalytische Reduktion von Kohlendioxid (CO_2) durch sichtbares Licht mit hoher Selektivität zu Kohlenmonoxid (CO). Ionische Flüssigkeiten zeigen hohes Potenzial als kooperatives Medium, da sie nicht nur große Konzentrationen an CO_2 lösen, sondern auch die Reduktion erleichtern können. Es werden daher Materialien für die photokatalytische Reduktion von CO_2 zu CO unter milden Bedingungen gesucht, die sowohl Photokatalysatorelemente als auch ionische Flüssigkeiten kombinieren.

Daher wurden in dieser Arbeit verschiedene Polymere – zusammengesetzt aus ionischer Flüssigkeit und photokatalytischen Elementen – durch radikalischer Copolymerisation der ionischen Flüssigkeit 1-Butyl-3-vinylimidazoliumchlorid und photokatalytisch aktiven Re- und Ru-Komplexen hergestellt. Dabei wurden unterschiedliche Verhältnisse von photokatalytischen Materialien mit Vinyl-funktionalisiertem Ligandensystem verwendet. Die gewünschten Materialien wurden mit hoher Ausbeute synthetisiert, und die Zusammensetzung der Polymere durch verschiedene analytische Methoden bestätigt.

Die approbierte gedruckte Originalversion dieser Diplomarbeit ist an der TU Wien Bibliothek verfügbar
The approved original version of this thesis is available in print at TU Wien Bibliothek.
TU WIEN Bibliothek Your knowledge hub

Table of contents

Acknowledgments III

Abstract IV

Kurzfassung V

Table of contents VI

Abbreviations – Acronyms IX

1. Introduction 1

1.1. Anthropogenic carbon dioxide emissions 1

1.2. Carbon capture and utilization 3

1.3. The European project CARBOFLOW: Streamlined CO_2 conversion in ionic liquids – a platform strategy for modern carbonylation chemistry 5

2. Theoretical background 7

2.1. The stability of carbon dioxide 7

2.2. General methods for the reduction of carbon dioxide 8

2.2.1. Chemical reduction of carbon dioxide 8

2.2.2. Electrochemical reduction of carbon dioxide 10

2.2.3. Biochemical reduction of carbon dioxide 12

2.3. Photochemical reduction of carbon dioxide 14

2.3.1. Homogeneous photocatalysis 14

2.3.2. Heterogeneous photocatalysis 18

2.3.3. State-of-the-art visible-light photocatalytic CO_2 reduction with transition metal complexes 20

2.4. The influence of ionic liquids on CO_2 reduction 23

2.5. Polymerized photocatalyst system 26

3. Aim of the thesis 27

4. Results and discussion 28

Die approbierte gedruckte Originalversion dieser Diplomarbeit ist an der TU Wien Bibliothek verfügbar
The approved original version of this thesis is available in print at TU Wien Bibliothek.
TU Bibliothek Your knowledge hub WIEN

4.1. Concept of the polymer synthesis ... 28
4.2. Synthesis of polymerizable monomers ... 30
4.2.1. Ionic liquid synthesis ... 30
4.2.2. Ligand synthesis ... 31
4.2.3. Catalytic monomers ... 34
4.3. Polymerization of monomers ... 36
4.4. Analysis ... 40
5. Conclusion and outlook ... 50
6. Experimental part ... 52
6.1. Materials and methods ... 52
6.2. Synthesis of monomer set ... 53
6.2.1. 1–Butyl–3–vinylimidazolium chloride (3) ... 53
6.2.2. 5,5′-Divinyl-2,2′-bipyridine (6) ... 54
6.2.3. Photocatalyst monomer of the cross-linked polymer (CLP-PC, 8) ... 55
6.2.4. Photosensitizer monomer of the cross-linked polymer (CLP-PS, 10) ... 56
6.2.5. *N*-(4-Vinylbenzyl)phthalimide (13) ... 57
6.2.6. 4-(Aminomethyl)styrene (15) ... 58
6.2.7. 4'-Methyl-*N*-(4-vinylbenzyl)-[2,2'-bipyridine]-4-carboxamide (17) ... 59
6.2.8. Photocatalyst monomer of the side-chain polymer (SCP-PC, 18) ... 60
6.2.9. Photosensitizer monomer of the side-chain polymer (SCP-PS, 19) ... 61
6.3. Polymerisation of monomers ... 62
6.3.1. General procedure for polymerisation in batch reactor mode (A) ... 62
6.3.2. General procedure for polymerisation in the autoclave (B) ... 62
6.3.3. Synthesis of polyionic liquid (PIL, 20) ... 63
6.3.4. Synthesis of cross-linked polymer (CLP, 21) ... 64
6.3.5. Synthesis of cross-linked polymer (CLP, 22) ... 65
6.3.6. Synthesis of cross-linked polymer (CLP, 23) ... 66
6.3.7. Synthesis of side-chain polymer (SCP, 24) ... 67

Die approbierte gedruckte Originalversion dieser Diplomarbeit ist an der TU Wien Bibliothek verfügbar
The approved original version of this thesis is available in print at TU Wien Bibliothek.
TU Bibliothek Your knowledge hub WIEN

6.3.8. Synthesis of side-chain polymer (SCP, 25) 68

7. Bibliography 69

8. List of figures 75

9. List of tables 77

Die approbierte gedruckte Originalversion dieser Diplomarbeit ist an der TU Wien Bibliothek verfügbar
The approved original version of this thesis is available in print at TU Wien Bibliothek.
TU WIEN Bibliothek Your knowledge hub

Abbreviations – Acronyms

AIBN	Azobisisobutyronitrile
bpy	Bipyridine
[bmim][PF_6]	1-Butyl-3-methylimidazolium hexafluorophosphate
CB	Conduction band
CLP	Cross-linked polymers
CLP-PC	Photocatalyst monomer of the CLP
CLP-PS	Photosensitizer monomer of the CLP
CO_2	Carbon dioxide
DBU	1,8-Diazabicyclo[5.4.0]undec-7-ene
DCM	Dichloromethane
DMAP	4-Dimethylaminopyridine
dmb	4,4'-Dimethyl-2,2'-bipyridine
DMF	*N,N*-Dimethylformamide
5,5'-dvbpy	5,5'-Divinyl-2,2'-bipyridine
E^0	Standard redox potential
EDC	1-Ethyl-3-(3-dimethylaminopropyl)carbodiimide
EE, EtOAc	Ethyl acetate
[emim][BF_4]	1-Ethyl-3-methylimidazolium tetrafluoroborate
FE	Faradaic efficiency
FT-IR	Fourier-transform infrared spectroscopy
HOMO	Highest occupied molecular orbital
ICP	Inductively coupled plasma spectroscopy
ISC	Intersystem crossing
IR	Infrared
LUMO	Lowest unoccupied molecular orbital
MLCT	Metal to ligand charge transfer
NMR	Nuclear magnetic resonance
OERS	One-electron reduced species
PC	Photocatalyst
PE	Petroleum ether
PIL	Polyionic liquid; polymerized ionic liquid
ppy	2-Phenylpyridine

Die approbierte gedruckte Originalversion dieser Diplomarbeit ist an der TU Wien Bibliothek verfügbar
The approved original version of this thesis is available in print at TU Wien Bibliothek.
TU Bibliothek Your knowledge hub WIEN

P[VBIm]	Poly(1-butyl-3-vinylimidazolium)
PS	Photosensitizer
$scCO_2$	Supercritical CO_2
SCP	Side-chain polymers
SCP-PC	Photocatalyst monomer of the SCP
SCP-PS	Photosensitizer monomer of the SCP
SET	Single-electron transfer
SILP	Supported ionic liquid phase
T-XRF	Total-reflection X-ray fluorescence spectroscopy
TGA	Thermogravimetric analysis
TLC	Thin-layer chromatography
TMS	Tetramethylsilane
UV-Vis	Ultraviolet–visible spectroscopy
VB	Valence band

Die approbierte gedruckte Originalversion dieser Diplomarbeit ist an der TU Wien Bibliothek verfügbar
The approved original version of this thesis is available in print at TU Wien Bibliothek.
TU Bibliothek Your knowledge hub WIEN

1. Introduction

1.1. Anthropogenic carbon dioxide emissions

Since the pre-industrial age, atmospheric carbon dioxide (CO_2) concentrations have risen from around 280 ppm to above 400 ppm in 2022 (see Figure 1) due to fossil fuel combustion and industrial processes combined with increasing global deforestation. CO_2 is a greenhouse gas, meaning it can trap the heat radiating from Earth's surface leading to a rise of the atmospheric temperature. Subsequently, this can lead to extreme weather conditions, such as drought and wildfire activity, on the one hand, and heavy precipitation, flooding, and tropical storm activity on the other hand. Furthermore, aquatic environments are affected, as an increase in greenhouse gases has been proven to be the cause of increasing sea surface temperatures, rising sea levels, and ocean acidification, due to absorption of CO_2.[2,3]

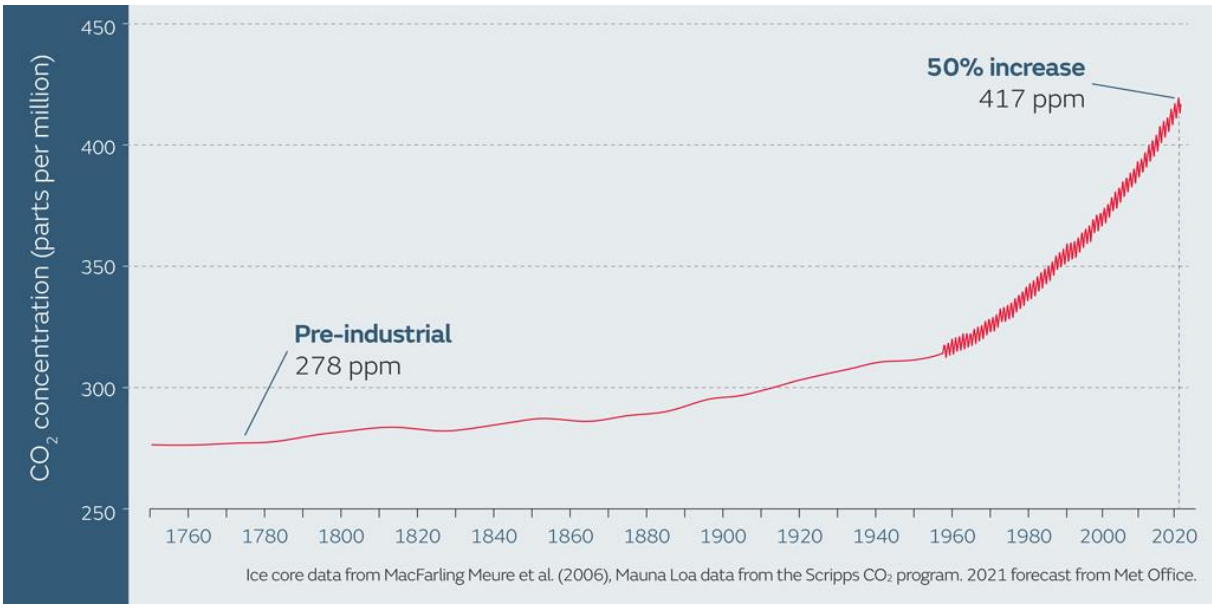

Figure 1: Atmospheric CO_2 concentrations from 1770 to 2021. Graphic taken from[4]

It has been proven that CO_2 is responsible for more than half of the heat trapped within the atmosphere since the industrial revolution, which is leading to current concerns of climate change. Natural CO_2 sinks, i.e., the terrestrial biosphere and the ocean, cannot equilibrate the CO_2 in the atmosphere because its rate of production through fossil fuel consumption, land-use change, and industrial processes is faster than the equilibration rate. Therefore, balance cannot be achieved.[5,6] Accordingly, the research into carbon capture and utilization technologies is important to mitigate these global developments. Ideally, CO_2 would be contained in a closed cycle, such as the one exemplified in Figure 2. Using renewable energy as power supply, CO_2 from the atmosphere can be recycled into value-added chemicals, fuels and feedstock for further

Die approbierte gedruckte Originalversion dieser Diplomarbeit ist an der TU Wien Bibliothek verfügbar
The approved original version of this thesis is available in print at TU Wien Bibliothek.
TU Bibliothek Your knowledge hub WIEN

use on a daily basis or for industrial applications, while the subsequent CO_2 emissions start the cycle anew.[7]

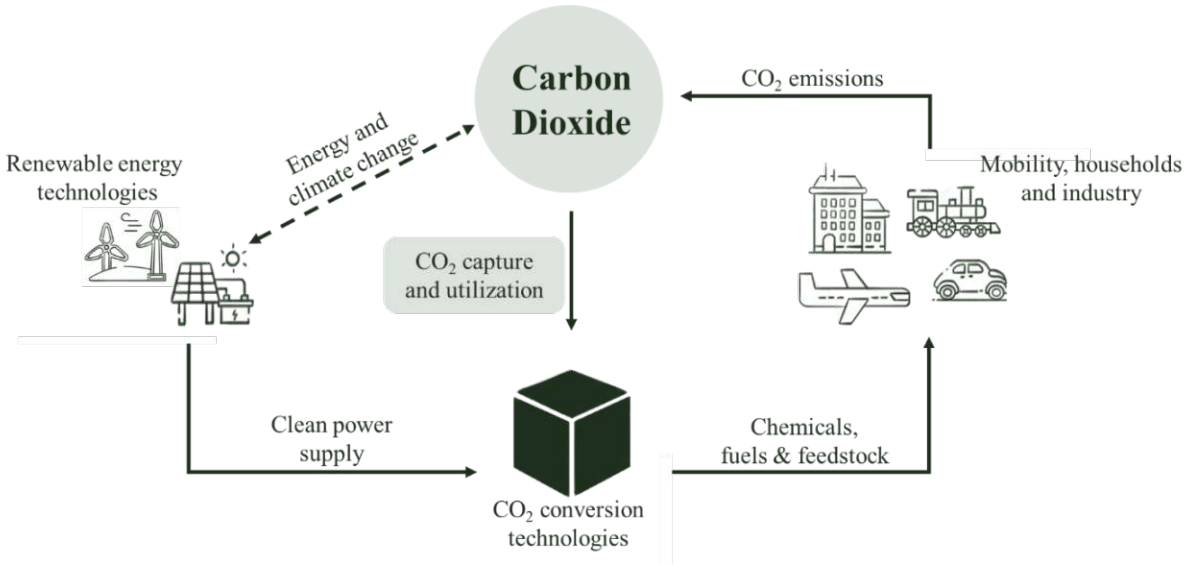

Figure 2: Closed CO_2 cycle. Graphic adapted from [7]

Die approbierte gedruckte Originalversion dieser Diplomarbeit ist an der TU Wien Bibliothek verfügbar
The approved original version of this thesis is available in print at TU Wien Bibliothek.

1.2. Carbon capture and utilization

Carbon capture and utilization describes the process of capturing, transporting, and utilizing carbon compounds, i.e., CO_2 and carbon monoxide (CO), through conversion to value-added chemicals (see Figure 3).

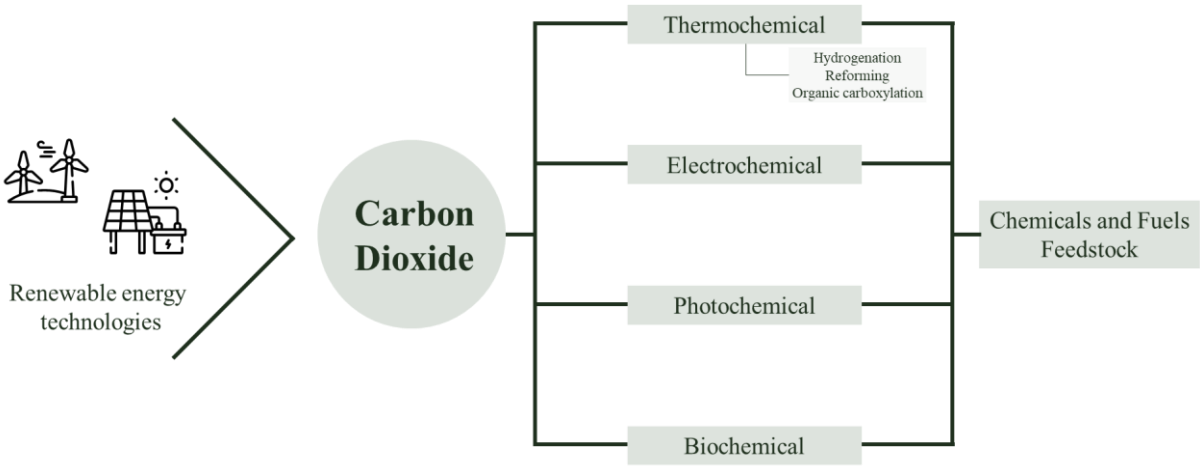

Figure 3: Pathways for the chemical utilization of CO_2. Graphic adapted from [7]

CO_2 is a stable and very inert compound, as carbon is in the highest oxidation state and in the lowest energy level. Therefore, high energy input is required for its valorization *via* conversion to other chemical compounds. The important issue to consider when discussing carbon capture and utilization procedures is that the CO_2 emitted through these procedures – be it through energy consumption, reagent production, etc. – should not be higher than the amount of captured CO_2 to begin with. Furthermore, the compounds synthesized through the fixation of CO_2 need to be of high demand for the developed process to have industrial value and significantly decrease the atmospheric CO_2 concentrations.[2]

CO_2 can either be directly extracted from the air or selectively captured when it is emitted from stationary sources of the industrial or energy sector. Carbon capture can be very effective when extracted from combustion streams. In combination with appropriate subterranean storage, it could prevent 65 to 80% of carbon emissions from entering the atmosphere.[8] By converting the captured CO_2 into high-value chemicals a step towards a closed carbon cycle can be taken. Complete decarbonization is not possible with the current standards and state-of-the-art technologies but by closing the cycle, at least, the current atmospheric CO_2 concentrations could be maintained constant.[9] Possible products from the valorization of CO_2 are fuels, polymers, and construction materials.[2]

Die approbierte gedruckte Originalversion dieser Diplomarbeit ist an der TU Wien Bibliothek verfügbar
The approved original version of this thesis is available in print at TU Wien Bibliothek.
TU Bibliothek Your knowledge hub WIEN

Hydrogenation into methanol, which is an intermediate in the production of synthetic fuels, as well as a building block in many other important chemical processes, is already highly researched, well-established and offers a possible pathway for carbon dioxide valorization. [10,11] The methanol plants in Iceland are a prime example for the potential of sustainable methanol production utilizing CO_2 from geothermal plants. By using renewable energy, such as geothermal energy and hydropower the methanol potential there is ~2150 million L/y.[12] Complications, however, often lie in the required energy consumption and H_2 production cost.[10,11] Further methods for CO_2 utilization can be the biocatalytic or electrochemical conversion to formic acid, [13,14] the electrochemical reduction to hydrocarbons on various metal catalysts, [15,16] or the conversion to polymeric materials.[2,17]

Die approbierte gedruckte Originalversion dieser Diplomarbeit ist an der TU Wien Bibliothek verfügbar
The approved original version of this thesis is available in print at TU Wien Bibliothek.
TU WIEN Bibliothek Your knowledge hub

1.3. The European project CARBOFLOW: Streamlined CO_2 conversion in ionic liquids – a platform strategy for modern carbonylation chemistry

Carbon monoxide (CO) is an important reduction product from CO_2. It can be used as C1 building block for the production of bulk and fine chemicals through carbonylation reactions, such as the Fischer-Tropsch synthesis of hydrocarbons. However, since CO is a highly toxic gas, it needs to be handled carefully. An innovative concept is, therefore, the valorization of CO_2 as feedstock for the production of carbonyl compounds with CO as intermediate.[18]

CARBOFLOW is a running research project in the group of Katharina Schröder at TU Wien and has received funding from the European Research Council (ERC) under the European Union's Horizon 2020 research and innovation programme (Grant agreement No. 864991). This project aims to replace CO with the more benign surrogate CO_2 as an abundant, non-toxic, and renewable carbon source.[19]

CARBOFLOW consists of three goals, the first one being the photocatalytic reduction of CO_2 in ILs, which act as solvent as well as co-catalyst, to obtain CO under mild conditions. The second goal is the investigation of carbonylation reactions in supercritical CO_2 ($scCO_2$), such as Pd catalyzed alkoxycarbonylations of alkenes and aminocarbonylation reactions. Lastly, the results of both goals should be combined to achieve a streamlined process for the direct formation of carbonyl compounds from CO_2 in $scCO_2$, as exemplified in Figure 4.[19]

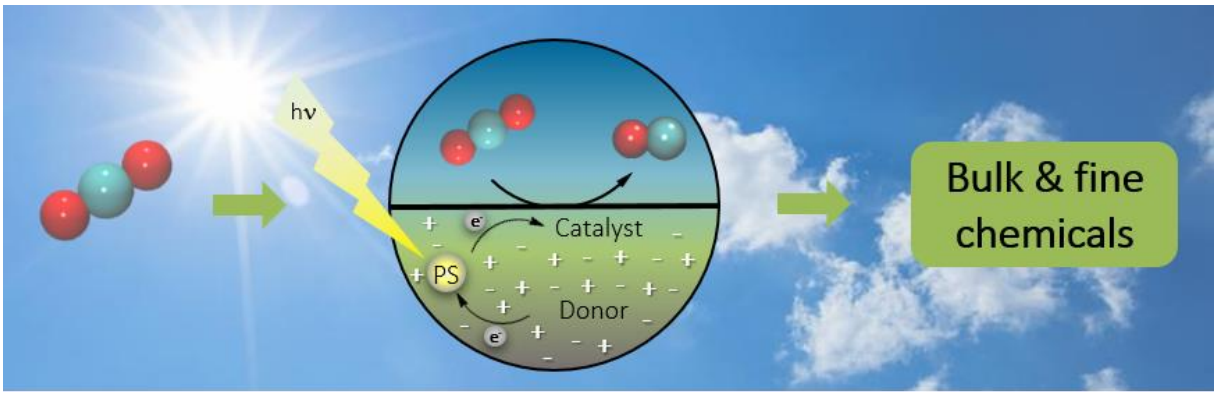

Figure 4: Process concept of CARBOFLOW. Graphic taken from [20]

This thesis is placed in the frame of goal one, aiming for the design of a photocatalytic system that can efficiently reduce CO_2 to CO in combination with ILs. ILs can be used as cooperative media since CO_2 is soluble in them in large concentrations.[1,19,21] Depending on the substitution pattern, the properties of ILs can be varied. Moreover, imidazolium-based ILs show a high

Die approbierte gedruckte Originalversion dieser Diplomarbeit ist an der TU Wien Bibliothek verfügbar
The approved original version of this thesis is available in print at TU Wien Bibliothek.
TU Bibliothek Your knowledge hub WIEN

affinity towards activation of CO_2 as they can form CO_2 adducts.[22] An important focus lies, therefore, on determining the optimal IL composition for the project purposes. Furthermore, Re complexes are to be investigated as photocatalysts in combination with Ru-based photosensitizers, as they have shown promising results for the selective photocatalytic reduction of CO_2 to CO.[23] By immobilizing the photocatalytic components and IL in a polymer framework, catalyst leaching can be avoided, and product separation and catalyst recycling is facilitated.[24]

Die approbierte gedruckte Originalversion dieser Diplomarbeit ist an der TU Wien Bibliothek verfügbar
The approved original version of this thesis is available in print at TU Wien Bibliothek.
TU WIEN Bibliothek Your knowledge hub

2. Theoretical background

2.1. The stability of carbon dioxide

Carbon is in its highest oxidation state in carbon dioxide and, therefore, rather unreactive. For a reaction to take place, usually a large energy input is required to overcome the high activation energy barrier. Some kinetic and thermodynamic considerations can promote a reaction. The term "catalysis" describes the acceleration of a chemical reaction induced by a catalyst, which can reduce the kinetic barrier. The reaction partner forms a bond with the catalyst, reacts to form the product and detaches again, leaving the catalyst in the original state, ready for the next reaction partner to attach.[25]

Additionally, possible pathways involve the reaction of CO_2 with high energy starting materials towards low energy products or the continuous removal of product from the reaction vessel to shift the equilibrium to the side of the product. Furthermore, energy can be supplied from an external source in the form of light or electricity.[26]

Efficient catalysts lower the reduction activation energy. One-electron reduction yields a CO_2 radical anion, which has a high potential (-1.9 V *vs*. NHE in water at pH 7). Multi-electron reduction processes are characterized by lower potentials and yield stable energy-rich products. The following equations [Eq. (1)-(5)] show examples of multi-electron CO_2 reductions and their potentials under standard conditions:[27,28]

$$CO_2(g) + 2\,H^+ + 2\,e^- \rightarrow CO(g) + H_2O(l) : -0.53\ \text{V}\ \textit{vs}.\ \text{NHE (at pH 7)} \quad (1)$$

$$CO_2(g) + 2\,H^+ + 2\,e^- \rightarrow HCOOH(aq) : -0.61\ \text{V} \quad (2)$$

$$CO_2(g) + 4\,H^+ + 4\,e^- \rightarrow HCHO(aq) + H_2O(l) : -0.48\ \text{V} \quad (3)$$

$$CO_2(g) + 6\,H^+ + 6\,e^- \rightarrow CH_3OH(aq) + H_2O(l) : -0.38\ \text{V} \quad (4)$$

$$CO_2(g) + 8\,H^+ + 8\,e^- \rightarrow CH_4(aq) + 2\,H_2O(l) : -0.24\ \text{V} \quad (5)$$

A two-electron reduction is thermodynamically less favored in comparison to the production of H_2 from protons. Therefore, the catalysts must be highly selective towards the reduction of CO_2, as well as be able to drive multi-electron reductions. Metal complexes can have multiple redox states in the metal center and the ligands, which makes multi-electron reductions possible.[28]

Die approbierte gedruckte Originalversion dieser Diplomarbeit ist an der TU Wien Bibliothek verfügbar
The approved original version of this thesis is available in print at TU Wien Bibliothek.
TU Bibliothek Your knowledge hub WIEN

2.2. General methods for the reduction of carbon dioxide

2.2.1. Chemical reduction of carbon dioxide

Methods for CO_2 reduction have been established, both in homogeneous and heterogeneous systems, for fast and selective product formation. In a homogeneous system, reactants and catalysts all operate in the same phase, mostly through solvation in an appropriate solvent. This leads to high reactivity and selectivity as well as efficient heat distribution. However, it complicates the recycling of the catalyst and the separation of reactants and products. Heterogeneous systems are based on the catalyst located in a different phase than the reactants or product. They allow easy product separation, catalyst recycling, and use in a continuous process, but have the drawback that oftentimes the activity and selectivity are limited.[29]

One of the most common reductants for CO_2 reduction is H_2. The reverse water gas shift (RWGS) reaction [Eq. (6)] can reduce CO_2 with H_2 to CO, which can then be further converted to synthetic fuels or platform chemicals. It is in competition with the Sabatier reaction [Eq. (7)] for methane production. At low temperatures, the latter is thermodynamically favored over RWGS. Active RWGS catalysts are required to selectively produce CO, such as the ones suggested in Table 1. The catalyst must be able to adsorb CO_2 and dissociate one C-O bond. The O can then be hydrogenated to H_2O. [30]

$$CO_2 + H_2 \leftrightarrow CO + H_2O \tag{6}$$

$$CO_2 + 4\ H_2 \leftrightarrow CH_4 + 2\ H_2O \tag{7}$$

Table 1: Selection of typical catalysts for homogeneous and heterogeneous RWGS reaction to CO.

Type	Catalyst	Solvent	Solid support	CO Selectivity	Ref.
homogeneous	$RuCl_3$ (with LiCl as co-catalyst)	NMP	-	84.8 mol%	[31]
	$Ru_3(CO)_{12}$-[PPN]Cl	NMP	-	40.3 mol%	[32]
heterogeneous	Pt nanoparticles	-	SiO_2	100%	[33]
	Pd-In nanoparticles	-	SiO_2	100%	[34]

The Sabatier reaction to form methane from CO_2 is a possible hydrogenation reaction to yield hydrocarbons through heterogenous catalysis. Ni, Ru and Rh can be applied as heterogeneous catalysts, in combination with H_2 at high pressures and temperatures. Moreover, aldehydes and alcohols can be formed through hydroformylation reactions from alkenes with H_2 and CO_2 utilizing a Ru catalyst. Importantly, the production of H_2 is highly energy demanding. It can be obtained from fossil-fuel sources or through water-splitting, which can be performed electrochemically, thermally, or photolytically. These processes require a considerable amount

Die approbierte gedruckte Originalversion dieser Diplomarbeit ist an der TU Wien Bibliothek verfügbar
The approved original version of this thesis is available in print at TU Wien Bibliothek.
TU Bibliothek Your knowledge hub WIEN

of electricity and are, therefore, very cost-demanding, although, it is noteworthy that renewable energy sources can be used. This is an important factor that needs to be considered in the grand scale for the efficient mitigation of CO_2.[26]

The reductive hydrogenative conversion of CO_2 is an important category of the different reduction processes of CO_2, as the overall Gibbs free energy of these reactions is often negative since water is formed as by-product. The conversion to methanol [Eq. (8)], which can be used as a liquid energy carrier, *via* this route, uses $Cu/ZnO/Al_2O_3$ as catalyst, and CO_2 and H_2 as raw materials. Again, the production of H_2 makes these processes very energy demanding.[26]

$$CO_2 + 3\ H_2 \leftrightarrow CH_3OH + H_2O \tag{8}$$

Alternatively, p-block element-containing reductants (E = B, Si, P, Al, Ga, Ge, Sn) have been investigated for the homogeneous reduction of CO_2. Since E-H bonds are weaker than H-H bonds, the formation of molecules or polymers with stronger E-O bonds is favored during CO_2 reduction. Therefore, this reduction method could also be considered as a potential oxidation process, where CO_2 acts as a soft oxidant of main group compounds. As depicted in Figure 5 CO_2 can be transformed to various reduction products using hydroboranes, hydrosilanes, or phosphines, among others, as stochiometric reductants. This research area is still in its earlier stages, yet seems very promising as it could yield a large variety of possible main group oxidation compounds in addition to the value-added chemicals from the CO_2 reduction.[35]

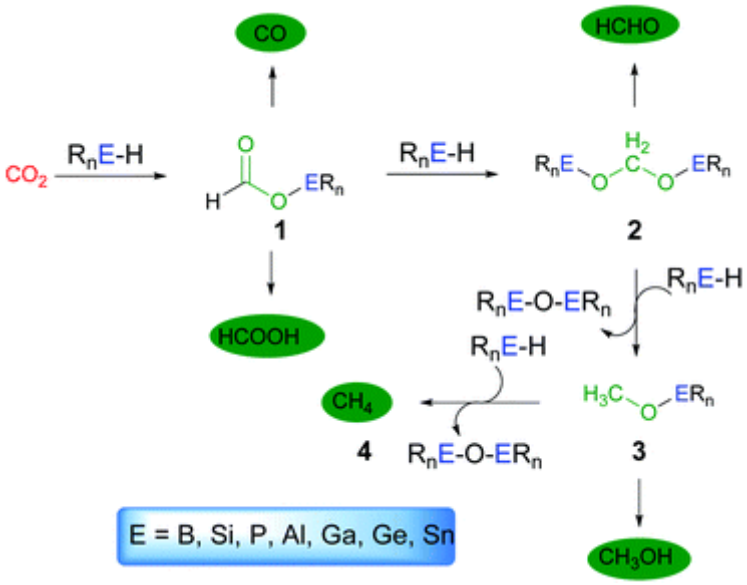

Figure 5: CO_2 reduction with p-block element-containing reductants. Graphic taken from[35]

Die approbierte gedruckte Originalversion dieser Diplomarbeit ist an der TU Wien Bibliothek verfügbar
The approved original version of this thesis is available in print at TU Wien Bibliothek.

A particularly interesting solvent for the reduction is supercritical CO_2. It can be used as solvent and reactant at the same time and since it has tunable solvation properties H_2 can be highly miscible in it. This makes for a very efficient energy and heat transfer. Furthermore, $scCO_2$ is easily separated from the product(s) by simply releasing the pressure. These properties make $scCO_2$ quite relevant for homogeneous CO_2 reductions, and, as shown in Table 2, a fair amount of research has already been conducted on the topic of CO_2 hydrogenation using $scCO_2$ as solvent. [36,37]

Table 2: Selection of CO_2 hydrogenation reactions in $scCO_2$ to formates. Table adapted from [36]

Catalyst precursor	Ligand	Additive	*P* (MPa) (H_2/CO_2)	T (°C)	TON	TOF (h^{-1})	Ref.
$[RuH_2(PMe_3)_4]$	PMe_3	Et_3N	8.5/12	50	3700	1400	[38]
$[RuCl(OAc)(PMe_3)_4]$	PMe_3	C_6F_5OH	7/12	50	32000	95000	[39]
$[RuCl(PMe_3)_3$(**NN1**)$]$	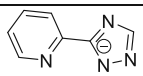 **NN1**	DBU	7/10	100	4800	1200	[40]
$[RuCl_2[P(OMe)_3]_4]$	$P(OME)_3$	DBU	7/10	100	6630	1655	[41]

2.2.2. Electrochemical reduction of carbon dioxide

The electrochemical reduction of CO_2 is a very promising technique for CO_2 mitigation that employs electrical energy and mild conditions to overcome the reduction barrier. Renewable energy, such as solar or wind, can be employed and water can be used instead of H_2, rendering this process more environmentally benign in comparison to other existing reduction methods.[42] By controlling the electrode overpotential and the operating temperature, CO_2 can be selectively reduced to value-added chemicals and fuels. As the reaction takes place at the interface of electrolyte and electrode, its conditions are customizable through selection of electrocatalysts, electrode potential, and electrolyte type and composition, to the direction of achieving high product selectivity and low CO_2 reduction overpotential. [7]

Generally, the reduction consists of three steps. First, CO_2 is chemisorbed to the catalytic surface. Then radical $*CO_2^{\bullet-}$anions are formed as a result of the transfer of electrons. Depending on the way the molecule is attached to the electrode surface, the carbon atoms can be protonated in different ways and the corresponding reduction products and water are formed. Lastly, the products are desorbed from the surface.[27,42] The electrons participating in the reduction step are transferred from the electrode to the catalyst, as depicted in Figure 6. The injection speed can be varied through the applied electrode potential, but it needs to be fast for an efficient

Die approbierte gedruckte Originalversion dieser Diplomarbeit ist an der TU Wien Bibliothek verfügbar
The approved original version of this thesis is available in print at TU Wien Bibliothek.
TU Bibliothek Your knowledge hub WIEN

electrocatalyst. Variations of the catalyst metal center and the corresponding ligands are also a possibility that can be exploited in order to reach optimal reduction conditions.[28]

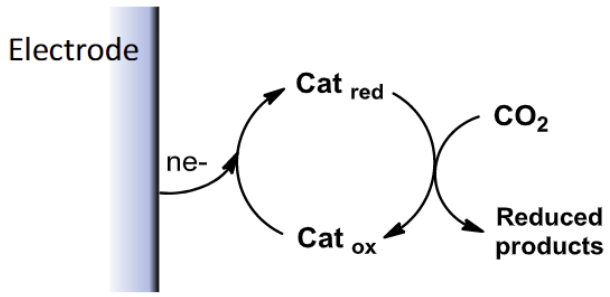

Figure 6: Scheme of the electrochemical reduction of CO_2. Graphic adapted from [28]

The difficulty of electrochemical CO_2 reductions lies in the competitive reduction of the protons in the electrolyte to H_2. Competitive H_2 formation can be circumvented by using electrode materials and catalysts that prefer carbon reduction, rather than proton reduction.[42]

Depending on the reaction conditions and materials used, common reduction products are methane, CO, formic acid, methanol, oxalic acid, and formaldehyde, among others.[7] A selection of possible electrocatalytic CO_2 reduction reactions and the correspondingly formed products has been summarized in Table 3. The standard redox potential (E^0) of the products (vs NHE, pH 7) and the Faradaic efficiency (FE), to describe the product selectivity of these reactions, is given.

Table 3: Selection of electrocatalytic CO_2 reduction reactions.

Electrodes	Electrolyte	Products	E^0 [27]	FE	Ref.
$Bi_2O_2CO_3$-coated carbon fiber (working electrode), Pt mesh (counter electrode), Ag/AgCl (reference electrode)	Aqueous $KHCO_3$ or $NaHCO_3$ solution (0.1–1.0 M)	Formic acid	-0.61 V	69%	[43]
Cu_2O electrodeposited on stainless steel (working electrode), Pt wire (counter electrode), Ag/AgCl (reference electrode)	Aqueous $KHCO_3$ solution (0.5 M)	Methanol	-0.38 V	38%	[44]
Cu foil (working electrode), Pt foil (counter electrode), Ag/AgCl-saturated KCl (reference electrode)	$NaClO_4$ in methanol (0.25 M, catholyte) KOH in methanol (0.3 M, anolyte)	Methane	-0.24 V	70.5%	[45]
Cu_2O film (working electrode), Pt wire (counter electrode), Ag/AgCl (reference electrode)	Aqueous $KHCO_3$ (0.1 M) and phosphate buffer (0.1 M K_2HPO_4, and 0.1 M KH_2PO_4)	Ethylene Ethanol	-0.34 V -0.33 V	34–39% 9–16%	[46]

Die approbierte gedruckte Originalversion dieser Diplomarbeit ist an der TU Wien Bibliothek verfügbar
The approved original version of this thesis is available in print at TU Wien Bibliothek.
TU Bibliothek Your knowledge hub WIEN

2.2.3. Biochemical reduction of carbon dioxide

Biochemical CO_2 reduction often relies on controlled photosynthetic technologies. Microalgae have demonstrated a high efficiency in fixing CO_2 using solar energy. Finding suitable algal strains has, therefore, been an interesting field of research. Open pond systems using algae have already been investigated and show that large areas are required for profitable CO_2 sequestration. The benefit of these open systems is that direct sunlight can be used, however, they can be easily contaminated, and the system parameters are at least partly dependent on environmental influences. There is the possibility to build a closed system bioreactor, where photosynthesis can occur in a regulated environment for optimal CO_2 uptake and conversion to carbohydrates, H_2 and oxygen. A closed system would facilitate environmental control, which would make it easier to sustain a monoculture and would lead to higher biomass concentrations. Generated biomass can be separated and converted into biofuels.[26]

Cyanobacteria are organisms that have the ability to fix CO_2. They are a micro-algal species that can live under mild and extreme weather conditions and contribute 20-30% of photosynthetic activity on earth. Depending on the strain, they have a photo- or chemoheterotrophic metabolism. Chemoheterotrophic strains metabolize CO_2 in the dark and continue with the phototrophic metabolism as soon as light is available. CO_2 is fixed by cyanobacteria through the enzyme RuBisCO, which has a low affinity for CO_2. However, carboxysomes encapsulate RuBisCO in the bacteria and increase its catalytic performance by accumulating CO_2 in the vicinity of its active site. The advantage of cyanobacteria is that they are easily genetically engineered, for example to enhance the affinity of RuBisCO, or the product production yield, making this field a highly active area of research. [47–50]

Methanogenic bacteria can fix CO_2 in a non-photosynthetic way. They can convert CO and H_2 or CO_2 and H_2 into methane and are responsible for over 50% of the methane released into the atmosphere. H_2 is, hereby, used as reducing agent, while CO_2 and CO are the carbon sources. *Methanobacterium formicium* and *Methanosarcina barkeri* can convert CO_2 into methane and are often used in a triculture system with *Rhodospirillum rubrum*, which converts CO and H_2O into CO_2 and H_2 in a first reaction step. Conventional methanation reactions require high temperatures and elevated pressure of 300 to 700 °C and 3 to 20 atm, respectively, while triculture systems only require low temperatures of 37 °C and are resistant to catalyst poisoning. As with a lot of other conventional CO_2 reduction methods, methanogenic bacteria are not viable for large scale CO_2 mitigation as H_2 is a key substance for the conversion to methane and

Die approbierte gedruckte Originalversion dieser Diplomarbeit ist an der TU Wien Bibliothek verfügbar
The approved original version of this thesis is available in print at TU Wien Bibliothek.
TU Bibliothek Your knowledge hub WIEN

the state-of-the-art formation of H_2 from natural gas *via* steam reforming is too energy-demanding for commercial applications.[26]

Die approbierte gedruckte Originalversion dieser Diplomarbeit ist an der TU Wien Bibliothek verfügbar
The approved original version of this thesis is available in print at TU Wien Bibliothek.
TU WIEN Bibliothek Your knowledge hub

2.3. Photochemical reduction of carbon dioxide

2.3.1. Homogeneous photocatalysis

Photochemistry is based on the ability of ultraviolet, visible, or infrared radiation to supply enough energy to overcome the activation energy barrier, which is not possible by simply employing thermal energy. The reactant has to be able to absorb radiation for an electron to enter an excited state in which it can react further. The amount of energy needed to excite an electron to a higher energy state is fixed, as the energy levels are quantized. Therefore, as is depicted in Figure 7, if light of the corresponding frequency can interact with the molecule, it is absorbed and an electron can transition from one electronic state (E_1) to another (E_2). Since there are many possible transitions between the different vibrational and rotational states of the electronic states, light with different wavelengths will lead to transitions to excited states, with the most probable transition giving the most intense peak. There are different types of electronic excitations, but in photochemistry molecules containing groups, where $\pi \rightarrow \pi^*$ and $n \rightarrow \pi^*$ transitions are possible, are more relevant, as is the case with reactants with π-systems. [51]

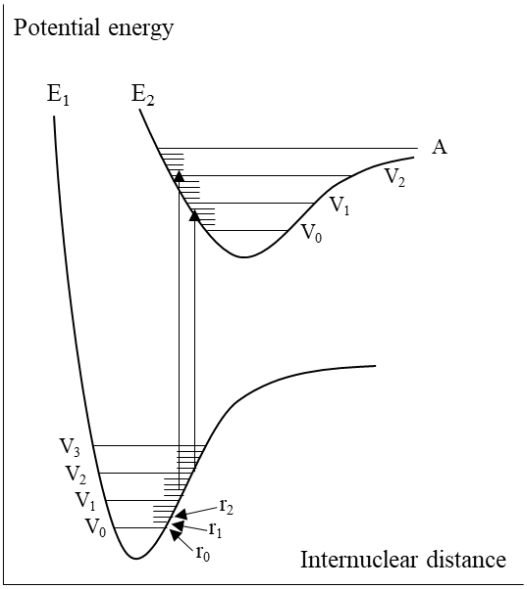

Figure 7: Potential energy curves for diatomic molecules, E: electronic state, V: vibrational state, r: rotational state. Graphic adapted from [51]

Die approbierte gedruckte Originalversion dieser Diplomarbeit ist an der TU Wien Bibliothek verfügbar
The approved original version of this thesis is available in print at TU Wien Bibliothek.

In photocatalysis photons are absorbed by the photocatalyst, promoting the electrons of the catalyst to a stable, long-lived, excited electronic state. In the ground state these species are not very effective single-electron transfer (SET) reagents. Only after excitation, they enter a state, in which they can efficiently engage in bimolecular electron-transfer reactions.[52] Figure 8 depicts the photoredox cycle, where after light absorption, an electron is excited from the highest occupied molecular orbital (HOMO) to the lowest unoccupied molecular orbital (LUMO) and yields Pcat* as excited species photocatalyst. Pcat* is a potent reductant and oxidant. It can subsequently participate either in an oxidative or reductive quenching cycle. In the oxidative cycle the high-energy electron can be used to reduce a reactant (A in Figure 8) and the photocatalyst is therefore used as the reductant. In the next step, the oxidized photocatalyst ($Pcat_{ox}^{+}$) can absorb an electron from a donor (D in Figure 8) and return to its original ground-state (Pcat). In the reductive cycle it can accept an electron, in the hole of the original HOMO from Pcat, from an electron donor. The reduced catalyst ($Pcat_{red}^{-}$) can, in the next step, reduce an acceptor *via* SET to give a reduced acceptor and again the original ground-state photocatalyst. The redox potentials of the single steps of these SET reactions can be customized depending on the ligands used.[52,53]

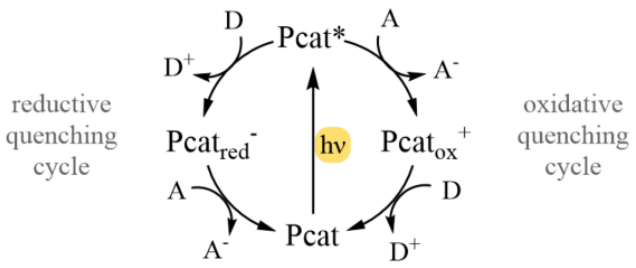

Figure 8: Exemplary photoredox cycle, Pcat: photocatalyst, D: electron donor, A: acceptor. Graphic adapted from [53]

Common photocatalysts are Ir-, Ru- or Re-based, e.g. $[Ru(bpy)_3]^{2+}$, $[Ru(dmb)_3]^{2+}$, $[Ir(bpy)_3]^{3+}$, fac-$Ir(ppy)_3$, or $ReCl(bpy)(CO)_3$ (see Figure 9).[26,54] Electron donors for reductive quenching cycles are usually tertiary amines, such as triethanolamine. Oxidative quenchers for the oxidative quenching cycle can be diazonium salts, polyhalomethanes, and dicyanobenzenes, among others.[52]

Die approbierte gedruckte Originalversion dieser Diplomarbeit ist an der TU Wien Bibliothek verfügbar
The approved original version of this thesis is available in print at TU Wien Bibliothek.

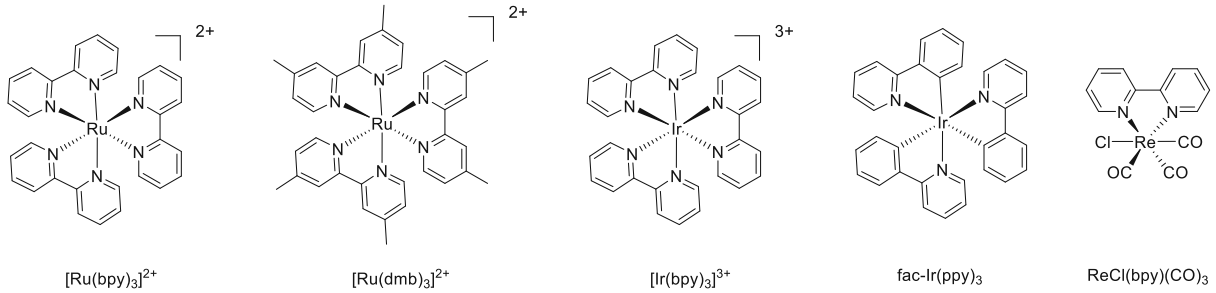

Figure 9: Chemical structures of $[Ru(bpy)_3]^{2+}$, $[Ru(dmb)_3]^{2+}$, $[Ir(bpy)_3]^{3+}$, fac- $Ir(ppy)_3$,and $ReCl(bpy)(CO)_3$.

A photosensitizer is another significant aspect of a photocatalytic system. A sensitizer absorbs the light and, as a consequence, an electron enters an excited electronic state. The excess energy is then transferred to a molecule in the environment and excites it in turn, while the sensitizer returns to the ground-state.[51] The energy transfer can occur either *via* radiative or *via* two different non-radiative transfer mechanisms, the Förster and the Dexter energy transfer (see Figure 10). The Förster energy transfer is based on dipolar interactions through space, as the transition moment dipoles of donor and acceptor couple. This means that no orbital overlap is required, making this mechanism possible over larger distances of 10 to 100 Å. Dexter energy transfer can be described as two simultaneous electron transfers, as is aptly depicted in Figure 10. It is a through-bond process and, therefore, orbital overlap is required, making this mechanism possible only for shorter distances of less than 10 Å. Consequently, the Förster mechanism is dominant at longer distances, while the Dexter mechanism is dominant at very short distances.[54]

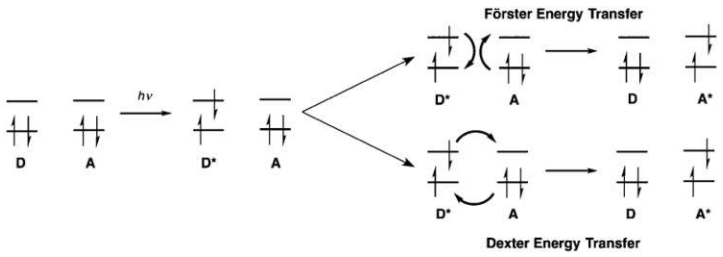

Figure 10: Mechanisms of the Förster and the Dexter energy transfer. Graphic taken from[54]

Die approbierte gedruckte Originalversion dieser Diplomarbeit ist an der TU Wien Bibliothek verfügbar
The approved original version of this thesis is available in print at TU Wien Bibliothek.

A schematic photocatalytic set-up for the reduction of CO_2 with a photosensitizer and a photocatalyst is depicted in Figure 11. After reductive quenching of the photosensitizer with an electron donor, the one-electron reduced photosensitizer can transfer an electron to reduce the photocatalyst. The sensitizer returns to the ground state and can start the cycle anew, while the reduced catalyst is a potent reducing agent for CO_2 reduction.[28]

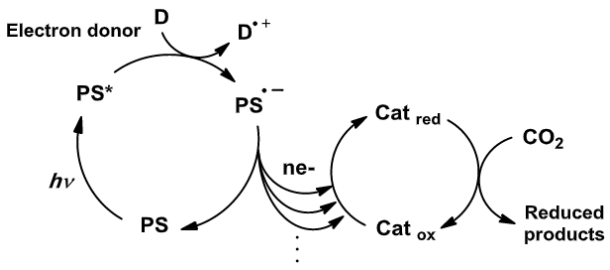

Figure 11: Photocatalytic system for the reduction of CO_2, PS: photosensitizer, Cat: photocatalyst, D: electron donor. Graphic taken from [28]

Different aspects affect the catalytic reduction, such as the back reaction, and different reaction pathways. This includes the possible coordination modes in metal complexes, which lead to different reduction products. Therefore, it is crucial to find the appropriate catalyst for the desired product outcome. Some possible metal-CO_2 complexes and their corresponding bonding modes are depicted in Table 4.[26]

Table 4: Structural types of metal-CO_2 complexes. Table adapted from [26]

Mode of bonding	Structural types of metal-CO_2 complexes	Type of M
η^1-O	M-O-C=O	U
η^1-C		Rh, Ir
η^1-C,O	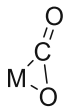	Ni, Rh, Fe, Pd
μ_2-η^2	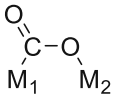	Pt, Ir/Zr, Ir/Os, Rh, Ru, Re/Ge
μ_2-η^3	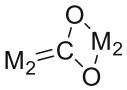	Re/Zr, Ru/Zr, Ru/Ti, Fe/Zr, Fe/Ti

Die approbierte gedruckte Originalversion dieser Diplomarbeit ist an der TU Wien Bibliothek verfügbar
The approved original version of this thesis is available in print at TU Wien Bibliothek.

2.3.2. Heterogeneous photocatalysis

Heterogeneous CO_2 reductions are usually carried out in a photocatalytic, electrochemical or photoelectrochemical manner. In Figure 12 and Figure 13 schematic depictions of these three methods are shown.

Photocatalytic heterogeneous CO_2 reduction is supposed to mimic natural photosynthesis by using solar energy and a semiconductor. As depicted in Figure 12a, when the energy absorbed is higher than the bandgap, electrons are excited from the valence band (VB) to the conduction band (CB). An equal number of holes to the electrons is generated in the VB. These electron-hole pairs separate and are transported to the surface where the catalytic CO_2 reduction and the oxidation of an electron donor or H_2O occur. For the reduction to be thermodynamically possible, the redox potential must be below the CB position. Metal oxides, nitrides, and metal sulfides, e.g., Cu_xO-TiO_2 composites, d^{10} metal nitride solid solutions, and CdS, have been proven to be active semiconductors, but, currently, sacrificial agents are still used as electron donors instead of water and the production evolution is still low, even lower when using water as electron donor. [55]

A comparison to heterogeneous electrochemical CO_2 reduction is shown in Figure 12b. The process is controllable through varying the potentials and reaction temperature, while the set-up is compact, as well as easy to scale up. The disadvantage is that, due to slow kinetics, high energy efficiency and selectivity is difficult to achieve.[55]

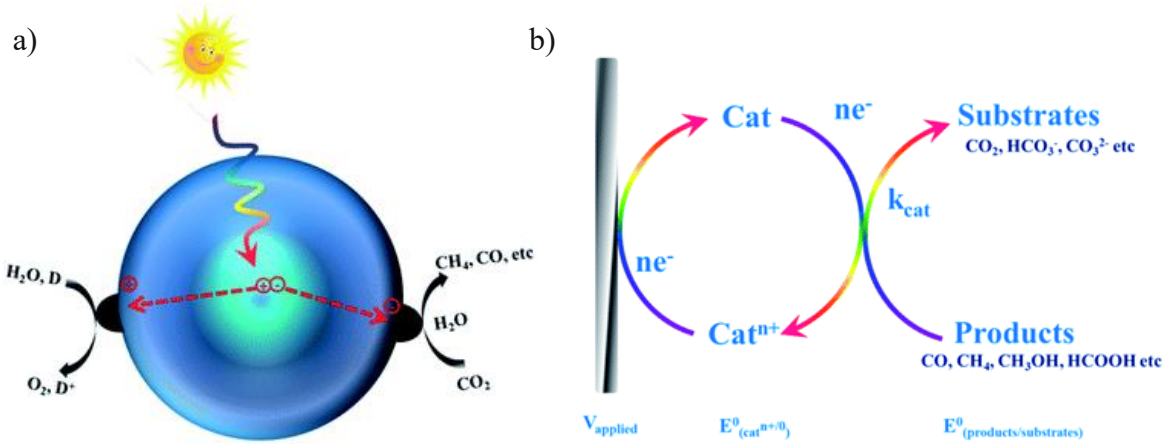

Figure 12: Heterogeneous CO_2 reduction methods: (a) photocatalytic reduction, (b) electrochemical reduction. Graphics taken from[55]

Die approbierte gedruckte Originalversion dieser Diplomarbeit ist an der TU Wien Bibliothek verfügbar
The approved original version of this thesis is available in print at TU Wien Bibliothek.
TU Bibliothek Your knowledge hub WIEN

Photoelectrochemical reduction of CO_2 is a combination of photo- and electrocatalysis. By combining these two modes of catalysis, a mutually beneficial interaction is introduced into these concurrent processes. The applied potential can improve the separation of the photo-induced electrons and holes of photocatalytic process, while light irradiation reduces the required overpotential of the electrocatalytic process. The photocathodes are made of semiconductor and act as both catalyst and light harvester (see Figure 13).

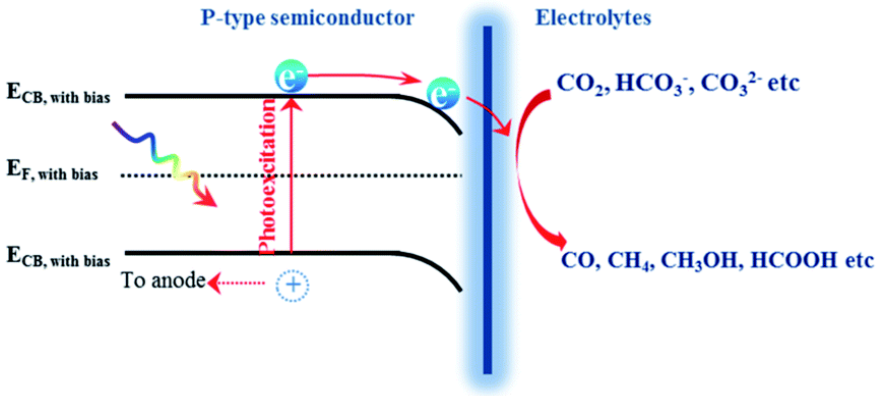

Figure 13: Photoelectrochemical reduction of carbon dioxide. Graphics taken from [55]

The semiconducting electrode can be used in its pure form or in combination with cocatalysts and form hybrid structures that show improved efficiency and selectivity. The cocatalysts can be metals or metal complex catalysts.[55] Possible semiconductors are presented in Table 5.

Table 5: Examples of semiconductor materials for photoelectrochemical CO_2 reduction.

Type	Material	Reduction product	Faradaic efficiency (%)	Ref.
Pure semiconductor	p-GaP	CH_4	Near 100%	[56]
Metal-modified semiconductor	Nanoporous Au thin film coupled on a Si electrode	CO	91%	[57]
Metal complex-modified semiconductor	Ru(II)–Re(I) supramolecular photocatalyst coupled on a NiO electrode	CO	71%	[58]

Die approbierte gedruckte Originalversion dieser Diplomarbeit ist an der TU Wien Bibliothek verfügbar
The approved original version of this thesis is available in print at TU Wien Bibliothek.

2.3.3. State-of-the-art visible-light photocatalytic CO_2 reduction with transition metal complexes

Several factors can affect the efficiency of the photocatalytic CO_2 reduction, such as solvents, temperature, CO_2 concentration, catalysts, photosensitizers, electron donors, and irradiation. The solvent has a general impact on the whole system; therefore, the choice of a proper solvent is very important. Weak coordinating ability to the catalyst and high solubility of CO_2 are required. *N,N*-Dimethylformamide, *N,N*-dimethylacetamide, *N*-methyl-2-pyrrolidone, and acetonitrile are often used. [28]

In this thesis a catalytic system consisting of derivatives of $[Re(bpy)(CO)_3Cl]$ and $[Ru(bpy)_3]^{2+}$ as photocatalyst and photosensitizer, respectively, was developed. This catalytic combination has been established in literature to be very efficient for CO_2 reduction.[59–61] $[Ru(bpy)_3]^{2+}$ is a prototypical photosensitizer. It absorbs at 452 nm and has a stable, long-lived excited electronic state. After absorption of a photon, an electron is excited from the metal-centered t_{2g} orbital to the ligand-centered π^* orbital in a metal-to-ligand charge transfer (MLCT). In this state, the metal center has been oxidized from Ru(II) to Ru(III), while a single-electron reduction has occurred in the ligand framework. Through a rapid intersystem crossing (ISC) the electron transfers from the singlet MLCT (^{1}MLCT) state to the lowest-energy triplet MLCT state (^{3}MLCT). This triplet state is a long-lived photoexcited state that can take part in a single-electron transfer reaction as both oxidant and reductant.[52] This process is pictured in Figure 14.

Die approbierte gedruckte Originalversion dieser Diplomarbeit ist an der TU Wien Bibliothek verfügbar
The approved original version of this thesis is available in print at TU Wien Bibliothek.
TU WIEN Bibliothek Your knowledge hub

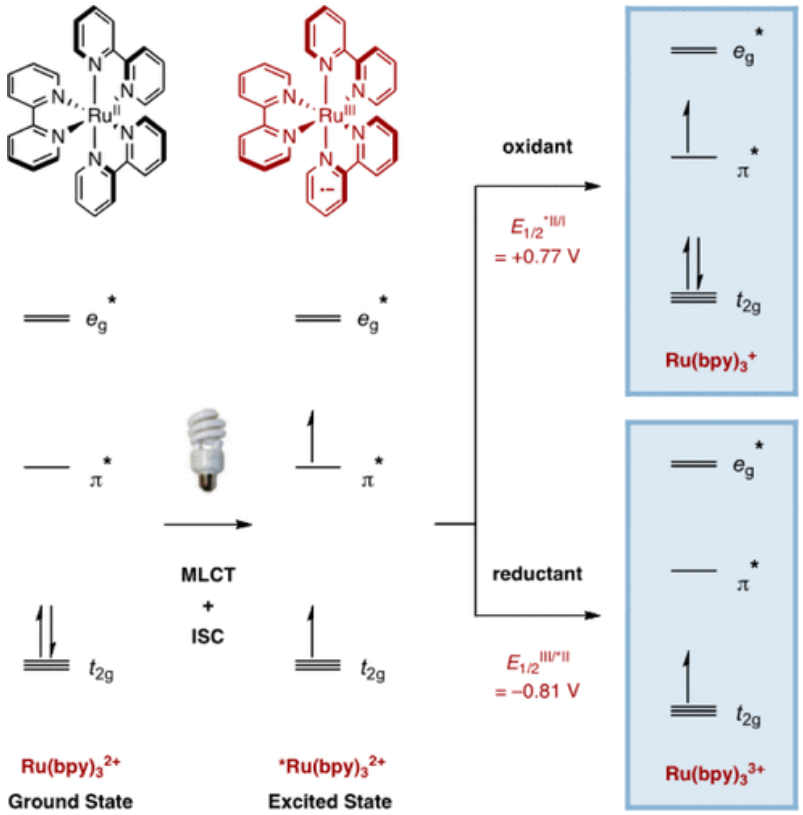

Figure 14: Molecular orbitals of $[Ru(bpy)_3]^{2+}$ after photoexcitation. Graphic taken from[52]

Re(I) complexes are highly efficient catalysts for CO_2 reduction and show a high product selectivity towards CO in photocatalytic reactions. Early studies in the 1980s from Hawecker, Lehn, and Ziessel showed that *fac*-Re(bpy)(CO)$_3$X (X= Cl^- and Br^-) can already reduce CO_2 to CO with high efficiency with a tertiary amine as electron donor. They proposed a reaction mechanism in which the photocatalytically produced one-electron reduced species can vacate a CO site for the CO_2, as can be seen in process (a) in Figure 15.[62] This pathway was not completely correct, as the CO ligand exchange takes too long for this to be the primary mechanism. Sullivan et al. proposed an alternative mechanism, shown in process b of Figure 15, in which the Cl^- is disassociated from the catalyst.[63] Neither of these mechanisms has been experimentally verified, since neither group reported a direct observation of the intermediates.[62,63]

Die approbierte gedruckte Originalversion dieser Diplomarbeit ist an der TU Wien Bibliothek verfügbar
The approved original version of this thesis is available in print at TU Wien Bibliothek.

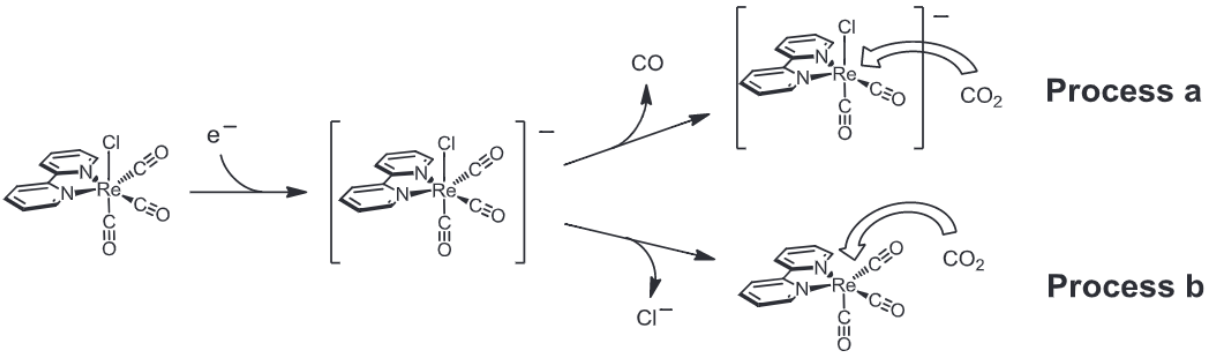

Figure 15: Proposed reaction mechanism for the reduction of CO_2 using fac-Re(bpy)(CO)$_3$Cl from Hawecker et al. (process a)[62] and Sullivan et al. (process b)[63]. Graphic taken from [28]

Ever since these early studies the reduction mechanism has been studied extensively, but as of right now, there are still a lot of unanswered questions. In 2018, Kuramochi, Ishitani, and Ishida published an extensive review where they highlighted the key points of what is already understood on this topic and discussed what needs to be further investigated. They stressed the importance of understanding the reaction mechanism and catalyst deactivation processes. It was possible to observe the intermediates in these processes in homogeneous systems using photosensitizers and electron donors, with spectroscopic methods and kinetic analyses, but still there is a lot of uncertainty with regard to their structure. The mechanisms proposed by different research groups often contradict each other and no general CO_2 reduction mechanism that explains all reactions under all conditions has been thus far reported.[28]

Die approbierte gedruckte Originalversion dieser Diplomarbeit ist an der TU Wien Bibliothek verfügbar
The approved original version of this thesis is available in print at TU Wien Bibliothek.

2.4. The influence of ionic liquids on CO_2 reduction

Ionic liquids are compounds with a melting point below 100 °C, consisting of a combination of cations and anions, some of which are depicted in Figure 16. They are characterized by thermal stability, high heat capacity, negligible vapor pressure, electric conductivity, and wide solvating range, among others. Due to this plethora of properties, which can be modified and tailored by using different ion combinations, they have a wide scope of applications, e.g., as solvents, electrolytes, for heat storage or separation processes.[64]

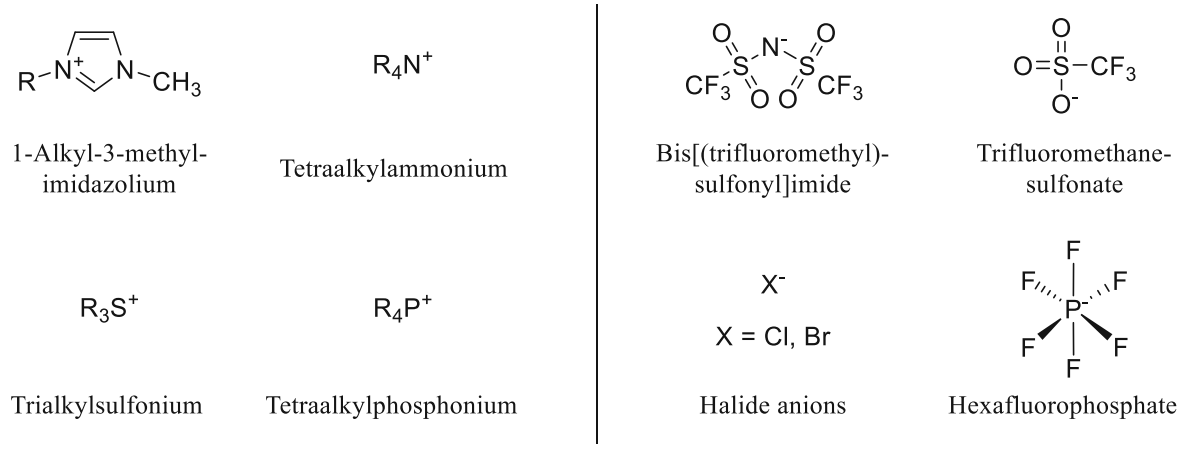

Figure 16: Typical IL cations and anions.

ILs have three key features that make them appealing in combination with CO_2, as seen in Figure 17). On the one hand, CO_2 is soluble in ILs and ILs can act as co-catalysts for CO_2 reduction. On the other, the catalyst for the reduction can be immobilized in an IL phase.

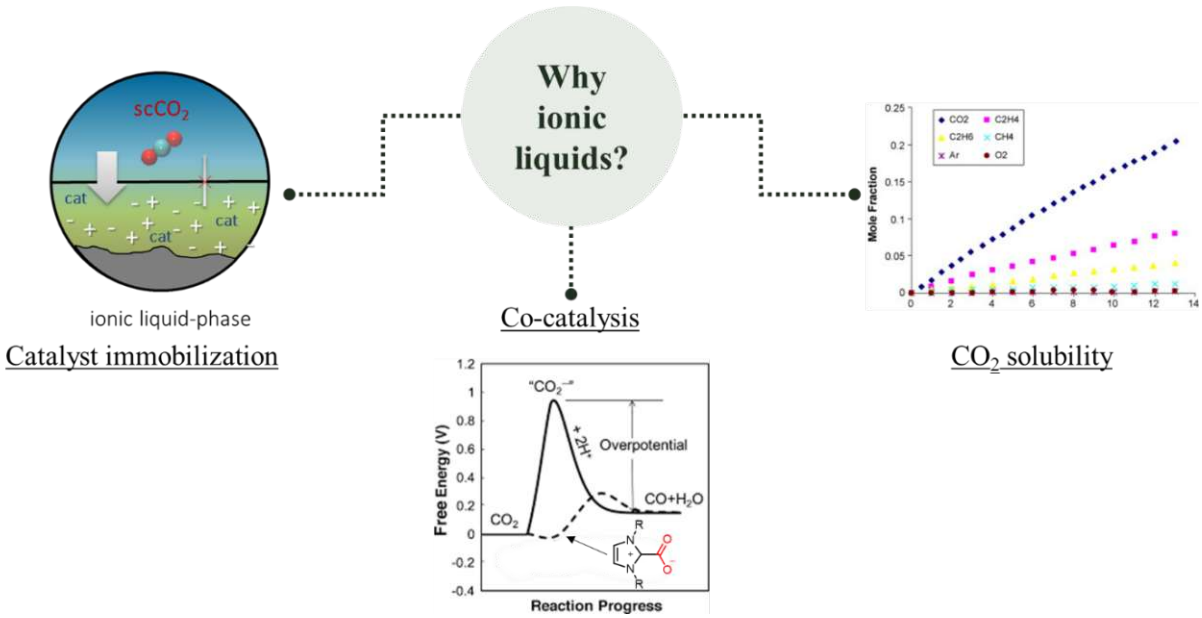

Figure 17: The benefits of ILs in combination with CO2. Graphs taken or adapted from [1,21]

Die approbierte gedruckte Originalversion dieser Diplomarbeit ist an der TU Wien Bibliothek verfügbar
The approved original version of this thesis is available in print at TU Wien Bibliothek.

Figure 18 depicts the solubility of different gases, i.e., CO_2, C_2H_4, C_2H_6, CH_4, Ar, and O_2, in the IL 1-n-butyl-3-methylimidazolium hexafluorophosphate ([bmim][PF_6]) at different pressures. H_2, CO, and N_2 were also investigated but showed solubilities below the detection limit, meaning they have low to no solubility in the IL. It is immediately visible that CO_2 has higher solubility in ILs in comparison to these other gases.[21] This is important, since other studies have demonstrated that $scCO_2$ can be used to extract organic products from the IL phase without any IL contamination of the CO_2 after the extraction[65] and due to the low volatile character of ILs the chances of contamination due to gaseous IL are extremely low to non-existent, regardless of the pressure and temperature of the experiments. Furthermore, since CO has a very low solubility in ILs, it is easily separated from the IL phase after the CO_2 reduction.[21]

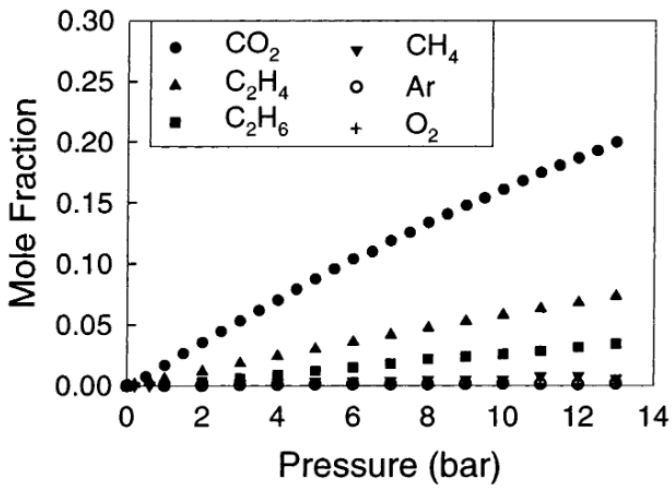

Figure 18: Solubility of different gases in the IL [bmim][PF_6] at 25°C. Graphic taken from[21]

In addition to this, ILs can co-catalyze the reduction of CO_2. The initial reduction barrier lowered when CO_2 is chemically absorbed into the IL phase forming a carboxylate-imidazolium zwitterion,[66] as seen in Figure 19. Importantly, this chemisorption must be strong enough to promote the CO_2 reduction, but not to the extent that it can deactivate the CO_2^- intermediate. The group of Rosen et al. showed that by adding ILs to the reaction system, the required applied potential could be lowered. In their example, an electrocatalytic system, where the IL 1-ethyl-3-methylimidazolium tetrafluoroborate ([emim][BF_4]) was added to the cathode compartment, was evaluated. The voltage was kept constant until a steady performance was achieved, which showed a decrease of the required potential for CO to be detectable, from 2.1 V to 1.5 V, in comparison to the same system without IL addition. This improvement alone is still not significant enough for commercial applications, but it shows that the addition of ILs is beneficial for CO_2 reduction reactions.[1]

Die approbierte gedruckte Originalversion dieser Diplomarbeit ist an der TU Wien Bibliothek verfügbar
The approved original version of this thesis is available in print at TU Wien Bibliothek.
TU Bibliothek Your knowledge hub WIEN

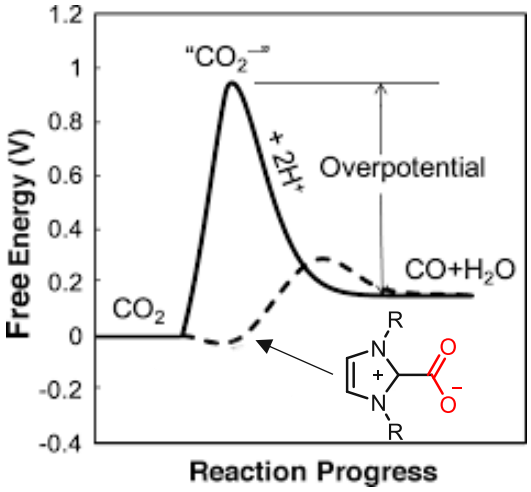

Figure 19: Scheme of the change in free energy of the CO_2 reduction in water (solid line) or IL (dashed line). Graphic adapted from [1]

For continous processes, the catalyst can be immobilized in a heterogeneous system, which facilitates catalyst separation and recycling. Commonly, a heterogeneous catalyst is a solid or supported on a solid, while the reactants are liquids or gases. A special form of a heterogeneous catalytic process is a biphasic system, as seen in Figure 20a, where the catalyst is immobilized in a liquid phase while the product forms a separate liquid phase.[67] Another novel heterogeneous approach is the use of a supported ionic liquid phase (SILP) (see Figure 20b). In this method a thin IL film is physisorbed on the surface of a porous solid support, e.g. silica. Catalytic materials can be bound into the IL phase and by modifying the IL anions and cations the properties can be optimized according to the application. [68] Leaching of the catalyst material is possible in these processes, since the catalyst is not chemically bound to the support material or solvent. Alternatively, the catalytic materials and ILs can be chemically bound into a polymer system to avoid this disadvantage.

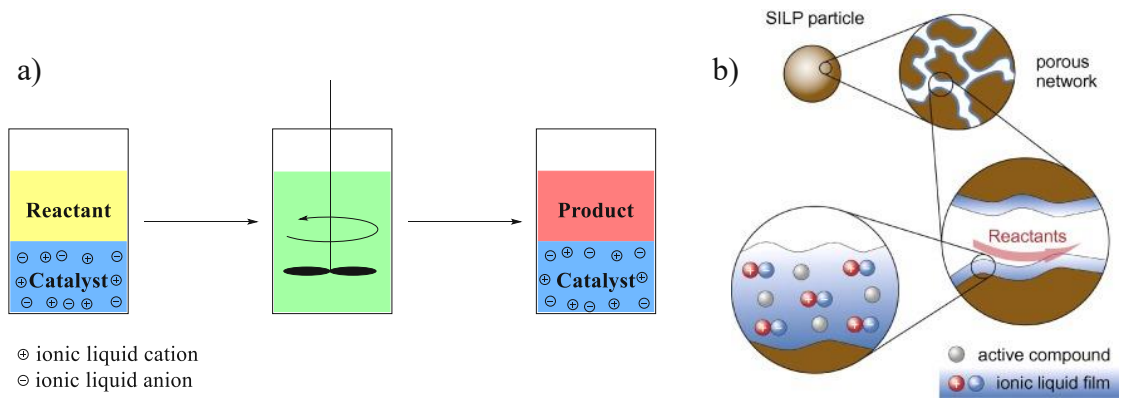

Figure 20: Schematic depictions of two heterogenous catalytic processes assisted by ionic liquids: (a) l-l-biphasic system, (b) SILP technology. Graphic (b) taken from [68]

Die approbierte gedruckte Originalversion dieser Diplomarbeit ist an der TU Wien Bibliothek verfügbar
The approved original version of this thesis is available in print at TU Wien Bibliothek.
TU Bibliothek Your knowledge hub WIEN

2.5. Polymerized photocatalyst system

Polymerized ILs, or polyionic liquids (PIL), have been investigated as solid adsorbents for CO_2. They are synthesized through radical polymerization of vinyl-substituted monomers. Possibly due to their micropores and porous structures, PILs have shown higher CO_2 sorption capacity, when compared to non-polymerized ILs. Therefore, PILs have gained interest for CO_2 separation and purification processes. Studies have shown that the adsorption capacity is dependent on the IL anion. In the example of poly(1-butyl-3-vinylimidazolium) (P[VBIm]) the adsorption capacity was increasing as follows: P[VBIm][Br] < P[VBIm][BF_4] < P[VBIm][SCN].[69]

The catalytic elements attached to the polymer system need to have polymerizable groups to covalently link and create a photocatalytic framework. This is achievable by adding vinyl groups to the ligands of the desired photocatalyst and -sensitizer. Through radical co-polymerization of the catalytic monomers and IL, a stable polymer system can be produced, in which photocatalytic elements are covalently linked to each other and to the IL, which is expected to prevent catalyst leaching. The alternative would be to add the catalytic elements to the polymer through post-modification, but this can lead to incomplete coordination and random metal anchoring, which can decrease the catalyst performance. Earlier studies by He et al., where a Re photocatalyst was directly polymerized with an IL into a Re-based porous organometallic polymer system has already shown that this system has a high CO_2 uptake and can absorb in the visible-light region. CO can be selectively produced with selectivity of up to 95.5% and H_2 evolution is suppressed. This catalytic system, therefore, seems to be a promising candidate for efficient CO_2 reduction.[70] Alternatively, Shimakoshi et al. have developed a polymer system for photocatalytic de-chlorination, in which a B_{12} catalyst and Ru photosensitizer are connected through a PIL backbone. The catalyst and sensitizer were polymerized through styrene moieties that were connected to the ligands *via* amide linkage.[71] This novel concept could be adapted for the photocatalytic reduction of CO_2, by adding a Re catalyst instead of B_{12} to the system.

Die approbierte gedruckte Originalversion dieser Diplomarbeit ist an der TU Wien Bibliothek verfügbar
The approved original version of this thesis is available in print at TU Wien Bibliothek.
TU WIEN Bibliothek Your knowledge hub

3. Aim of the thesis

Photocatalytic reduction of CO_2 is a promising field of research for CO_2 valorization. Visible-light photoreduction offers the opportunity to reduce CO_2 under mild conditions using catalysts that can be modified to yield optimal results. Ionic liquids have shown advantageous properties in combination with CO_2 reduction as solvent and co-catalyst.

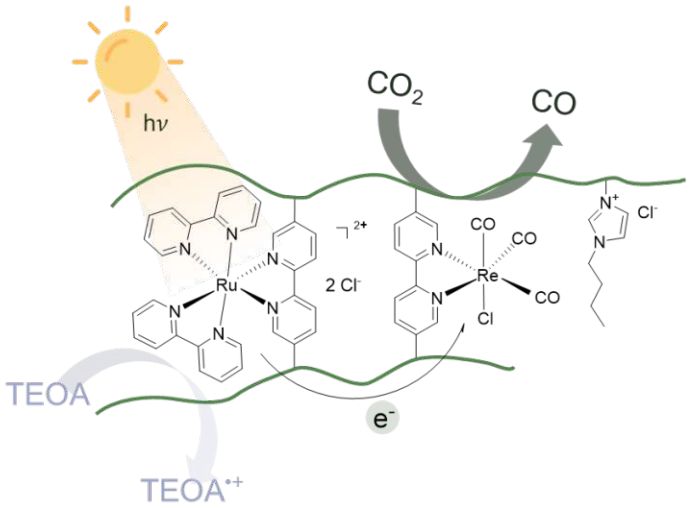

Figure 21: Schematic concept for carbon dioxide valorization via photocatalytic reduction.

In this thesis, the beneficial properties of ILs are combined with an established photochemical system, consisting of a Re photocatalyst and a Ru photosensitizer, into a novel polymeric framework to create an efficient method for selective visible-light CO_2 photoreduction under benign reaction conditions, as is depicted schematically in Figure 21. Furthermore, the polymeric system is analyzed to ensure the correct product formation and photochemical properties.

Die approbierte gedruckte Originalversion dieser Diplomarbeit ist an der TU Wien Bibliothek verfügbar
The approved original version of this thesis is available in print at TU Wien Bibliothek.

4. Results and discussion

4.1. Concept of the polymer synthesis

To synthesize a photocatalytically active polymer, two general transformations are required. As depicted in Figure 22 on the example of a cross-linked polymer, photosensitizer and catalyst need to be modified with a polymerizable group, such as a vinyl or styrene group. Both groups yield chemically and thermally stable polymers. The photocatalytically active polymers are thus obtained *via* free radical co-polymerization, which is based on the addition of monomers to a growing polymer chain, of the vinyl-substituted catalyst and sensitizer complexes and the IL 1-butyl-3-vinylimidazolium chloride.

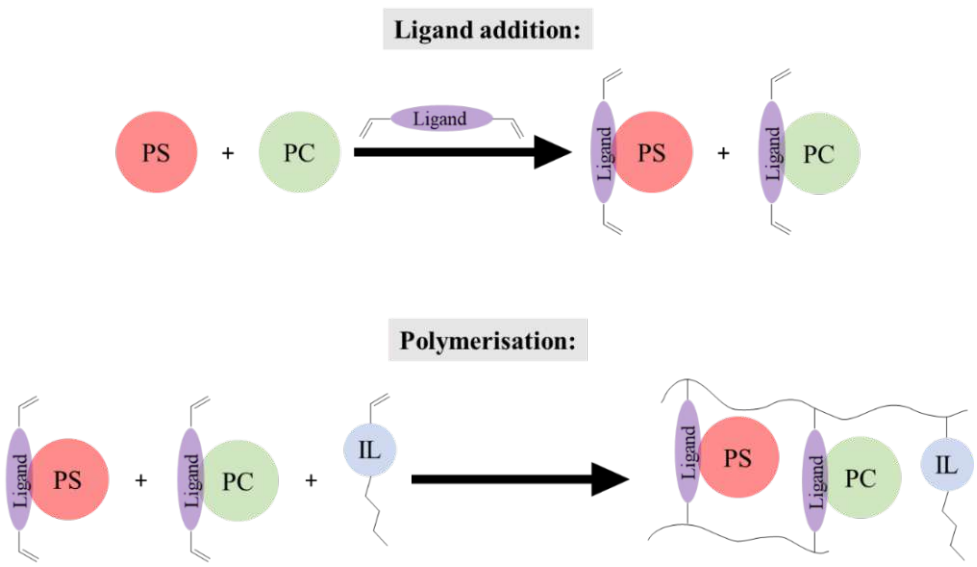

Figure 22: Schematic concept of the synthesis of a photocatalytically active cross-linked polymer, PS: photosensitizer, PC: photocatalyst, IL: ionic liquid.

For cross-linked polymers (CLP), the ligands were disubstituted with two vinyl groups, while for the side-chain polymers (SCP), the ligands were monosubstituted with a polymerizable side chain, which consists of a styrene moiety that was connected to the ligand *via* amide linkage. The monomers are depicted in Figure 23. For the remainder of this thesis the monomers will be called CLP-PC and CLP-PS, respectively, for the catalyst and photosensitizer monomers of the CLP and, analogously, SCP-PC and SCP-PS for the catalyst and photosensitizer monomers of the SCP.

Die approbierte gedruckte Originalversion dieser Diplomarbeit ist an der TU Wien Bibliothek verfügbar
The approved original version of this thesis is available in print at TU Wien Bibliothek.
TU Bibliothek Your knowledge hub WIEN

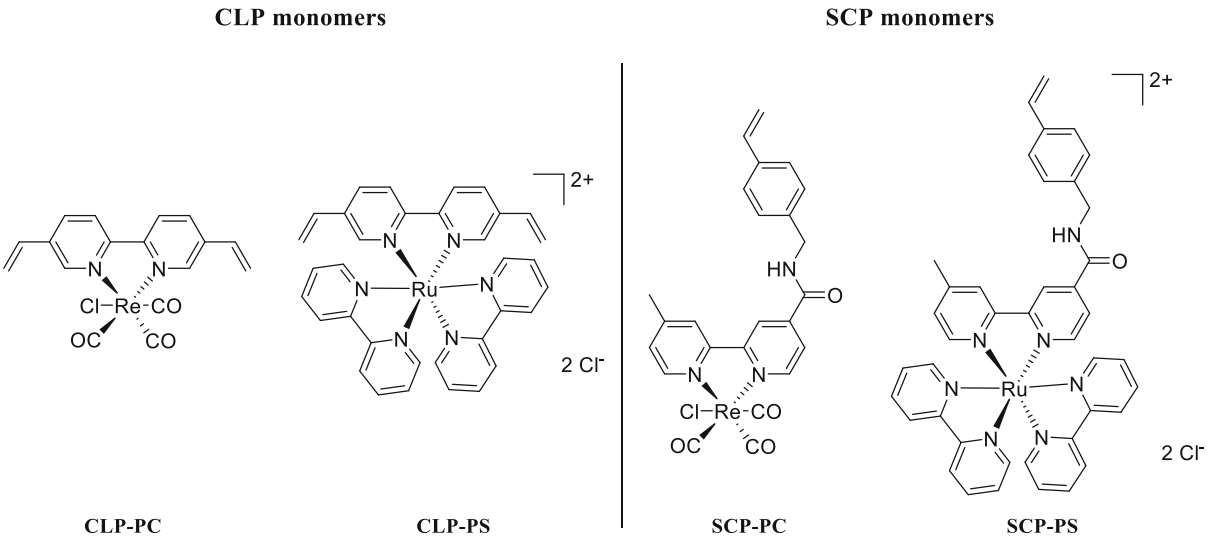

Figure 23: Structures of the polymerizable photocatalytic monomers: CLP-PC, CLP-PS, SCP-PC, and SCP-PS.

The polymer backbone is represented by wavy lines in all polymer depictions throughout this thesis, as the polymers are irregularly substituted; thus, no accurate chemical structure can be provided (see Figure 24).

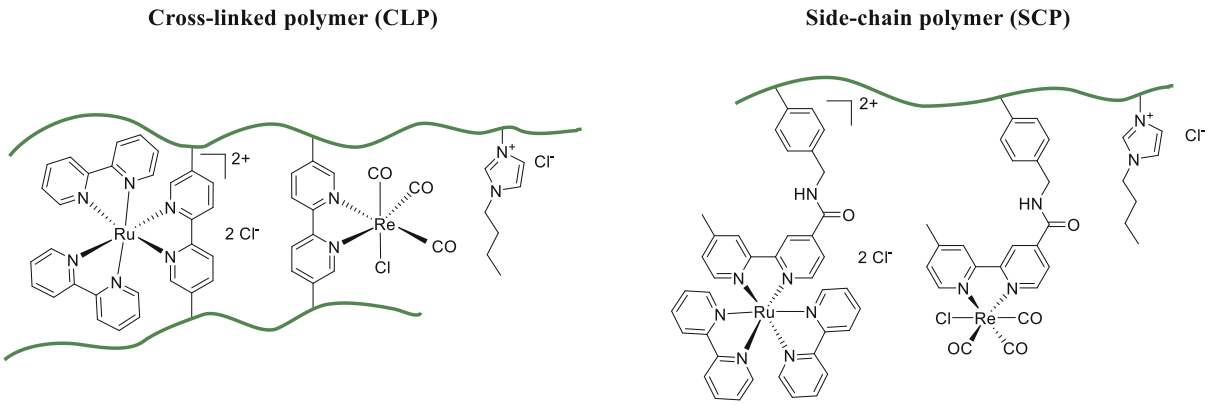

Figure 24: Schematic structures of the CLP, and SCP.

Die approbierte gedruckte Originalversion dieser Diplomarbeit ist an der TU Wien Bibliothek verfügbar
The approved original version of this thesis is available in print at TU Wien Bibliothek.

4.2. Synthesis of polymerizable monomers

4.2.1. Ionic liquid synthesis

Ionic liquids have shown beneficial properties in the field of CO_2 reduction, as was already discussed in chapter 2.4. Since there are almost unlimited possible IL ion combinations with different properties each, the cations and anions can be matched to the specific application. The role of the cation is more complex, as CO_2 interaction strongly depends on the chemical structure. Imidazolium based ILs were chosen for this thesis, since prior studies have already shown that this type of IL is capable of capturing high concentrations of CO_2. Cations and anions form a network in which CO_2 fills the interstices and associates fitting to the often spherical anion. Importantly, imidazolium based ILs can also act as co-catalysts for CO_2 reductions, since they can form stable activating intermediates by CO_2 coordinating to the IL. This is caused by the C2 position of the imidazolium ring featuring an acidic proton that, after deprotonation, can trap CO_2 in a *N*-heterocyclic carbene (NHC)-CO_2 adduct. The substituents of the imidazolium base have an influence on the reduction as well. Longer alkyl chains have exhibited a positive impact on the absorption of CO_2. They offer more free volume for the gas to occupy.[72,73] However, an increase in the alkyl chain length also leads to higher viscosity and steric hindrance. This inhibits the catalytic kinetics and decreases the activity for CO reduction.[74] Therefore, a butyl substituent was chosen for the imidazole ring. To be able to covalently link the IL into the final polymer framework, a vinyl substituent is needed on the imidazole ring as well. Maginn et al. have determined that the anion also plays a major role in regard to the solubility of CO_2 in imidazolium based ILs.[75] Thus, the CO_2 solubility varies depending on the anion, with methide and [NTf_2] anions showing high solubilities in general. This impact of the anion can be based on acid/base interactions, interactions with fluorous alkyl chains, and the polarizability, i.e., the solubility parameter, of the ILs. In general, the chloride anion does not have a remarkably high CO_2 capture capability, but it was chosen for the IL anion of this thesis since chloride is also a ligand of the photocatalyst, and therefore, the number of different elements present in the system could be minimized.[76]

Hence, the IL used in this thesis is 1-butyl-3-vinylimidazolium chloride. It was obtained through quaternization of 1-vinylimidazole with 1-chlorobutane at 70 °C for 48 h under solvent-free conditions under argon. To avoid polymerization through thermal initiation or discoloration of the product, the polymer had to be synthesized at low temperatures for a prolonged amount of time. The crude was washed with ethyl acetate to remove any remaining 1-chlorobutane. After drying the solid *in vacuo,* the desired IL was obtained with a high yield of 75% (see Figure 25).

Die approbierte gedruckte Originalversion dieser Diplomarbeit ist an der TU Wien Bibliothek verfügbar
The approved original version of this thesis is available in print at TU Wien Bibliothek.
TU Bibliothek Your knowledge hub WIEN

The IL needs to be stored under dry and inert conditions, since, on the one hand, the IL is very hygroscopic and, on the other hand, if not stored carefully, the vinyl group could be deactivated through auto-polymerization. Therefore, the IL was kept in a desiccator under vacuum after the synthesis. [77]

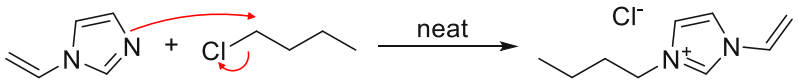

Figure 25: Mechanism for the synthesis of 1-butyl-3-vinylimidazolium chloride.

4.2.2. Ligand synthesis

The vinyl substituents were added to the bipyridine (bpy) ligand of the CLP-PC and CLP-PS *via* a palladium catalyzed *Suzuki-Miyauru coupling* mechanism, as is depicted in Figure 26. Palladium(II) acetate and triphenylphosphine form the catalyst bis-(triphenylphosphine)-palladium(II)-diacetate, to which 5,5′-dibromo-2,2′-bipyridine can be added in an oxidative addition step (OA). Through transmetalation (TM), using dicaesium carbonate as a base, the vinyl group of potassium vinyltrifluoroborate is added to the catalyst and, finally, the product can be separated in a reductive elimination step (RE) to obtain the CLP ligand 5,5’-divinyl-2,2’-bipyridine (5,5’-dvbpy) in a high yield of 70%. This coupling mechanism has the advantage that only mild reaction conditions are required and the organoboron reagent is stable and not harmful to the environment. Furthermore, organotrifluoroborate salts specifically are stable at high temperature as well as towards air and moisture. Due to their insolubility in many apolar solvents, remaining starting material can be easily separated. Additionally, the B-F bonds are very strong making the cleavage of the vinyl group favorable. [78]

Die approbierte gedruckte Originalversion dieser Diplomarbeit ist an der TU Wien Bibliothek verfügbar
The approved original version of this thesis is available in print at TU Wien Bibliothek.
TU Bibliothek Your knowledge hub WIEN

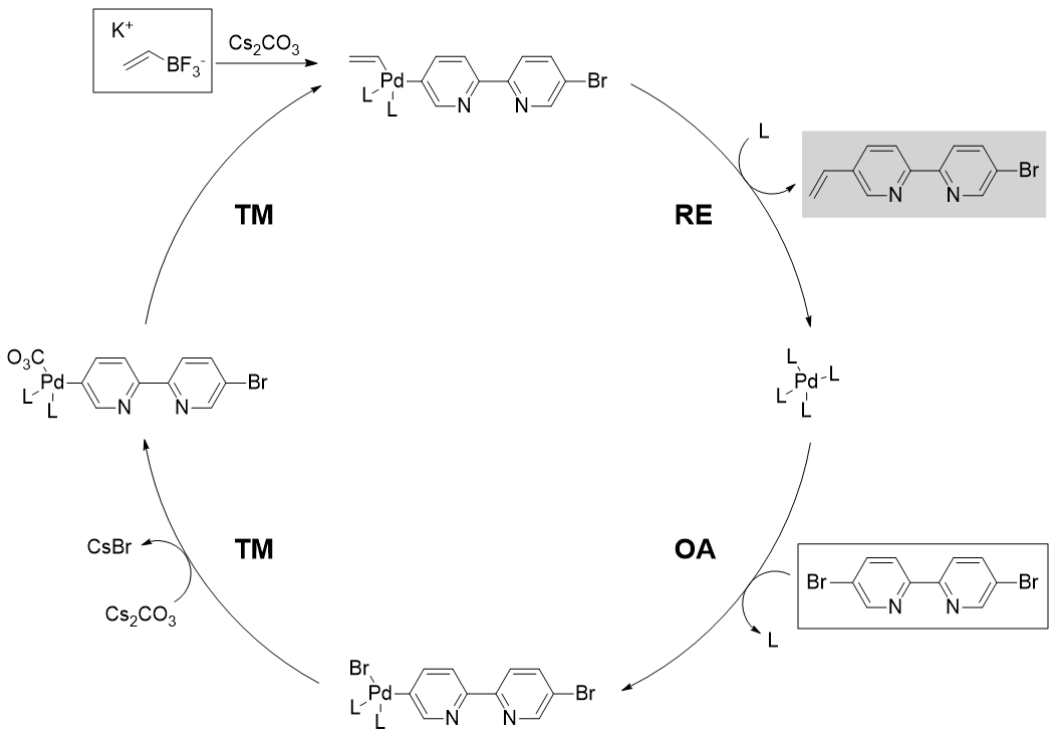

Figure 26: Mechanism for the synthesis of 5,5'-divinyl-2,2'-bipyridine, RE: reductive elimination, OA: oxidative addition, TM: transmetalation.

The vinyl group was incorporated into the ligand of the SCP-PC and SCP-PS in the form of a side chain that was added to the carboxylic acid derivative of bpy. First, the 4-(aminomethyl)styrene was synthesized via the *Gabriel synthesis* from 4-vinylbenzyl chloride. This method selectively produces primary amines and avoids the notorious over-alkylation. As depicted in Figure 27, phthalimide is added to 4-vinylbenzyl chloride *via* an S_N2 reaction [Figure 27 (1)]. This produces *N*-(4-vinylbenzyl)phthalimide. Only one alkyl group can be added to the *N*-atom of the phthalimide, hence, over-alkylation is not possible.[79] Through hydrazinolysis of *N*-(4-vinylbenzyl)phthalimide [Figure 27 (2)] according to the *Ing-Manske procedure* 4-(aminomethyl)styrene was obtained.[51]

Die approbierte gedruckte Originalversion dieser Diplomarbeit ist an der TU Wien Bibliothek verfügbar
The approved original version of this thesis is available in print at TU Wien Bibliothek.

(1) Formation of *N*-(4-vinylbenzyl)phthalimide:

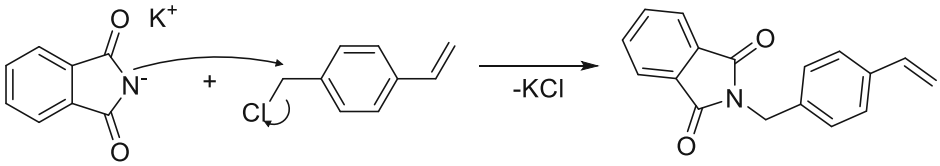

(2) Hydrazinolysis of N (4-vinylbenzyl)phthalimide:

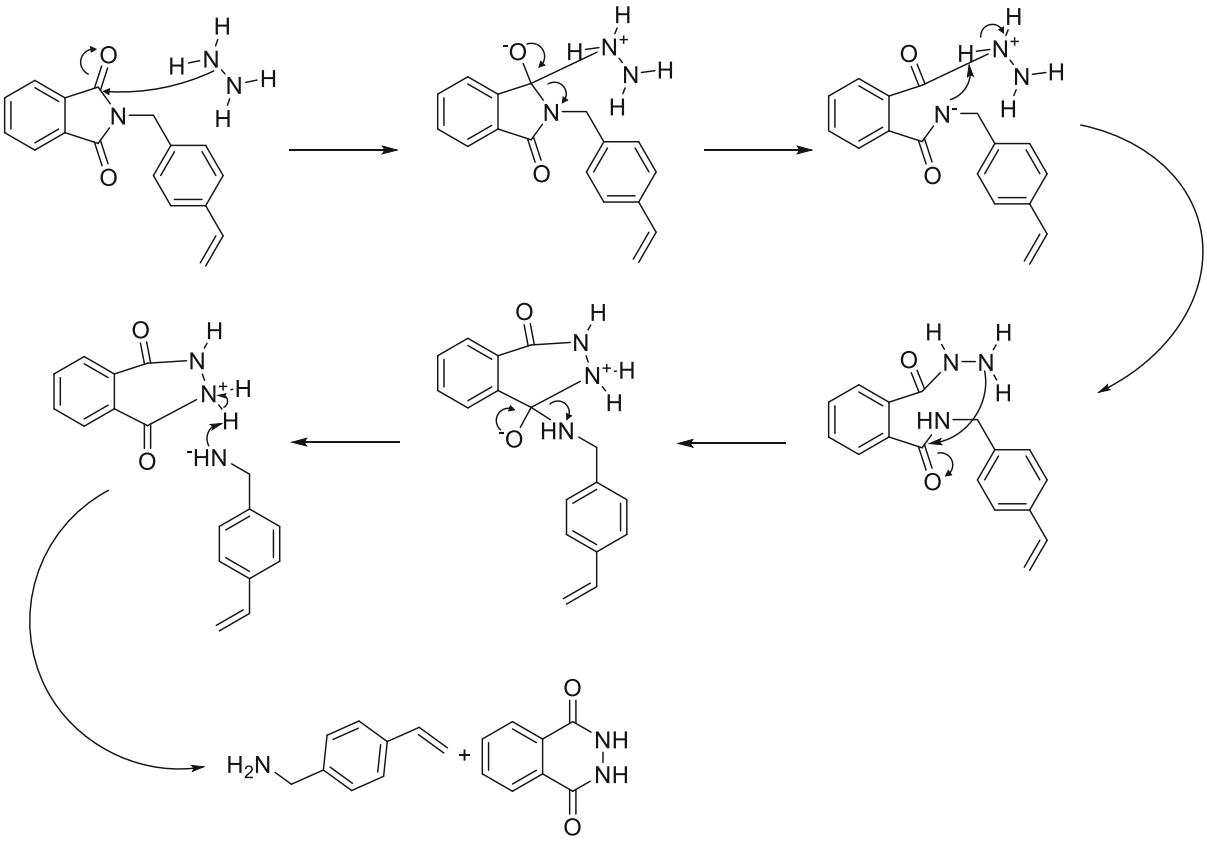

Figure 27: Mechanism of the Gabriel synthesis

Then, 4-(aminomethyl)styrene was added to 4'-methyl-2,2'-bipyridine-4-carboxylic acid through an amidation reaction with 1-ethyl-3-(3-dimethylaminopropyl)carbodiimide (EDC) and 4-dimethylaminopyridine (DMAP) as the coupling agents, as is depicted in Figure 28. 4'-Methyl-*N*-(4-vinylbenzyl)-[2,2'-bipyridine]-4-carboxamide was obtained as the SCP ligand in a yield of 35%. In an attempt to increase the yield, hydroxybenzotriazole, commonly used as additive for coupling reactions with EDC to activate the carbonic acid by forming an active ester,[80] was added to another reaction mixture. The other variables were not changed. The yield slightly decreased to 31% while doing so. Since both the carboxylic acid and the amine are bulky molecules, the incomplete reaction could be explained by steric hindrance. Moreover, the reaction mixture needs to be cooled for four hours at the beginning, which indicates that this amidation with these additives is exothermic, which could lead to thermal decomposition of starting material.[80]

Die approbierte gedruckte Originalversion dieser Diplomarbeit ist an der TU Wien Bibliothek verfügbar
The approved original version of this thesis is available in print at TU Wien Bibliothek.
TU Bibliothek Your knowledge hub WIEN

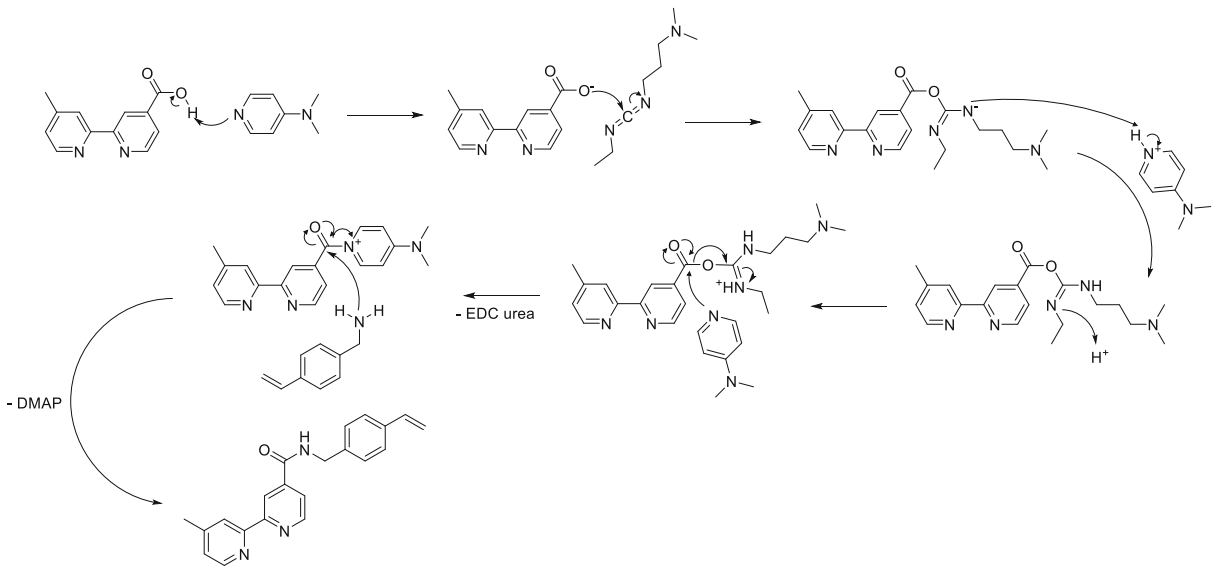

Figure 28: Mechanism for the amidation of 4-(aminomethyl)styrene and 4'-methyl-2,2'-bipyridine-4-carboxylic acid.

4.2.3. Catalytic monomers

The CLP-PC and SCP-PC were synthesized by exchanging two CO ligands of pentacarbonylchlororhenium(I) with the previously prepared vinyl-substituted bpy ligands, as shown in Figure 29 on the example of SCP-PC. The oxidation state of the Re center is maintained during this substitution. No special work-up was required. The finished products were filtered off and washed with toluene. CLP-PC was obtained as a yellow powder with a yield of 80%, while SCP-PC was obtained as an orange powder with a yield of 26%. An excess amount of starting material was not used for the synthesis since the they are relatively expensive. Therefore, using an excess amount of them was not desirable.

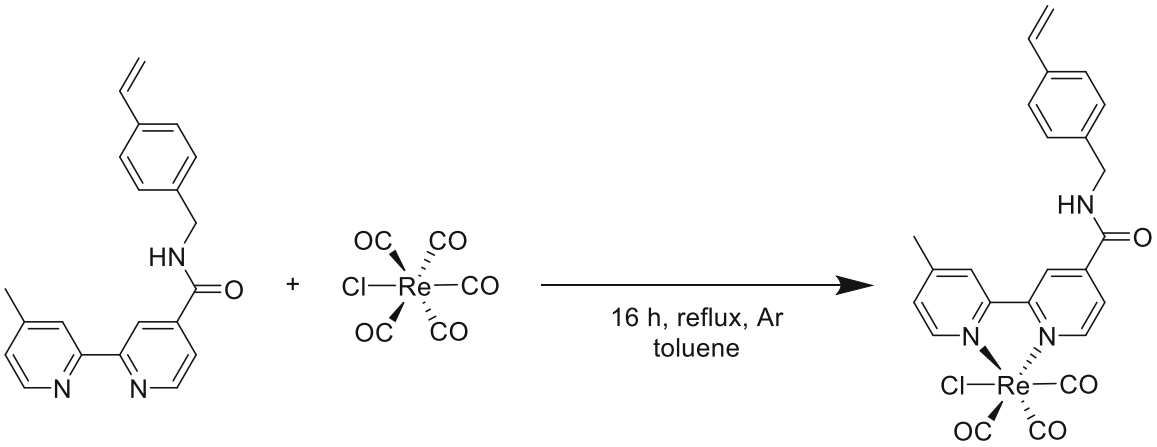

Figure 29: Ligand exchange of pentacarbonylchlororhenium(I) on the example of SCP-PC.

Die approbierte gedruckte Originalversion dieser Diplomarbeit ist an der TU Wien Bibliothek verfügbar
The approved original version of this thesis is available in print at TU Wien Bibliothek.

The CLP-PS and SCP-PS were synthesized by exchanging the two chloride ligands of *cis*-bis(2,2′-bipyridine)dichlororuthenium(II) with the previously prepared vinyl-substituted bpy ligands, as shown in Figure 30 on the example of SCP-PS. The oxidation state of the Ru center is not changed during this substitution. Therefore, two chloride anions compensate the positive charge of the complex. The work-up of these complexes consisted of several solvation and precipitation steps, to remove any excess starting materials and, since the last solvent used was water, the final products were dried over anhydrous phosphorus pentoxide for a prolonged amount of time to ensure that they were completely dry. Both photosensitizer monomers were obtained as dark violet solids with very high yields of 98% for CLP-PS and 95% for SCP-PS.

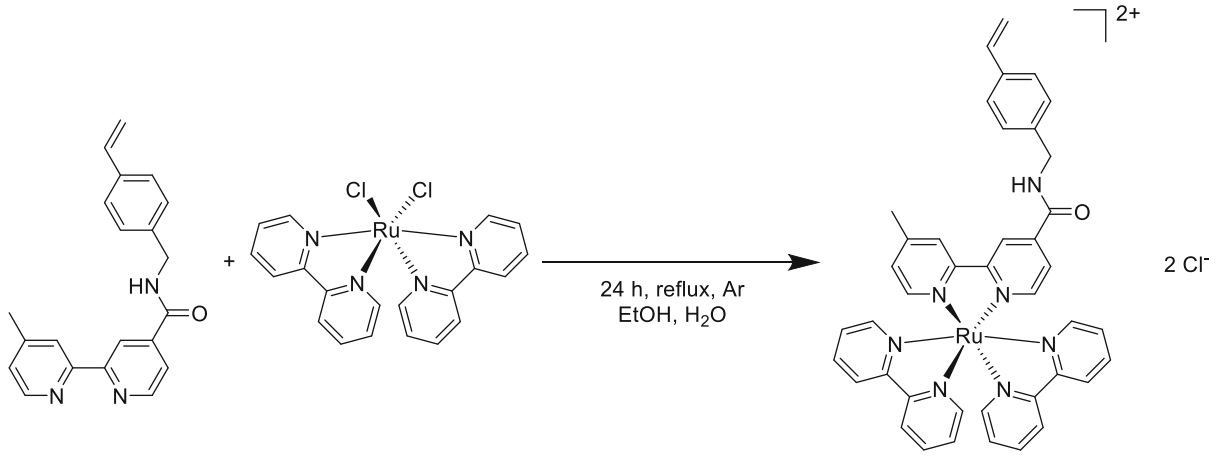

Figure 30: Ligand exchange of cis-bis(2,2'-bipyridine)dichlororuthenium(II) on the example of SCP-PS.

Die approbierte gedruckte Originalversion dieser Diplomarbeit ist an der TU Wien Bibliothek verfügbar
The approved original version of this thesis is available in print at TU Wien Bibliothek.

4.3. Polymerization of monomers

After completion of the polymerizable monomer set, the appropriate polymerization technique was investigated. The mechanism of free-radical polymerization is shown in Figure 31. It requires as radical initiator to start. Azobisisobutyronitrile (AIBN) is a commonly used as such, since it can thermally disassociate at low temperatures, does not form oxygenated by-products, and does not induce any change in color. The disassociated initiator starts the polymerization through the addition of a polymerizable monomer to the radical. The monomers need to be chosen according to the application as well as polymerization process. Some monomers are too stable due to resonance stabilization of the radicals and are, therefore, inhibited from further reaction since the resonance stabilization is lost after polymerization. This can happen, for example, to propylene and isobutylene. In this thesis vinyl and styrene were used as polymerizable groups. They are very reactive and form chemically stable polymers. For the synthesis of polystyrene thermal initiation is even enough; AIBN is not required. Furthermore, the required ligands could be added easily since vinyl and styrene are modifiable.[81]

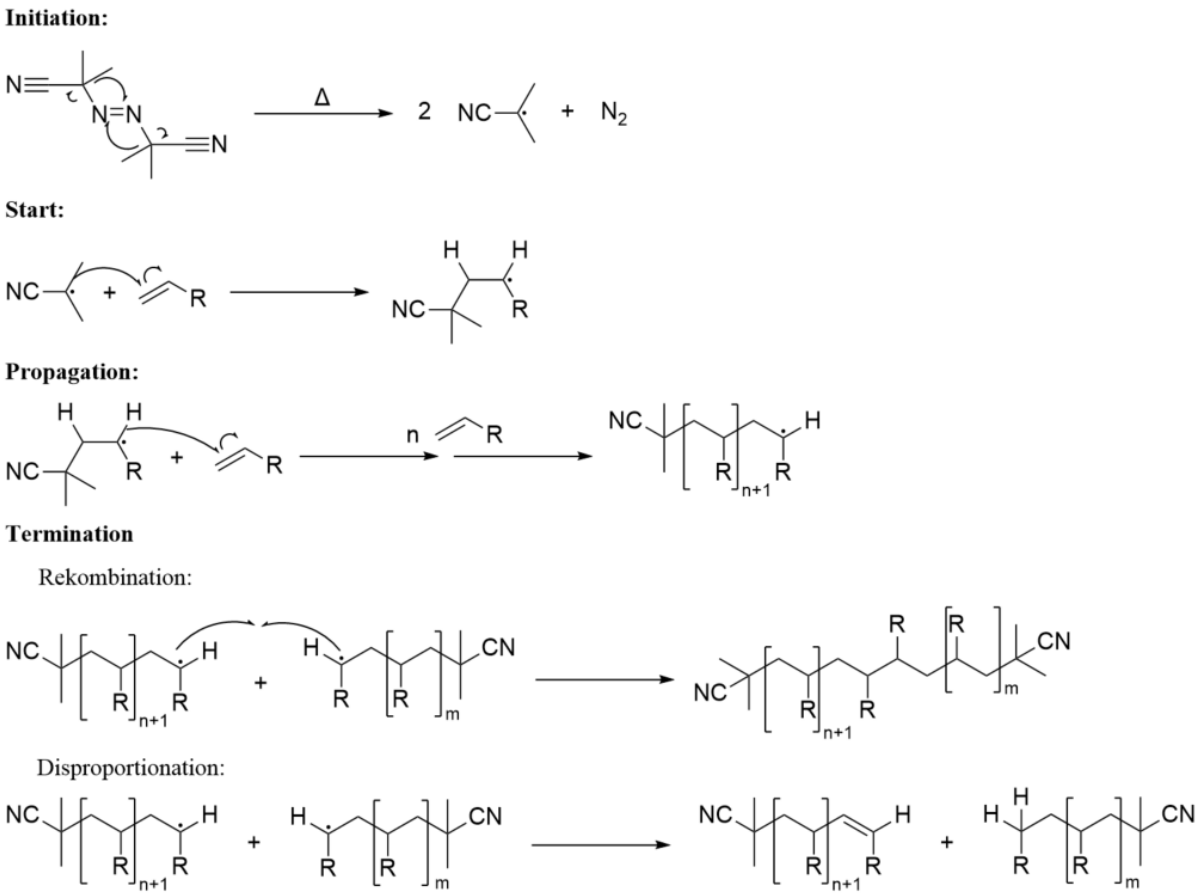

Figure 31: Mechanism of a radical polymerization

Die approbierte gedruckte Originalversion dieser Diplomarbeit ist an der TU Wien Bibliothek verfügbar
The approved original version of this thesis is available in print at TU Wien Bibliothek.

Initially, the polymerization was performed under moderate pressure in a microwave vial. To avoid undesired inhibition, e.g., through oxygen from the air, the polymerization had to be carried out under an inert atmosphere. Reaction of just the IL with AIBN using *N,N*-Dimethylformamide (DMF) as solvent yielded the polymerized IL. After precipitation in acetone, the brown solid could be filtered off easily and a yield of 87% was achieved.

Preliminary ^{1}H NMR analysis of the PIL (see Figure 33) proved that polymerization was successful with this method and could be expanded to the polymerizations of the photocatalytic materials. The vinyl substituted monomers were combined in different ratios and polymerized analogous to the PIL. First, the CLP was synthesized, and high yields (see Table 6 and Table 7) were achieved by combining one photocatalytically active complex, either the Re photocatalyst (PC) or the Ru photosensitizer (PS), with IL. Since the PC and PS are very precious, this was done to investigate, whether the polymerization method for the PIL could be adapted for the photocatalytic polymers without risking too much of the PC and PS. This was repeated for the SCP in combination with only SCP-PS. With these polymers showing satisfactory results, in respect to their yields and analysis, a polymer framework containing all photocatalytic elements and IL was synthesized with different monomer ratios. As mentioned in chapter 2.3.3, by using Ru as a PS photoreductions induced by visible light are possible. For optimal results, an excess of PS is used. Furthermore, since the IL acts as back-bone for immobilization, as well as co-catalyst, an even larger excess is needed, to evenly distribute the PC and PS in the polymer framework and provide as many catalytic sites as possible. Therefore, the final ratios, as seen in Table 6 and Table 7, were chosen. This offered a variety of polymers for future photo-experiments.

Die approbierte gedruckte Originalversion dieser Diplomarbeit ist an der TU Wien Bibliothek verfügbar
The approved original version of this thesis is available in print at TU Wien Bibliothek.
TU Bibliothek Your knowledge hub WIEN

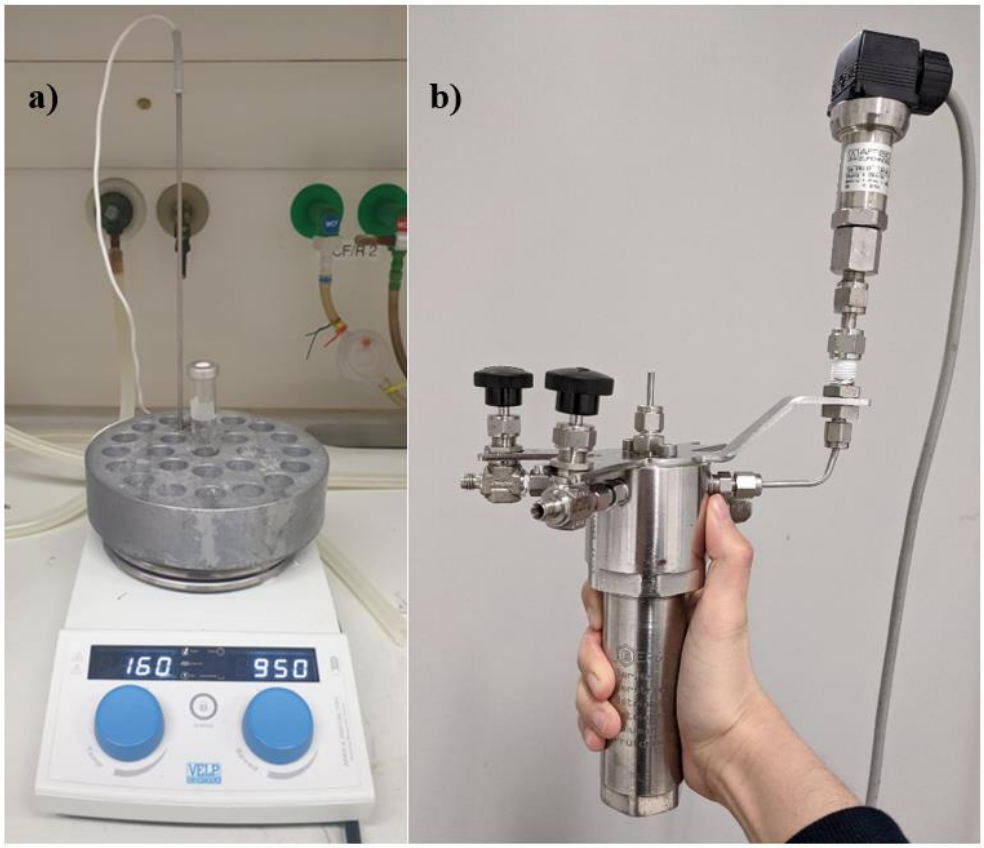

Figure 32: Polymerization reaction vessel, a: non-autoclave reaction, b: autoclave reaction.

Since, at first, the polymerization was carried out in a closed microwave vial, as seen in Figure 32a, a small amount of pressure was also applied to the reaction, which seemed to have a favorable effect. As described in [Eq. (9)], an increase in pressure enhances the reaction rate (k), but only if the activation volume ($\Delta V^{\ddagger}$) is negative. This applies to reactions, where the number of molecules decrease after product formation, which is the case for polymerization reactions.[51]

$$\frac{\delta \, lnk}{\delta p} = \frac{\Delta V^{\ddagger}}{RT} \tag{9}$$

As a result of this observation, the polymerizations of the complete photocatalytic frameworks were carried out in the autoclave at 50 bar and 100 °C (see Figure 32b). This has the advantage of working in a controlled inert environment with the addition of typical high pressure chemistry benefits, such as a faster reaction time. The polymeric materials, seen in Figure 24, were obtained as brown solids with high yields, as can be seen in Table 6 and Table 7.

Die approbierte gedruckte Originalversion dieser Diplomarbeit ist an der TU Wien Bibliothek verfügbar
The approved original version of this thesis is available in print at TU Wien Bibliothek.
TU WIEN Bibliothek Your knowledge hub

Table 6: Yields of the CLPs, Re: Re photocatalyst, Ru: Ru photosensitizer.

Ratio Re	Ru	IL	Inert gas atmosphere	Solvent	t (h)	T (°C)	*P* (bar)	Yield (%)
1	0	1	Ar	DMF	24	160	1.013	quant.
1	0	90	N_2	DMF	24	100	50.0	82
0	1	1	N_2	DMF	24	100	50.0	57
0	1	9	Ar	DMF	24	160	1.013	51
1	10	50	N_2	DMF	24	100	50.0	91
1	10	90	N_2	DMF	24	100	50.0	85
1	10	120	N_2	DMF	24	100	50.0	85

Table 7: Yields of the SCPs, Re: Re photocatalyst, Ru: Ru photosensitizer.

Ratio Re	Ru	IL	Inert gas atmosphere	Solvent	t (h)	T (°C)	*P* (bar)	Yield (%)
0	1	9	Ar	DMF	24	160	1.013	64
1	10	50	N_2	DMF	24	100	50.0	84
1	10	90	N_2	DMF	24	100	50.0	76
1	10	120	N_2	DMF	24	100	50.0	75

Die approbierte gedruckte Originalversion dieser Diplomarbeit ist an der TU Wien Bibliothek verfügbar
The approved original version of this thesis is available in print at TU Wien Bibliothek.
TU WIEN Bibliothek Your knowledge hub

4.4. Analysis

The PIL was still partly soluble in chloroform to an extent that made ^{1}H NMR analysis possible. As can be seen in Figure 33, the obtained signals were broad peaks, which indicated that the polymerization was accomplished. Polymers have broad signals in conventional ^{1}H NMR spectra due to their poor molecular rotation and each repeat unit being surrounded by a slightly different configuration of repeat units, which leads to very small chemical shifts for each unit. The polymers, including photocatalytic components, not just IL, were not soluble enough in any conventional solvents, i.e., acetone, chloroform, dimethyl sulfoxide, or methanol, to record their ^{1}H NMR spectra. Therefore, they were analysed *via* fourier transform infrared (FT-IR) spectroscopy, ultraviolet–visible (UV-Vis) spectroscopy, thermogravimetric analysis (TGA), and total-reflection X-ray fluorescence spectroscopy (T-XRF).

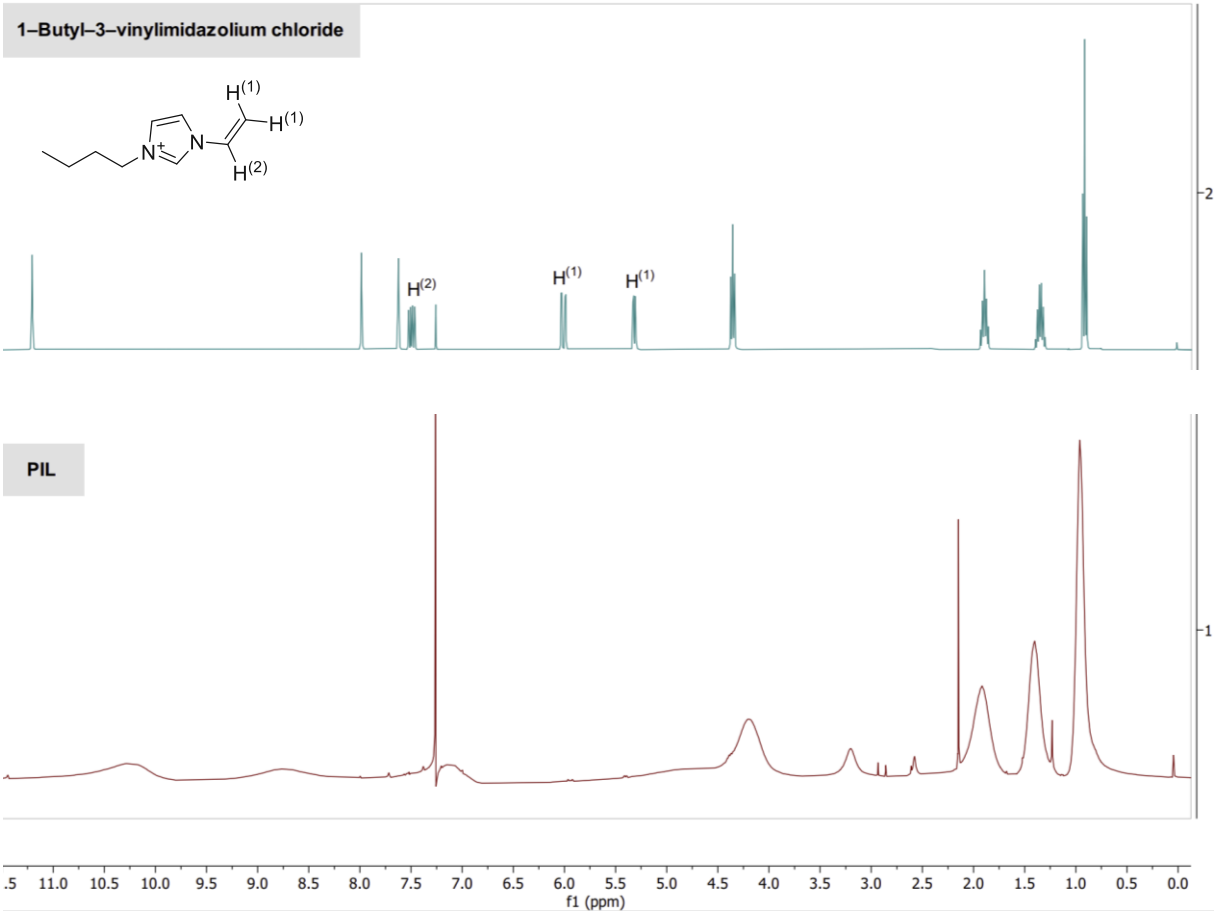

Figure 33: ^{1}H NMR of 1-butyl-3-vinylimidazolium chloride and PIL.

FT-IR spectroscopy provides an infrared spectrum of a component, be it liquid, gaseous or solid, by measuring the absorbed IR radiation over a broad spectrum. Since it can be applied on solid materials, the solvation of the polymers is not necessary. The atomic vibrations of specific functional groups or substances, induced by the absorbed radiation, correspond to different

Die approbierte gedruckte Originalversion dieser Diplomarbeit ist an der TU Wien Bibliothek verfügbar
The approved original version of this thesis is available in print at TU Wien Bibliothek.
TU Bibliothek Your knowledge hub WIEN

signals at different wavenumbers in the spectrum. By evaluating the IR spectra, identification, whether the specific components were bound into the polymer framework, was possible.

Figure 34 depicts the FT-IR spectra of the IL, the PIL, the CLP-PC, a CLP with a 1:1 ratio of photocatalyst to IL, and a CLP with a Re:Ru:IL ratio of 1:10:90. Signals between 2025 and 1870 cm^{-1} correspond to the stretching vibrations of CO ligands of Re. They are clearly visible in the spectra of the Re monomer and the polymers. The vibration of the imidazole ring of the IL occurs at 1465 cm^{-1}, while the CH-vibrations of the imidazole ring correspond to the signal peaks at 1542 and 1567 cm^{-1}. Therefore, it can be safely concluded that the photocatalyst and IL are properly built into the polymer frameworks.

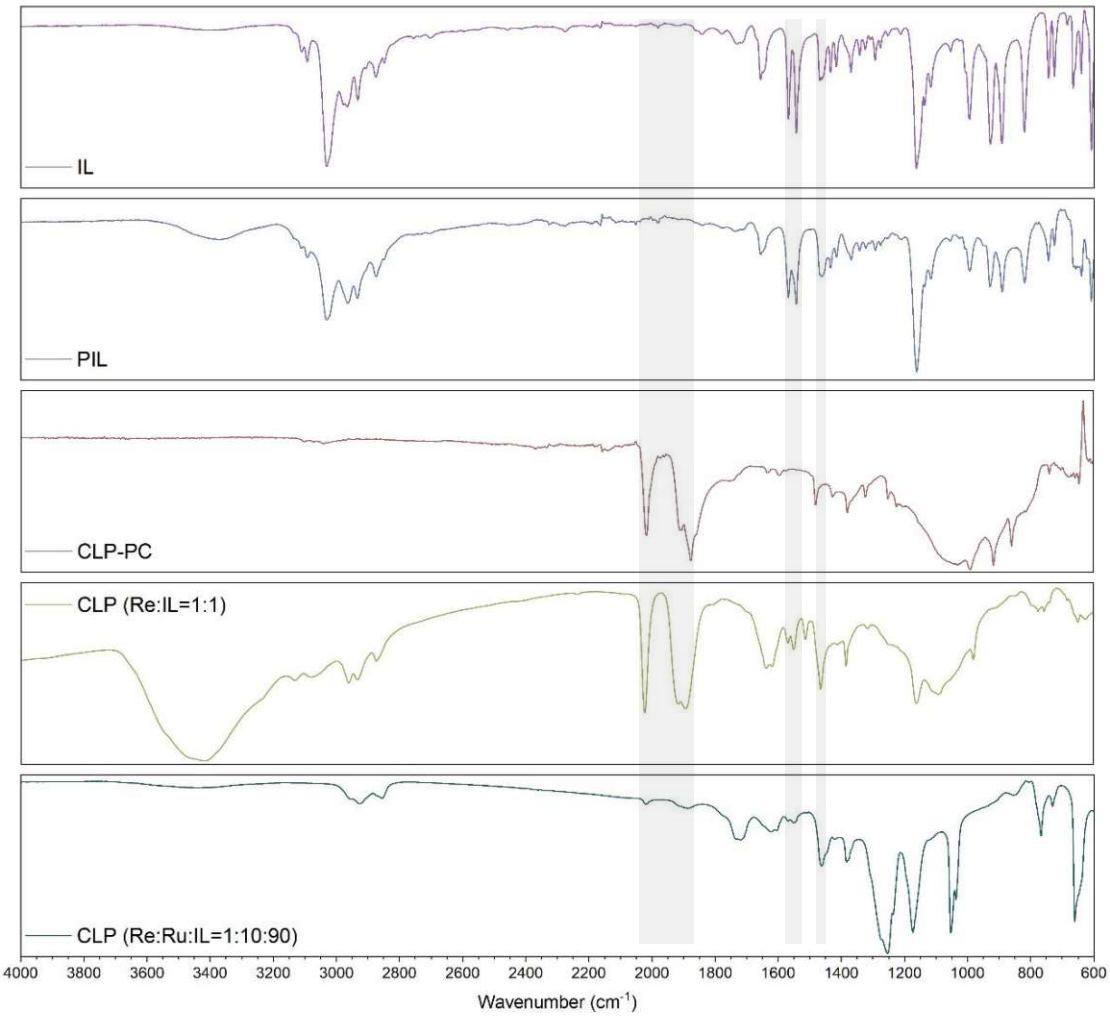

Figure 34: FT-IR spectra of the IL, PIL, CLP-PC, and two CLPs.

Die approbierte gedruckte Originalversion dieser Diplomarbeit ist an der TU Wien Bibliothek verfügbar
The approved original version of this thesis is available in print at TU Wien Bibliothek.
TU Bibliothek Your knowledge hub WIEN

Analogous results were obtained for the spectra of the other polymers, meaning the polymerization was successful and it was possible to construct the desired photocatalytic polymer framework.

UV-Vis spectroscopy measures the extinction of light by a sample. The absorbance from the sample can be measured at different wavelengths to provide spectral information. By absorbing photons of a specific energy, electrons can be excited to enter a higher energy state, as is needed for the photocatalytic experiments. This means that with the information gathered *via* UV-Vis spectroscopy, the spectral properties of the polymers in general and whether polymerization had any effect on them could be determined.

Figure 36 shows the UV-Vis spectra of reference materials and the complete polymers in a 1:10:90 ratio of PC:PS:IL. The spectra of $[Ru(bpy)_3][PF_6]_2$ and $Re(bpy)(CO)_3Cl$ were measured as reference for the monomolecular functional units and compared to the spectra of the CLP and SCP. Prior to measurement, they were dissolved in acetonitrile with a concentration of 0.25 mg/mL for the polymers and 0.03 mg/mL for the reference materials. The polymers were left in an ultra-sound bath in closed vials for at least four hours to ensure that as much of the polymers as possible was dissolved. There was always insoluble material remaining, but an adequate amount migrated to the solution phase to allow the measurement of the spectra.

Comparing the CLP to the SCP shows that they have very similar absorption spectra, indicating that the substitution pattern at the bpy unit has a low impact on the spectra. The polymers vary in their absorbance, which was expected, since there was probably a difference in the concentration of the measured samples, as the dissolved amount varied for each polymer. The absorbance at around 275 nm can be attributed to a ligand-centered transition, but more important for the purposes of this thesis is the broad signal at around 400 to 500 nm. The double peak corresponds to the MLCT transition of the Ru photosensitizer depicted in Figure 35. An MLCT promotes an electron from a metal- to ligand-based orbital. The enhanced redox activity of the exited state in comparison to the ground state is based on this spatial redistribution of electron density, leading to more efficient photocatalytic properties.[82]

Die approbierte gedruckte Originalversion dieser Diplomarbeit ist an der TU Wien Bibliothek verfügbar
The approved original version of this thesis is available in print at TU Wien Bibliothek.
TU WIEN Bibliothek Your knowledge hub

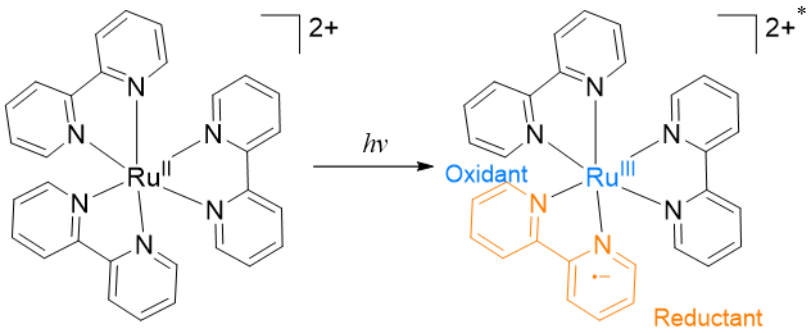

Figure 35: Schematic depiction of a metal-to-ligand charge transfer state in $[Ru(bpy)_3]^{2+}$. Graphic redrawn from[82]

The MLCT peak in Figure 36 is visible for the polymers and the Ru reference, but not for the Re reference. This proves that the PS is built into the polymer framework with a small red-shift of around 5 nm compared to $[Ru(bpy)_3][PF_6]_2$. The red shift is probably caused by the substituent effects of the electron donating methyl and aminomethyl groups of the modified ligands.[83] This information is important, because this means that the photocatalytic reduction of CO_2 should be possible with the generated polymer framework at the desired wavelength of > 445 nm. At around 360 nm the Re reference has a signal that can also be attributed to a MLCT of the Re complex.[84] This signal, however, is outside of the visible-light region and, therefore, not relevant for the project goal.

Die approbierte gedruckte Originalversion dieser Diplomarbeit ist an der TU Wien Bibliothek verfügbar
The approved original version of this thesis is available in print at TU Wien Bibliothek.

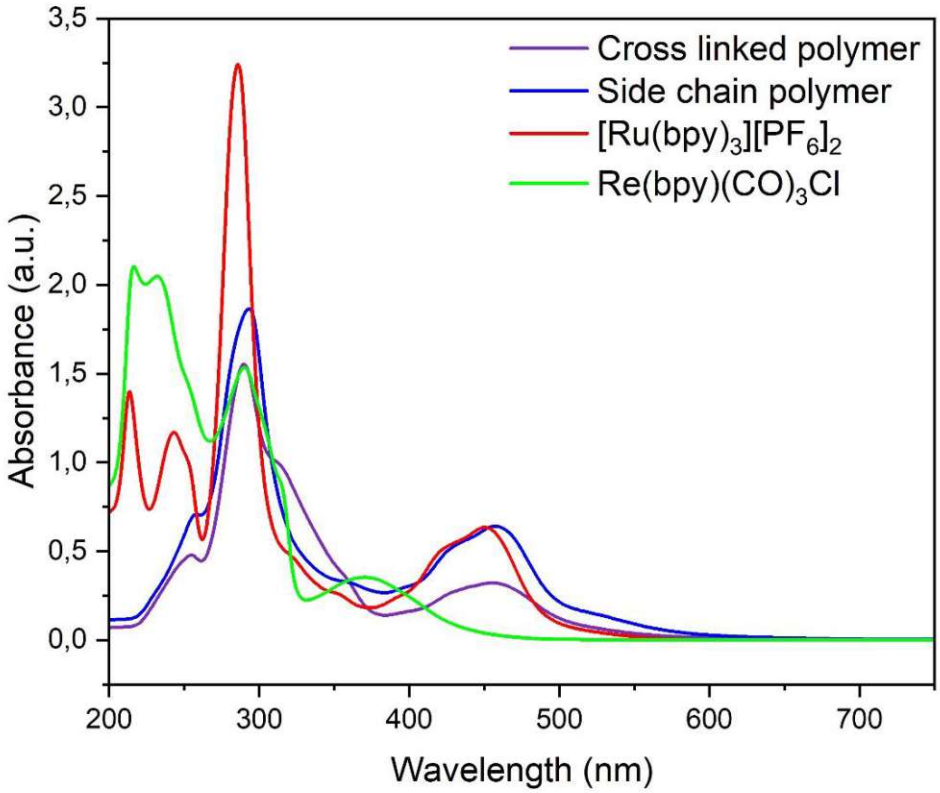

Figure 36: UV-Vis spectra of a CLP, SCP, $[Ru(bpy)_3][PF_6]_2$, and $Re(bpy)(CO)_3Cl$.

Figure 37 depicts the SCPs in different ratios. The spectra of the individual polymers look similar. They differ in their absorbance, which can be ascribed to the difference in solubility. Imidazolium based ILs show a good solubility in acetonitrile.[85] Increasing IL content should, consequently, lead to an increased solubility. Interestingly, the SCP with a Re:Ru:IL ratio of 1:10:90 has the highest absorbance, which would signify a higher solubility, since every sample was treated in an identical fashion. The samples were dissolved in acetonitrile, in which the Ru monomer is highly soluble. If the amount of Ru units is higher in this SCP than in the other polymers that might result in an increased solubility and, hence, a higher absorbance. Nevertheless, the absorbance maxima of the spectra are in the same wavelength regions for each polymer. This means that all the synthesized polymers may be used for photocatalytic reduction of CO_2, according to the intended concept of the project.

Die approbierte gedruckte Originalversion dieser Diplomarbeit ist an der TU Wien Bibliothek verfügbar
The approved original version of this thesis is available in print at TU Wien Bibliothek.
TU WIEN Bibliothek Your knowledge hub

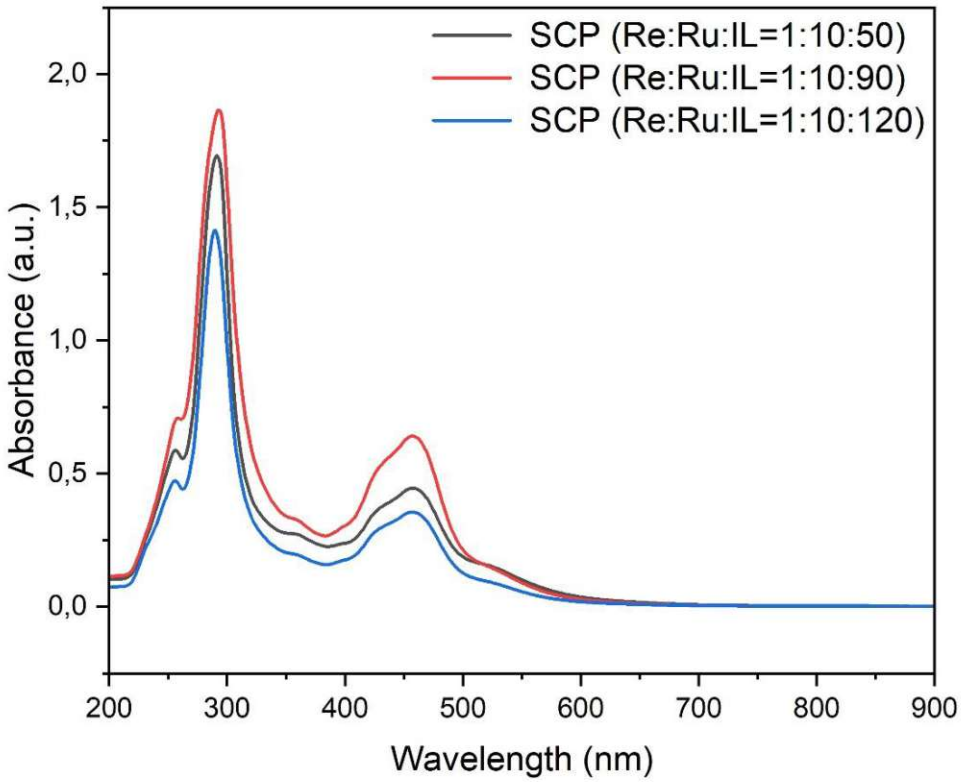

Figure 37: UV-Vis spectra of SCPs in different ratios.

Thermogravimetric analysis is a method used to determine the thermal behavior of a sample. By gradually heating up a sample, the mass change can be measured, which provides information about the phase transitions, decompositions, but also possible contaminations.

The results of a TGA of the simple PIL and three photocatalytically active polymers are depicted in Figure 38. The polymers show similar mass loss behavior. The first significant mass change occurs up to 100 °C, which can be attributed to water evaporating from the sample. ILs are hydrophilic and, therefore, water from the atmosphere is absorbed by the sample. Storing the sample in a dry environment prior to measurement is important. After water evaporation, the mass remains constant until approximately 240 °C. At this temperature organic matter starts to decompose, which leaves only the metal components of the PC and PS in the sample. The PIL, which does not contain a photocatalytic complex, exhibits the most significant mass loss. The CLP with a Re:IL ratio of 1:90 has a low metal content and shows only a slightly lower mass loss than the PIL. Compared to that, the CLP with a Ru:IL ratio of 1:9 and SCP still have maintained around half of their initial mass, since they have high amounts of the Re and/or Ru complex in the polymer framework as opposed to the PIL.

Die approbierte gedruckte Originalversion dieser Diplomarbeit ist an der TU Wien Bibliothek verfügbar
The approved original version of this thesis is available in print at TU Wien Bibliothek.
TU Bibliothek Your knowledge hub WIEN

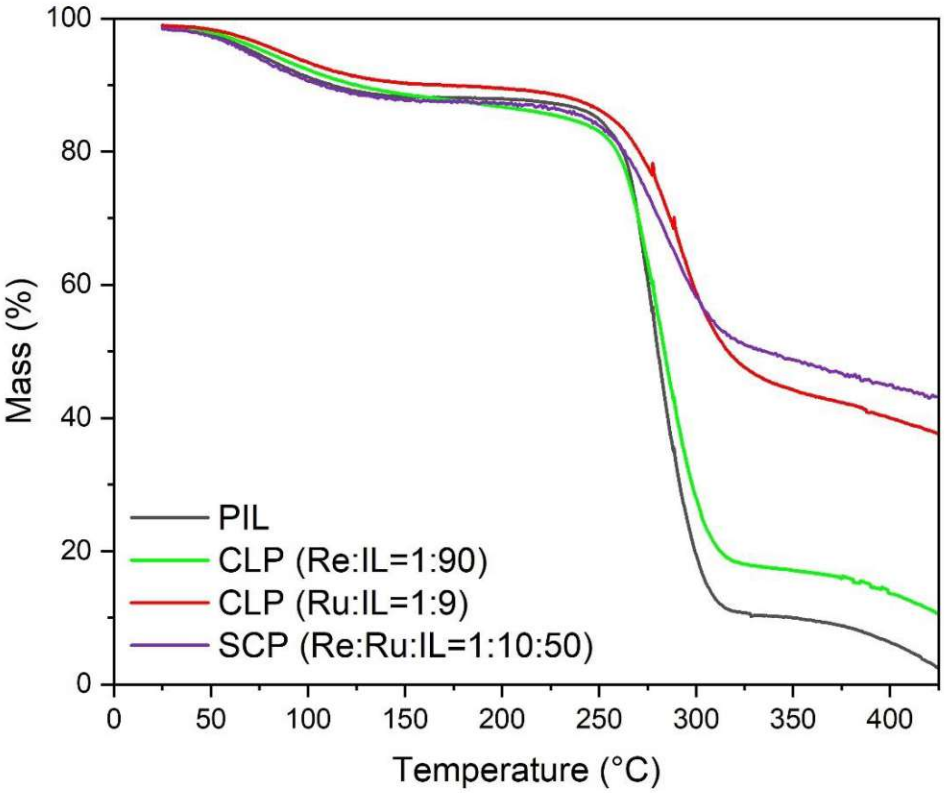

Figure 38: TGA results of the PIL, two CLPs in different monomer ratios, and an SCP.

T-XRF spectroscopy was employed to obtain the first approximate quantitative results for the ratio of Re photocatalyst to Ru photosensitizer in the polymers. This type of spectroscopy is non-destructive and is suitable for both solid and liquid samples, which meant that there was no need to try and solubilize the polymers in a solvent. After irradiation of the samples with X-rays from a W or Mo source, an electron can be excited to a higher energy state. Another electron can fall into the now vacant spot and, by doing so, emits a fluorescent X-ray, as graphically represented in Figure 39. The energy of the X-ray corresponds to the difference between the two states and is characteristic for each element.[86] Quantitative analysis is possible by using a standard or comparing the signals of the peaks of two different elements. This way a ratio of the measured components can be calculated.

Die approbierte gedruckte Originalversion dieser Diplomarbeit ist an der TU Wien Bibliothek verfügbar
The approved original version of this thesis is available in print at TU Wien Bibliothek.

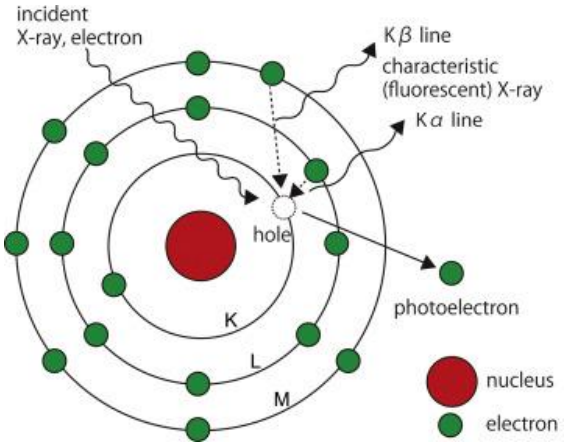

Figure 39: Schematic concept of characteristic X-ray generation for T-XRF spectroscopy. Graphic taken from [86]

The tungsten continuous spectrum of a CLP is shown in Figure 40 as an example. By comparing the intensity of the Re L lines with the Ru K lines the ratio of Re to Ru was calculated for the polymers in a 1:10:50 and 1:10:90 ratio of Re:Ru:IL. The chloride content of the IL is also measurable with this approach. However, in this case, the Cl signal overlaps with the Ru Lα line and, therefore, cannot be quantified. Thus, only the ratio of Re to Ru *via* T-XRF was measured. This signal overlap was also the reason for choosing the Ru K lines for the Re to Ru ratio calculation. The results are presented in Table 8.

Die approbierte gedruckte Originalversion dieser Diplomarbeit ist an der TU Wien Bibliothek verfügbar
The approved original version of this thesis is available in print at TU Wien Bibliothek.

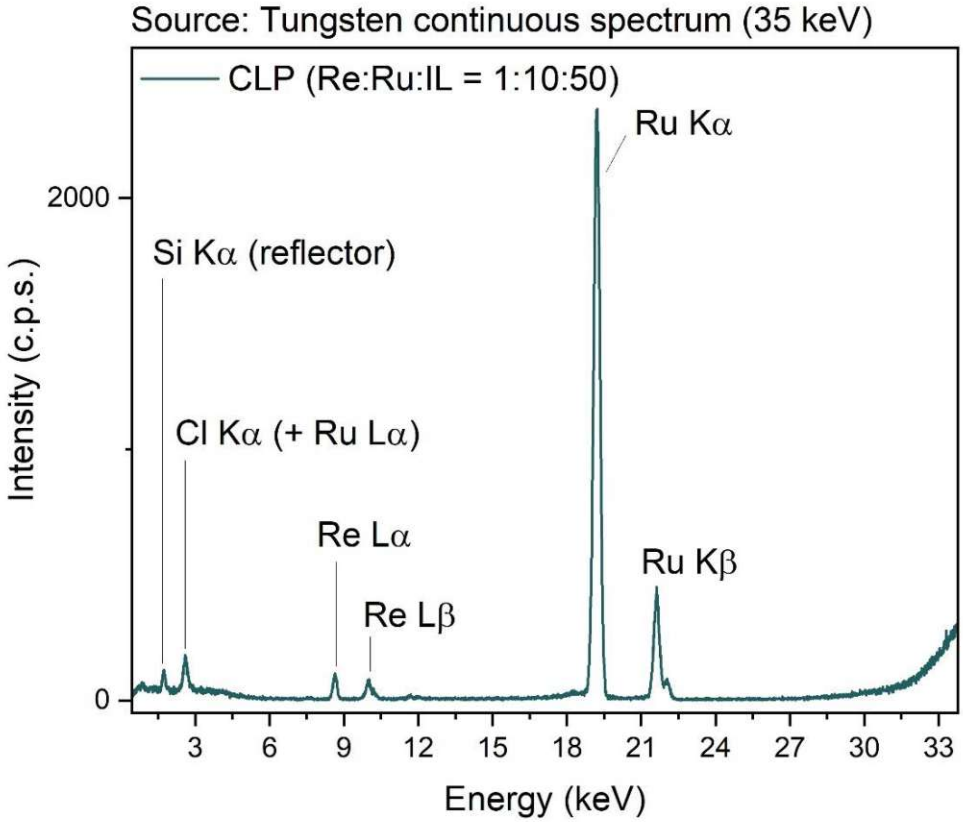

Figure 40: T-XRF spectrum of a CLP.

Table 8: T-XRF values of the CLPs, and SCPs.

	Entry	Theoretical ratio Re:Ru:IL	Measured ratio Re:Ru:IL
CLP	1	**1:10**:50	**1: 9**:x
	2	**1:10**:90	**1:14**:x
SCP	3	**1:10**:50	**1:11**:x
	4	**1:10**:90	**1:40**:x

The results of the T-XRF measurements vary only slightly for most polymers but are, approximately, still in the desired range. This indicates that the monomers are mostly built into the polymer framework the way they were intended. Entry 4 in Table 8 has a Ru content that is four times higher than the theoretical one. The isolated yield of this polymer was similar to the other SCPs, meaning one component should not be in the framework more or less than was intended. If that were the case, it should have been reflected in a corresponding increase or decrease in yield. However, the high Ru content would explain why the absorbance of this polymer was higher, considering the UV-Vis spectra (see Figure 37). As mentioned before, the Ru monomer is highly soluble in acetonitrile and, therefore, a higher Ru content would make the polymer possibly a little more soluble in acetonitrile. The IL content could not be measured

Die approbierte gedruckte Originalversion dieser Diplomarbeit ist an der TU Wien Bibliothek verfügbar
The approved original version of this thesis is available in print at TU Wien Bibliothek.
TU Bibliothek Your knowledge hub WIEN

with this method. Therefore, more measurements are required to determine the ratio of the individual components in the polymer framework. Inductively coupled plasma (ICP) spectroscopy is a method, where the sample is destroyed through the measurement, but it offers very precise quantitative and qualitative results and is planned for the near future.

Die approbierte gedruckte Originalversion dieser Diplomarbeit ist an der TU Wien Bibliothek verfügbar
The approved original version of this thesis is available in print at TU Wien Bibliothek.
TU WIEN Bibliothek Your knowledge hub

5. Conclusion and outlook

In this thesis, the synthesis of novel photocatalytic polymers for the reduction of carbon dioxide was successfully developed and optimized. State-of-the-art photocatalysts and photosensitizers were combined with ionic liquids, which are advantageous for carbon dioxide reduction, thereby, creating a polymer framework, which blends the desirable properties of the individual components into one. Through radical co-polymerization of vinyl-substituted monomers two different polymer-types were synthesized, a cross-linked polymer and a side-chain polymer.

For the cross-linked polymer, 5,5′-divinyl-2,2′-bipyridine, a vinyl-disubstituted ligand for photo-active Re and Ru complexes, was devised. These difunctionalized monomers created a cross-link in the polymer with a vinyl-monosubstituted ionic liquid as the base.

For the side-chain polymer, the ligand of the photo-active components, 4'-methyl-*N*-(4-vinylbenzyl)-[2,2'-bipyridine]-4-carboxamide, was substituted with a polymerizable side-chain. The polymerization of these complexes with vinyl-substituted ionic liquid yielded a polymer with a backbone constructed from the individual photocatalytic repeat units and ionic liquid.

Qualitative T-XRF measurements detected the photosensitizer and photocatalyst in the polymers, while the ionic liquid was qualitatively identified *via* IR measurements. UV-Vis spectroscopy measurements confirmed the absorption of visible light in the desired region for the photocatalytic reduction of carbon dioxide at > 445 nm and that the absorption was not heavily affected by the different polymer frameworks. Thermogravimetric analysis determined the thermal stability of the obtained polymers up to 200 °C.

The polymers, however, require further analysis. Solid-state MAS NMR could clarify the structure of the polymers, while ICP measurements are necessary to fully quantify the content concentrations. Additionally, BET measurements, cyclic voltammetry, and many other analytical methods could yield interesting results for the polymers, which is a task planned for the near future.

Photoexperiments are out of the scope of this thesis, although research is ongoing and promising. Preliminary photo-reductive experiments in liquid phase have already demonstrated the formation of carbon monoxide from carbon dioxide using the synthesized polymer as photocatalytic system. The objective for the future is to use the polymer for the reduction in a

Die approbierte gedruckte Originalversion dieser Diplomarbeit ist an der TU Wien Bibliothek verfügbar
The approved original version of this thesis is available in print at TU Wien Bibliothek.
TU Bibliothek Your knowledge hub WIEN

biphasic system with the catalyst in solid form and the substrate in gas form, followed by *in situ* gas chromatographic analysis.

Die approbierte gedruckte Originalversion dieser Diplomarbeit ist an der TU Wien Bibliothek verfügbar
The approved original version of this thesis is available in print at TU Wien Bibliothek.
TU Bibliothek Your knowledge hub WIEN

6. Experimental part

6.1. Materials and methods

All chemicals purchased from commercial suppliers were used without further purification unless otherwise noted. Dry solvents intended for anhydrous reactions were pre-distilled and desiccated on Al_2O_3 columns (PURESOLV, Innovative Technology).

Column chromatography was carried out on standard manual glass columns using silica gel from Merck (40-63 µm) with pre-distilled solvents. TLC analysis was performed on precoated aluminum-backed plates from Merck (silica gel 60 F_{254}). UV active compounds were visualized at 254 nm.

^{1}H and ^{13}C NMR spectra were recorded on a Bruker Avance UltraShield 400 MHz spectrometer and chemical shifts were reported in ppm from TMS with the solvent resonance as the internal standard. Coupling constants (*J*) are given in Hz. For NMR purposes, the following. multiplicities are reported using the following abbreviations: s = singlet, d = doublet, t = triplet, q = quartet, m = multiplet, dd = doublet of doublets, brs = broad singlet.

Infrared (IR) spectra were recorded on a Perkin-Elmer Spectrum 65 FT IR spectrometer equipped with a specac MK II Golden Gate Single Reflection ATR unit.

UV-Vis spectroscopy was performed on a JASCO V-670 spectrophotometer with a spectral test range of 190 to 900 nm.

Thermogravimetric analysis was conducted on a Netzsch STA 449 F1 system. The temperature was increased from 25 °C to 500 °C with a rate of 5 °C/min.

Total-reflection X-ray fluorescence spectroscopy was performed using an Atomika 8030C X-ray fluorescence Analyser, which operates with a total reflection geometry using an energy-dispersive Si(Li)-detector. The measurements were performed with the Tungsten continuous spectrum excitation mode (35 keV) at 50 kV and 47 mA, for 100 s live time.

Die approbierte gedruckte Originalversion dieser Diplomarbeit ist an der TU Wien Bibliothek verfügbar
The approved original version of this thesis is available in print at TU Wien Bibliothek.
TU Bibliothek Your knowledge hub WIEN

6.2. Synthesis of monomer set

6.2.1. 1–Butyl–3–vinylimidazolium chloride (3)

Procedure adapted from literature:[77]

1-Vinylimidazole (**1**, 4.85 mL, 53.6 mmol, 1.0 equiv.) was sealed in a 20 mL microwave vial equipped with a stirring bar and placed under Ar atmosphere. Butyl chloride (**2**, 6.7 mL, 64.3 mmol, 1.2 equiv.) was added *via* syringe. The reaction mixture was stirred at 70 °C for 48 h.

The lower phase of the resulting two-phase system was washed thrice with EtOAc, upon which it turned solid under heat generation. The solid was washed thrice with EtOAC and dried *in vacuo*. The desired product **3** was obtained as a colorless powder (7.454 g, 75%).

^{1}H NMR (400 MHz, $CDCl_3$): δ 11.18 (s, 1H, H-arom), 8.01 (t, J = 1.9 Hz, 1H, H-arom), 7.64 (t, J = 1.9 Hz, 1H, H-arom), 7.48 (dd, J = 15.7, 8.7 Hz, 1H, -*CH*=CH_2), 6.02 (dd, J = 15.7, 2.9 Hz, 1H, =CH_2), 5.30 (dd, J = 8.7, 3.0 Hz, 1H, =CH_2), 4.35 (t, J = 7.4 Hz, 2H, N-CH_2-CH_2-), 1.95 – 1.83 (m, 2H, -CH_2-CH_2-CH_2-), 1.41 – 1.27 (m, 2H, -CH_2-CH_3), 0.90 (t, J = 7.4 Hz, 3H, -CH_3).

^{13}C NMR (400 MHz, $CDCl_3$): δ 136.61 (C-arom), 128.51 (=CH_2), 122.73 (C-arom), 119.46 (C-arom), 109.42 (-*CH*=CH_2), 50.10 (N-CH_2-CH_2-), 32.09 (-CH_2-CH_2-CH_2-), 19.48 (-CH_2-CH_3), 13.46 (-CH_3).

FT-IR (ATR, ν/cm^{-1}): 1656, 1567 (C-H), 1542 (C-H), 1465 (imidazole ring), 927 (C=C)

The obtained analytical data was in agreement with literature.[87–89]

Die approbierte gedruckte Originalversion dieser Diplomarbeit ist an der TU Wien Bibliothek verfügbar
The approved original version of this thesis is available in print at TU Wien Bibliothek.

6.2.2. 5,5′-Divinyl-2,2′-bipyridine (6)

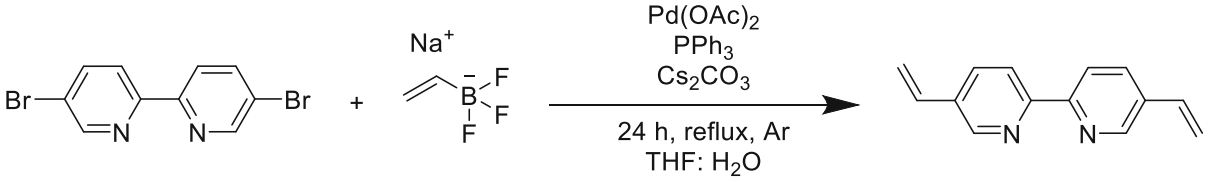

$C_{14}H_{12}N_2$
208.26

4 **5** **6**

Procedure adapted from literature:[70,90,91]

5,5′-Dibromo-2,2′-bipyridine (**4**, 250.0 mg, 0.796 mmol, 1.0 equiv.), potassium vinyltrifluoroborate (**5**, 397.8 mg, 2.95 mmol, 3.7 equiv.), palladium(II) acetate (3.6 mg, 0.016 mmol, 0.02 equiv.), triphenylphosphine (11.1 mg, 0.042 mmol, 0.05 equiv.) and dicaesium carbonate (726.4 mg, 2.23 mmol, 2.8 equiv.) were sealed in a 20 mL microwave vial equipped with a stirring bar and placed under Ar atmosphere. THF (13 mL) and water (0.53 mL) were degassed and added *via* syringe. The reaction mixture was stirred under reflux for 24 h.

After cooling to room temperature, water (14 mL) was added and the mixture was extracted with EtOAc (10 mL × 3). The combined organic layers were dried over anhydrous sodium sulfate, after which the solvent was removed under reduced pressure (20 mbar). The resulting crude was bound to silica gel and purified *via* column chromatography (4:1:0.25 = PE:EtOAc:TEA, $R_f = 0.4$). The desired product **6** was obtained as a colorless powder (116.6 mg, 70%)

^{1}H NMR (400 MHz, $CDCl_3$): δ 8.67 (s, 2H, H-arom), 8.37 (d, J = 8.3 Hz, 2H, H-arom), 7.86 (dd, J = 8.3, 2.3 Hz, 2H, H-arom), 6.77 (dd, J = 17.1, 11.0 Hz, 2H, -*CH*=CH_2), 5.90 (d, J = 17.7 Hz, 2H, =CH_2), 5.42 (d, J = 11.0 Hz, 2H, =CH_2).

^{13}C NMR (400 MHz, $CDCl_3$): δ 155.19 (C-arom), 147.95 (C-arom), 133.60 (-*CH*=CH_2), 133.46 (C-arom), 133.11 (C-arom), 120.92 (C-arom), 116.47 (=CH_2).

FT-IR (ATR, ν/cm^{-1}): 3000, 1627, 1589, 1465, 1363, 1024, 910 (C=C), 843

The obtained analytical data was in agreement with literature.[70,89,92]

Die approbierte gedruckte Originalversion dieser Diplomarbeit ist an der TU Wien Bibliothek verfügbar
The approved original version of this thesis is available in print at TU Wien Bibliothek.
TU Bibliothek Your knowledge hub WIEN

6.2.3. Photocatalyst monomer of the cross-linked polymer (CLP-PC, 8)

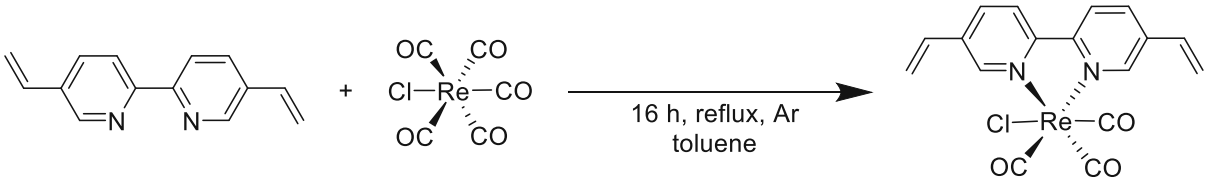

$C_{17}H_{12}ClN_2O_3Re$
513,95

6 **7** **8**

Procedure adapted from literature:[70]

5,5′-Divinyl-2,2′-bipyridine (**6**, 41.0 mg, 0.197 mmol, 1.0 equiv.), pentacarbonylchlororhenium(I) (**7**, 71.3 mg, 0.197 mmol, 1.0 equiv.) and toluene (20 mL) were mixed under inert conditions in a single-neck flask equipped with a stirring bar. The reaction mixture was stirred under reflux for 16 hours under Ar atmosphere.

After cooling to room temperature, the solid was filtered off and washed thrice with dry toluene. It was dried *in vacuo*. The desired product **8** was obtained as a yellow powder (81.3 mg, 80%).

^{1}H NMR (400 MHz, DMSO): δ 8.98 (s, 2H, H-arom), 8.75 (d, J = 8.6 Hz, 2H, H-arom), 8.55 (dd, J = 8.6, 2.1 Hz, 2H, H-arom), 7.03 (dd, J = 17.8, 11.2 Hz, 2H, -*CH*=CH_2), 6.29 (d, J = 17.7 Hz, 2H, =CH_2), 5.68 (d, J = 11.2 Hz, 2H, =CH_2).

FT-IR (ATR, ν/cm^{-1}): 2017 (CO), 1875 (CO), 1478, 1377, 1251, 915 (C=C), 856

The obtained analytical data was in agreement with literature.[70]

Die approbierte gedruckte Originalversion dieser Diplomarbeit ist an der TU Wien Bibliothek verfügbar
The approved original version of this thesis is available in print at TU Wien Bibliothek.
TU WIEN Bibliothek Your knowledge hub

6.2.4. Photosensitizer monomer of the cross-linked polymer (CLP-PS, 10)

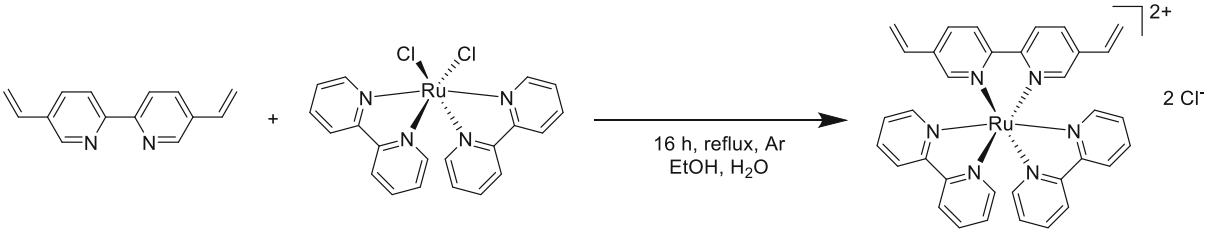

$C_{34}H_{28}N_6RuCl_2$
692,61

6 **9** **10**

Procedure adapted from literature:[90,91,93]

5,5′-Divinyl-2,2′-bipyridine (**6**, 35.4 mg, 0.170 mmol, 1.0 equiv.), *cis*-bis(2,2′-bipyridine)dichlororuthenium(II) hydrate (**9**, 123.5 mg, 0.255 mmol, 1.5 equiv.) were sealed in a 20 mL microwave vial equipped with a stirring bar and placed under Ar atmosphere. Dry ethanol (8.2 mL) and water (0.82 mL) were degassed and added *via* syringe. The reaction mixture was stirred under reflux for 16 h.

After cooling to room temperature, the solvent was removed under reduced pressure (20 mbar). The resulting crude was dissolved in acetonitrile (5 mL) and subsequently precipitated in diethyl ether (100 mL). The solid was separated and dissolved in double-distilled water (5 mL). Insoluble residues were separated through a sintered glass filter. Acetonitrile (5 mL) was added to the filtrate and then the solvent was removed under reduced pressure (20 mbar). The solid was dried over phosphorus pentoxide for 48 h to afford the desired product **10** as a dark violet solid (115.1 mg, 98%).

^{1}H NMR (400 MHz, MeOD): δ 8.73 (d, J = 9.3 Hz, 4H, H-arom), 8.65 (d, J = 8.5 Hz, 2H, H-arom), 8.27 (dd, J = 8.6, 2.0 Hz, 2H, H-arom), 8.18 – 8.12 (m, 4H, H-arom), 7.91 – 7.80 (m, 4H, H-arom), 7.68 (d, J = 2.0 Hz, 2H, H-arom), 7.56 – 7.48 (m, 4H, H-arom), 6.59 (dd, J = 17.7, 11.1 Hz, 2H, -*CH*=CH_2), 5.88 (d, J = 17.6 Hz, 2H, =CH_2), 5.48 (d, J = 11.1 Hz, 2H, =CH_2).

FT-IR (ATR, ν/cm^{-1}): 3004, 1600, 1462, 1442, 1312, 1246, 1156, 1122, 1068, 986, 917 (C=C), 852, 765 (C-H)

The obtained ^{1}H NMR analytical data was in agreement with literature.[94,95]

Die approbierte gedruckte Originalversion dieser Diplomarbeit ist an der TU Wien Bibliothek verfügbar
The approved original version of this thesis is available in print at TU Wien Bibliothek.
TU WIEN Bibliothek Your knowledge hub

6.2.5. *N*-(4-Vinylbenzyl)phthalimide (13)

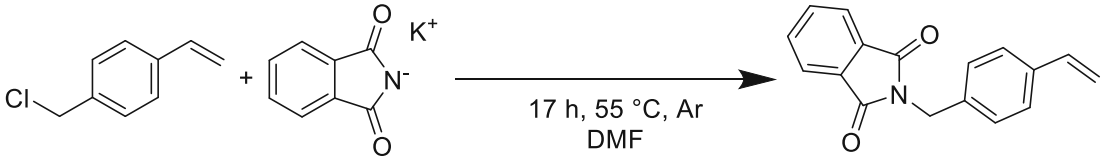

$C_{17}H_{13}NO_2$
263,30

11 **12** **13**

Procedure adapted from literature:[96]

4-Vinylbenzyl chloride (**11**, 4.0597 g, 26.6 mmol, 1.0 equiv.), potassium phthalimide (12, 5.0745 g, 27.4 mmol, 1.03 equiv.) and dry DMF (25 mL) were mixed in a 3-neck-flask equipped with a stirring bar and placed under Ar atmosphere. The reaction mixture was stirred at 55 °C for 17 h.

The solvent was removed at reduced pressure (20 mbar) and the resulting solid material was dissolved in chloroform (40 mL). Insoluble residues were filtered off and washed with chloroform (10 mL × 3). The combined organic extracts were washed with 0.2 M NaOH (15 mL) and water (15 mL × 2) and dried over anhydrous sodium sulfate, after which the solvent was removed under reduced pressure (20 mbar). The resulting crude was crystallized from methanol to afford **13** as a white solid (5.4105 g, 77%).

^{1}H NMR (400 MHz, $CDCl_3$): δ 7.89 – 7.67 (m, 4H, H-arom), 7.43 – 7.31 (m, 4H, H-arom), 6.67 (dd, J = 17.6, 10.9 Hz, 1H, -*CH*=CH_2), 5.71 (dd, J = 17.6, 0.9 Hz, 1H, =CH_2), 5.22 (dd, J = 10.9, 0.9 Hz, 1H, =CH_2), 4.83 (s, 2H, N-CH_2-).

The obtained analytical data was in agreement with literature.[96]

Die approbierte gedruckte Originalversion dieser Diplomarbeit ist an der TU Wien Bibliothek verfügbar
The approved original version of this thesis is available in print at TU Wien Bibliothek.
TU Bibliothek Your knowledge hub WIEN

6.2.6. 4-(Aminomethyl)styrene (15)

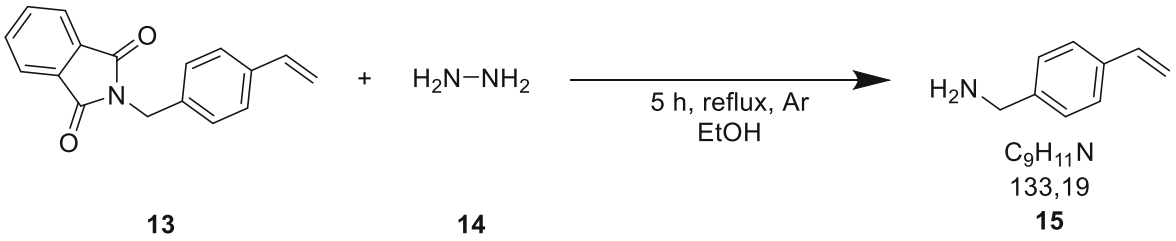

Procedure adapted from literature:[96]

N-(4-Vinylbenzyl)phthalimide (**13**, 9.000 g, 34.2 mmol, 1.0 equiv.) was dissolved in EtOH (abs., 47 mL) in a 3-neck-flask equipped with a stirring bar and placed under Ar atmosphere. Hydrazine hydrate (**2**, 50 – 60%, 4.66 mL, 47.9 mmol, 1.4 equiv.) dissolved in EtOH (abs., 4.6 mL) was added *via* syringe. The reaction mixture was stirred at reflux for 2.5 h, until full conversion of **13** was verified *via* TLC (eluent: toluene).

The solvent was removed at reduced pressure (20 mbar). The resulting solid material was dissolved in chloroform (80 mL) and washed with 20% NaOH (80 mL). The aqueous phase was extracted with chloroform (75 mL × 3). The combined organic extracts were dried over anhydrous sodium sulfate, after which the solvent was removed under reduced pressure (20 mbar). The resulting crude was purified *via* kugelrohr distillation. The desired product **15** was obtained as a colorless oil (3.309 g, 73%).

^{1}H NMR (400 MHz, $CDCl_3$): δ 7.41 – 7.23 (m, 4H, H-arom), 6.71 (dd, J = 17.6, 10.9 Hz, 1H, -*CH*=CH_2), 5.73 (dd, J = 17.6, 1.0 Hz, 1H, =CH_2), 5.22 (dd, J = 10.9, 1.0 Hz, 1H, =CH_2), 3.84 (s, 2H, N-C*H*$_2$-), 1.57 (s, 2H, -NH_2).

^{13}C NMR (400 MHz, $CDCl_3$): δ 143.10 (C-arom), 136.65 (-*CH*=CH_2), 136.31 (C-arom), 127.35(2C, C-arom), 126.49 (2C, C-arom), 113.54 (=CH_2), 46.35 (N-CH_2-).

The obtained analytical data was in agreement with literature.[96]

Die approbierte gedruckte Originalversion dieser Diplomarbeit ist an der TU Wien Bibliothek verfügbar
The approved original version of this thesis is available in print at TU Wien Bibliothek.
TU Bibliothek Your knowledge hub WIEN

6.2.7. 4'-Methyl-*N*-(4-vinylbenzyl)-[2,2'-bipyridine]-4-carboxamide (17)

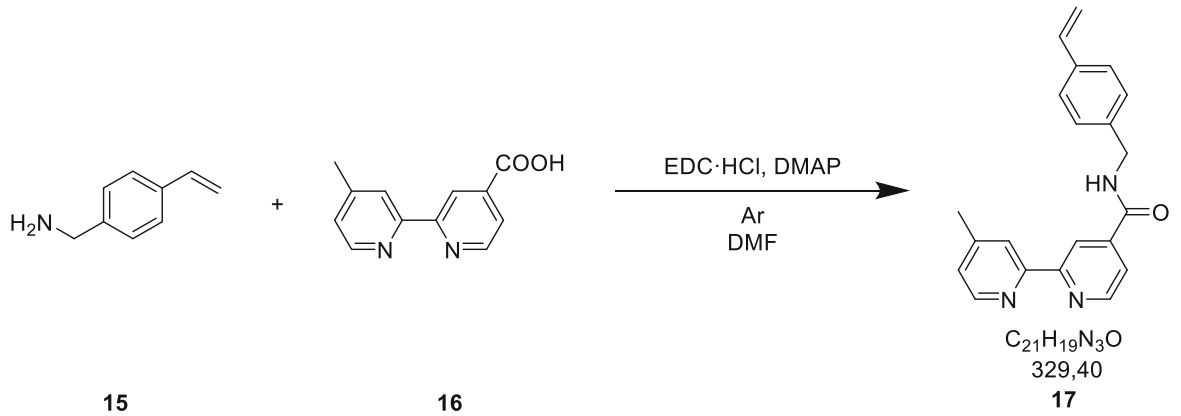

Procedure adapted from literature:[93]

4'-Methyl-2,2'-bipyridine-4-carboxylic acid (**16**, 250.0 mg, 1.17 mmol, 1.0 equiv.), EDC·HCl (511.5 mg, 2.67 mmol, 2.29 equiv.) and DMAP (325.9 mg, 2.67 mmol, 2.29 equiv.) were dissolved in DMF (4.2 mL), sealed in a 20 mL microwave vial equipped with a stirring bar and placed under Ar atmosphere. The mixture was cooled to 0 °C. 4-(Aminomethyl)styrene (**15**, 188.7 mg, 1.42 mmol, 1.2 equiv.) was added. The reaction mixture was first stirred at 0 °C for 4 h and then at room temperature for 24 h.

The solution was precipitated in an aqueous sodium carbonate solution (pH > 10), filtered off and dried *in vacuo*. The resulting crude was crystallized from methanol to afford **17** as a purple solid (134.0 mg, 35%).

^{1}H NMR (400 MHz, $CDCl_3$): δ 8.78 (d, *J* = 5.0 Hz, 1H, H-arom), 8.60 (s, 1H, H-arom), 8.48 (d, *J* = 4.9 Hz, 1H, H-arom), 8.25 (s, 1H, H-arom), 7.79 (dd, *J* = 5.0, 1.8 Hz, 1H, H-arom), 7.43 – 7.27 (m, 4H, H-arom), 7.14 (d, *J* = 5.0 Hz, 1H, H-arom), 6.85 (s, *J* = 5.6 Hz, 1H, NH), 6.70 (dd, *J* = 17.6, 10.9 Hz, 1H, -*CH*=CH_2), 5.74 (dd, *J* = 17.6, 0.9 Hz, 1H, =CH_2), 5.25 (dd, *J* = 10.8, 0.9 Hz, 1H, =CH_2), 4.64 (d, *J* = 5.7 Hz, 2H, -CH_2-), 2.44 (s, 3H, -CH_3).

^{13}C NMR (400 MHz, $CDCl_3$): δ 165.56 (C=O), 157.15 (C-arom), 155.10 (C-arom), 150.28 (C-arom), 149.06 (C-arom), 148.58 (C-arom), 142.56 (C-arom), 137.34 (C-arom), 137.18 (-*CH*=CH_2), 136.42 (C-arom), 128.43 (C-arom), 126.77 (C-arom), 125.36 (C-arom), 122.29 (C-arom), 122.00 (C-arom), 117.34 (C-arom), 114.31 (=CH_2), 44.14 (-CH_2-), 21.34 (-CH_3).

The obtained ^{1}H NMR data was in agreement with literature.[93]

Die approbierte gedruckte Originalversion dieser Diplomarbeit ist an der TU Wien Bibliothek verfügbar
The approved original version of this thesis is available in print at TU Wien Bibliothek.
TU Bibliothek Your knowledge hub WIEN

6.2.8. Photocatalyst monomer of the side-chain polymer (SCP-PC, 18)

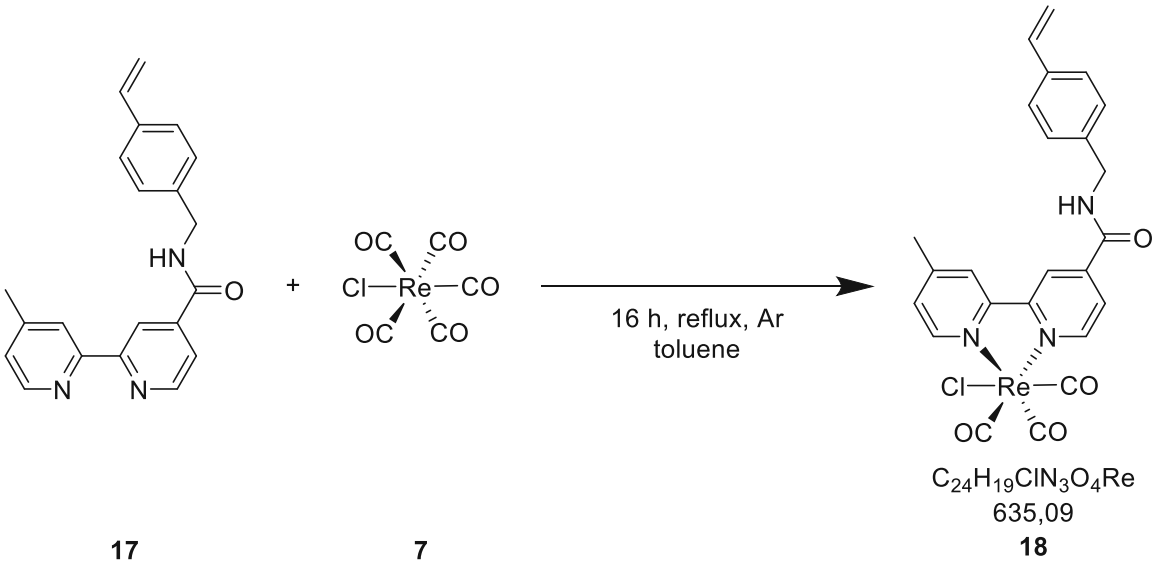

Procedure adapted from literature:[70]

4'-Methyl-*N*-(4-vinylbenzyl)-[2,2'-bipyridine]-4-carboxamide (**17**, 25.9 mg, 0.079 mmol, 1.0 equiv.), pentacarbonylchlororhenium(I) (**7**, 29.0 mg, 0.079 mmol, 1.0 equiv.) and toluene (7.9 mL) were sealed in a 20 mL microwave vial equipped with a stirring bar and placed under Ar atmosphere. The reaction mixture was stirred under reflux for 16 hours.

After cooling to room temperature, the solid was filtered of and washed thrice with dry toluene. It was dried *in vacuo*. The desired product **18** was obtained as an orange powder (13.0 mg, 26%).

^{1}H NMR (400 MHz, $CDCl_3$): δ 9.00 (d, J = 5.9 Hz, 1H, H-arom), 8.73 (d, J = 5.7 Hz, 2H, H-arom, NH), 8.56 (m, 2H, H-arom), 8.08 (m, 2H, H-arom), 7.84 (dd, J = 5.7, 1.7 Hz, 1H, H-arom), 7.46 – 7.29 (m, 3H, H-arom,), 6.71 (dd, J = 17.6, 10.9 Hz, 1H, -*CH*=CH_2), 5.81 – 5.71 (m, 1H, =CH_2), 5.27 (d, J = 10.9 Hz, 1H, =CH_2), 4.58 (s, 2H, -CH_2-), 2.41 (s, 3H, -CH_3).

FT-IR (ATR, ν/cm^{-1}): 2022 (CO), 1894 (CO), 1738, 1456, 1373, 1220, 930 (C=C), 850

Die approbierte gedruckte Originalversion dieser Diplomarbeit ist an der TU Wien Bibliothek verfügbar
The approved original version of this thesis is available in print at TU Wien Bibliothek.
TU WIEN Bibliothek Your knowledge hub

6.2.9. Photosensitizer monomer of the side-chain polymer (SCP-PS, 19)

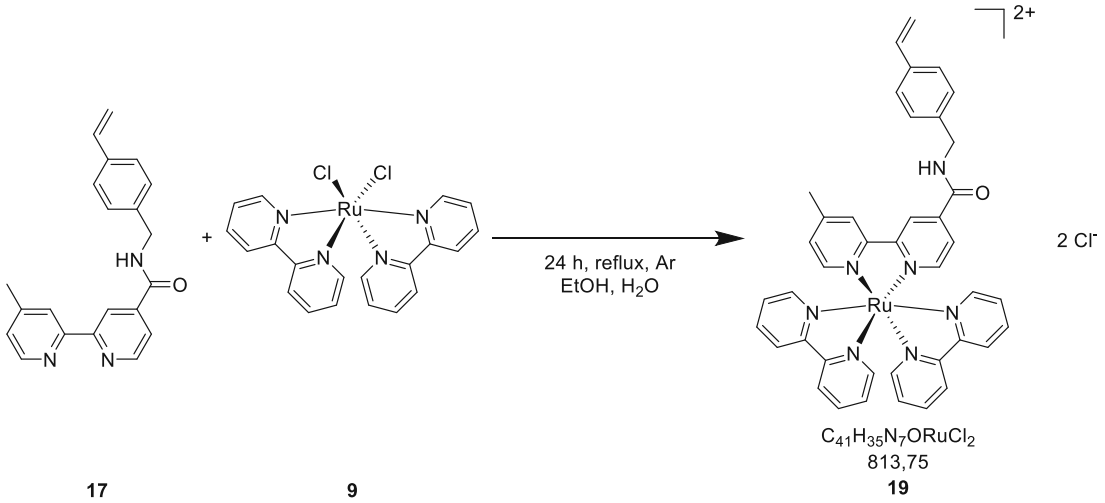

Procedure adapted from literature:[91,93]

4'-Methyl-*N*-(4-vinylbenzyl)-[2,2'-bipyridine]-4-carboxamide (**17**, 50.0 mg, 0.152 mmol, 1.0 equiv.), *cis*-bis(2,2′-bipyridine)dichlororuthenium(II) hydrate (**9**, 147.0 mg, 0.304 mmol, 2.0 equiv.) were sealed in a 20 mL microwave vial equipped with a stirring bar and placed under Ar atmosphere. Dry ethanol (3.41 mL) and water (0.09 mL) were degassed and added *via* syringe. The reaction mixture was stirred under reflux for 24 h.

After cooling to room temperature, the solvent was removed under reduced pressure (20 mbar). The resulting crude was dissolved in acetonitrile (5 mL) and subsequently precipitated in diethyl ether (100 mL). The solid was separated and dissolved in double-distilled water (5 mL). Insoluble residues were separated through a sintered glass filter. Acetonitrile (10 mL) was added to the filtrate and then the solvent was removed under reduced pressure (20 mbar). The solid was dried over phosphorus pentoxide for a minimum of 48 h to afford the desired product **19** as a dark violet solid (116.9 mg, 95%).

^{1}H NMR (400 MHz, MeOD): δ 9.14 (d, J = 2.0 Hz, 1H, H-arom), 8.74 (m, 6H, NH, H-arom), 8.16 (m, 5H, H-arom), 7.98 (d, J = 6.0 Hz, 2H, H-arom), 7.91 – 7.78 (m, 4H, H-arom), 7.66 (d, J = 6.0 Hz, 1H, H-arom), 7.56 – 7.29 (m, 8H, Ph, H-arom), 6.73 (dd, J = 17.6, 11.0 Hz, 1H, -*CH*=CH_2), 5.77 (dd, J = 17.7, 1.0 Hz, 1H, =CH_2), 5.23 (dd, J = 10.9, 1.0 Hz, 1H, =CH_2), 4.63 (s, 2H, -CH_2-), 2.62 (s, 3H, -CH_3).

FT-IR (ATR, ν/cm^{-1}): 1658 (C=O), 1543 (N-H), 1115, 917 (C=C)

The obtained analytical data was in agreement with literature.[93]

Die approbierte gedruckte Originalversion dieser Diplomarbeit ist an der TU Wien Bibliothek verfügbar
The approved original version of this thesis is available in print at TU Wien Bibliothek.
TU Bibliothek Your knowledge hub WIEN

6.3. Polymerisation of monomers

6.3.1. General procedure for polymerisation in batch reactor mode (A)

Procedure adapted from literature:[69]

The required amounts of reactants, 2,2′-azobis(2-methylpropionitrile) (AIBN) and dimethylformamide (DMF) were sealed in a 20 mL microwave vial equipped with a stirring bar in the glovebox under Ar atmosphere. The reaction mixture was stirred under reflux for 24 h.

After cooling to room temperature, the product was precipitated in acetone (dry) and dried *in vacuo*.

The products were obtained as brown solids.

6.3.2. General procedure for polymerisation in the autoclave (B)

Procedure adapted from literature:[69]

The required amounts of reactants, AIBN and DMF were sealed in an 8 mL screw-cap vial equipped with a stirring bar in the glovebox under Ar atmosphere. The reaction was carried out in the autoclave under N_2 atmosphere for 24 h, at 100 °C, at elevated pressures.

After cooling to room temperature, the product was precipitated in acetone (dry) and dried *in vacuo*.

The products were obtained as brown solids.

Die approbierte gedruckte Originalversion dieser Diplomarbeit ist an der TU Wien Bibliothek verfügbar
The approved original version of this thesis is available in print at TU Wien Bibliothek.
TU WIEN Bibliothek Your knowledge hub

6.3.3. Synthesis of polyionic liquid (PIL, 20)

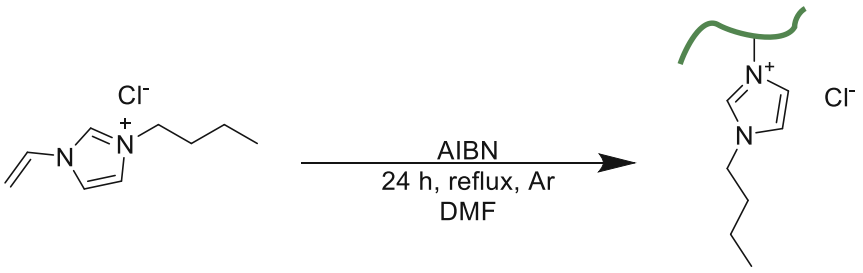

3 **20**

Preparation according to procedure **A** from 1–butyl–3–vinylimidazolium chloride (**3**, 500.0 mg, 2.68 mmol, 1.0 equiv.), AIBN (0.4 mg, 0.003 mmol, 0.001 equiv.) and DMF (dry, 1 mL) gave **20** as a brown solid (436.2 mg, 87%).

^{1}H NMR (400 MHz, $CDCl_3$): δ10.26 (brs, 1H, -N-*CH*-), 8.75 (s, 1H, -N-*CH*-), 7.11 (brs, 1H, -N-*CH*-), 4.19 (brs, 2H, N-C*H*$_2$-CH$_2$-), 3.20 (brs, 1H, polymer backbone), 1.92 (brs, 2H, -CH$_2$-C*H*$_2$-CH$_2$-), 1.40 (brs, 2H, -*CH*$_2$-CH$_3$), 0.95 (brs, 3H, -CH$_3$).

FT-IR (ATR, ν/cm^{-1}): 3030, 2963, 1568 (C-H), 1543 (C-H), 1464 (imidazole ring), 1162

The obtained FT-IR data was in agreement with literature.[97]

Die approbierte gedruckte Originalversion dieser Diplomarbeit ist an der TU Wien Bibliothek verfügbar
The approved original version of this thesis is available in print at TU Wien Bibliothek.
TU Bibliothek Your knowledge hub WIEN

6.3.4. Synthesis of cross-linked polymer (CLP, 21)

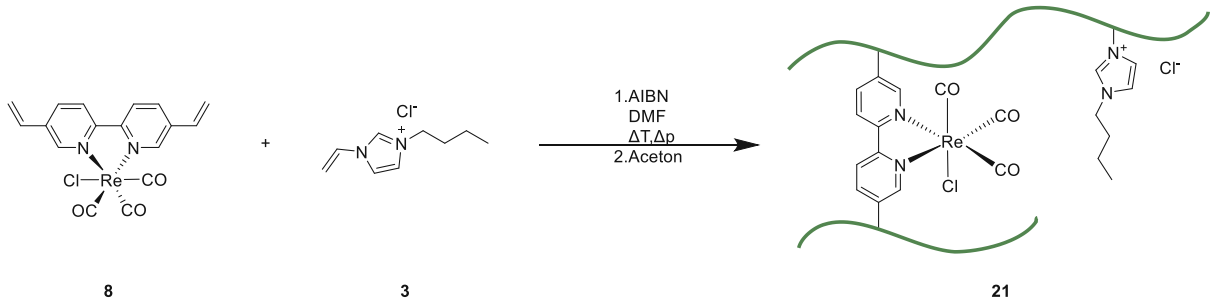

Product	Synthesis Procedure	Starting material ratio		Starting material amount		AIBN	DMF	Yield
		8	**3**	**8**	**3**			
21a	**A**	1	1	22.0 mg 0.043 mmol	8.0 mg 0.043 mmol	$7 \cdot 10^{-3}$ mg $4 \cdot 10^{-5}$ mmol 0.001 equiv.	0.3 mL	43.1 mg quant.
21b	**B**	1	90	20.0 mg 0.039 mmol	654.0 mg 3.5 mmol	0.6 mg 0.004 mmol 0.09 equiv.	2.7 mL	553.8 mg 82%

Autoclave conditions for **21b**: N_2 atmosphere, 24 h, 100 °C, 52.8 bar

21a: FT-IR (ATR, ν/cm^{-1}): 2962, 2023 (CO), 1892 (CO), 1571 (C-H), 1546 (C-H), 1465 (imidazole ring), 1163

21b: FT-IR (ATR, ν/cm^{-1}): 3049, 2959, 2015 (CO), 1895 (CO), 1569 (C-H), 1551 (C-H), 1462 (imidazole ring), 1163

Die approbierte gedruckte Originalversion dieser Diplomarbeit ist an der TU Wien Bibliothek verfügbar
The approved original version of this thesis is available in print at TU Wien Bibliothek.

6.3.5. Synthesis of cross-linked polymer (CLP, 22)

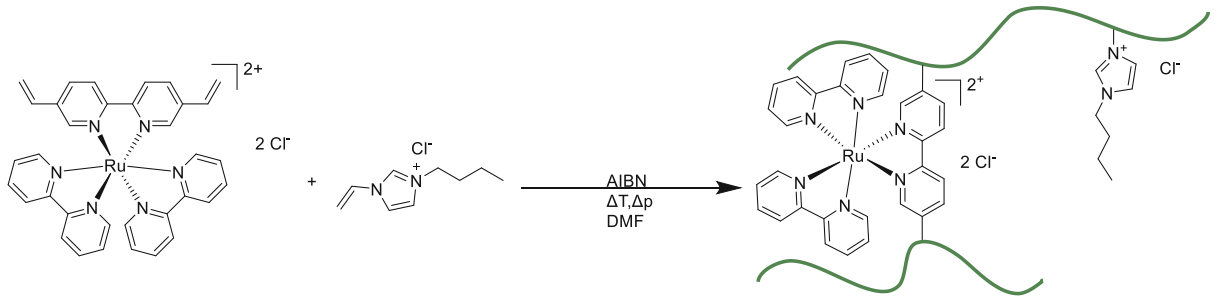

10 3 22

Product	Synthesis Procedure	Starting material ratio		Starting material amount		AIBN	DMF	Yield
		10	**3**	**10**	**3**			
22a	**B**	1	1	50.0 mg 0.072 mmol	13.5 mg 0.072 mmol	0.1 mg $7 \cdot 10^{-4}$ mmol 0.009 equiv.	0.4 mL	36.3 mg 57%
22b	**A**	1	9	42.5 mg 0.062 mmol	103.1 mg 0.553 mmol	0.1 mg $6 \cdot 10^{-4}$ mmol 0.009 equiv.	0.5 mL	74.8 mg 51%

Autoclave conditions for **22a**: N_2 atmosphere, 24 h, 100 °C, 52.8 bar

22a: FT-IR (ATR, ν/cm^{-1}): 3066, 2961, 1652, 1602, 1575 (C-H), 1464 (imidazole ring), 1380, 1245, 1160, 849, 770

22b: FT-IR (ATR, ν/cm^{-1}): 3066, 2959, 1649, 1602, 1569 (C-H), 1551 (C-H), 1464 (imidazole ring), 1379, 1264, 1162

Die approbierte gedruckte Originalversion dieser Diplomarbeit ist an der TU Wien Bibliothek verfügbar
The approved original version of this thesis is available in print at TU Wien Bibliothek.
TU Bibliothek Your knowledge hub WIEN

6.3.6. Synthesis of cross-linked polymer (CLP, 23)

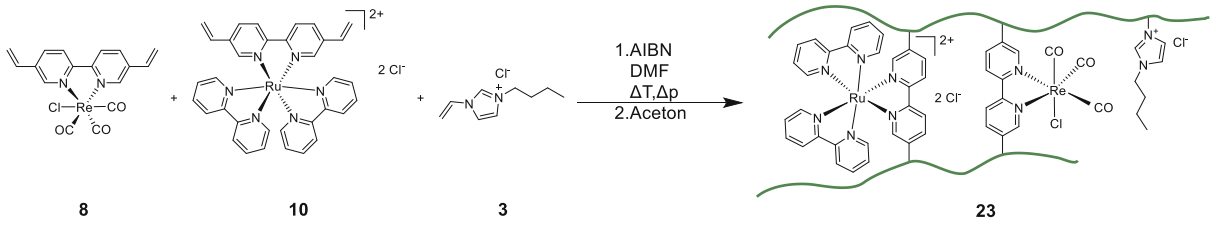

Preparation according to procedure **B**:

Product	Starting material ratio			Starting material amount			AIBN	DMF	Yield
	8	**10**	**3**	**8**	**10**	**3**			
23a	1	10	50	2.3 mg $4.4\cdot10^{-3}$ mmol	30.5 mg $4.4\cdot10^{-2}$ mmol	41.1 mg 0.22 mmol	0.04 mg $2\cdot10^{-4}$ mmol 0.05 equiv.	0.1 mL	67.0 mg 91%
23b	1	10	90	1.7 mg $3.4\cdot10^{-3}$ mmol	23.4 mg $3.4\cdot10^{-2}$ mmol	56.8 mg 0.30 mmol	0.05 mg $3\cdot10^{-4}$ mmol 0.09 equiv.	0.3 mL	69.6 mg 85%
23c	1	10	120	2.0 mg $3.9\cdot10^{-3}$ mmol	26.9 mg $3.9\cdot10^{-2}$ mmol	87.1 mg 0.47 mmol	0.08 mg $5\cdot10^{-4}$ mmol 0.12 equiv.	0.4 mL	98.4 mg 85%

Autoclave conditions:

23a: N_2 atmosphere, 24 h, 100 °C, 50.0 bar

23b: N_2 atmosphere, 24 h, 101 °C, 60.0 bar

23c: N_2 atmosphere, 24 h, 100 °C, 61.0 bar

23a: FT-IR (ATR, ν/cm^{-1}): 3017, 2970, 2016 (CO), 1885 (CO), 1568 (C-H), 1548 (C-H), 1463 (imidazole ring), 1162

23b: FT-IR (ATR, ν/cm^{-1}): 3029, 2971, 2022 (CO), 1890 (CO), 1570 (C-H), 1550 (C-H), 1464 (imidazole ring), 1159

23c: FT-IR (ATR, ν/cm^{-1}): 3062, 2958, 2019 (CO), 1890 (CO), 1570 (C-H), 1553 (C-H), 1465 (imidazole ring), 1160

Die approbierte gedruckte Originalversion dieser Diplomarbeit ist an der TU Wien Bibliothek verfügbar
The approved original version of this thesis is available in print at TU Wien Bibliothek.
TU Bibliothek Your knowledge hub WIEN

6.3.7. Synthesis of side-chain polymer (SCP, 24)

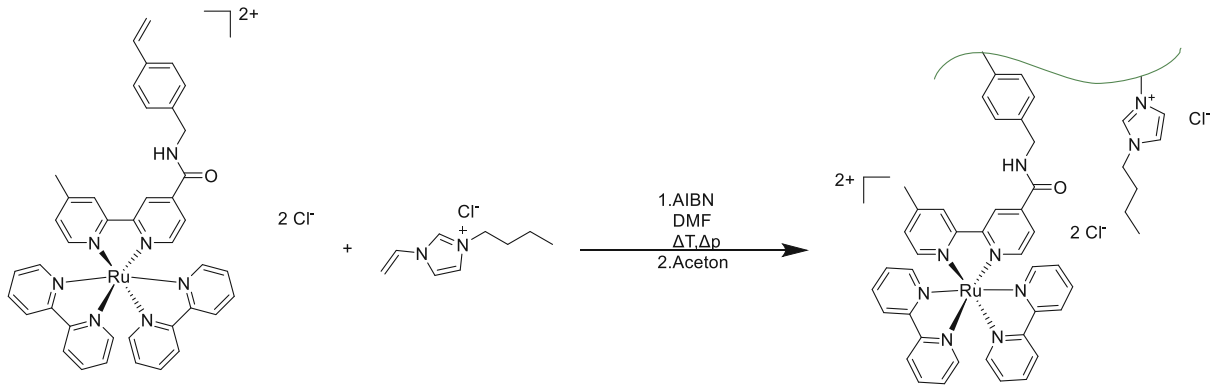

19 **3** **24**

Preparation according to procedure **A** from 1–butyl–3–vinylimidazolium chloride (**3**, 82.7 mg, 0.443 mmol, 9.0 equiv.), compound **19** (40.0 mg, 0.049 mmol, 1.0 equiv.), AIBN (0.1 mg, $4 \cdot 10^{-4}$ mmol, 0.009 equiv.) and DMF (dry, 0.3 mL) gave **24** as a brown solid (78.7 mg, 64%).

FT-IR (ATR, ν/cm^{-1}): 3059, 2959, 1650, 1569 (C-H), 1551 (C-H), 1460 (imidazole ring), 1440, 1267, 1162

Die approbierte gedruckte Originalversion dieser Diplomarbeit ist an der TU Wien Bibliothek verfügbar
The approved original version of this thesis is available in print at TU Wien Bibliothek.
TU WIEN Bibliothek Your knowledge hub

6.3.8. Synthesis of side-chain polymer (SCP, 25)

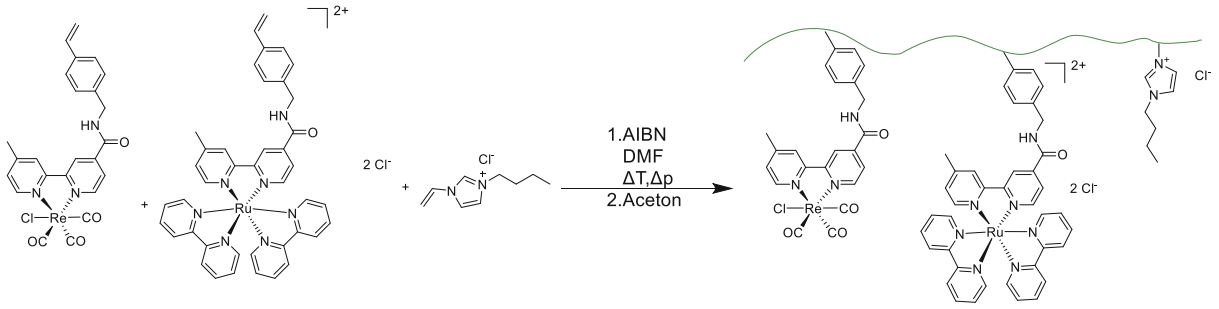

Preparation according to procedure **B**:

Product	Starting material ratio			Starting material amount			AIBN	DMF	Yield
	18	**19**	**3**	**18**	**19**	**3**			
25a	1	10	50	3.5 mg $5.5\cdot10^{-3}$ mmol	44.8 mg $5.5\cdot10^{-2}$ mmol	51.4 mg 0.28 mmol	0.05 mg $3\cdot10^{-4}$ mmol 0.05 equiv.	0.1 mL	83.9 mg 84%
25b	1	10	90	2.5 mg $3.9\cdot10^{-3}$ mmol	32.1 mg $3.9\cdot10^{-2}$ mmol	66.2 mg 0.35 mmol	0.06 mg $4\cdot10^{-4}$ mmol 0.09 equiv.	0.2 mL	76.2 mg 76%
25c	1	10	120	2.5 mg $3.9\cdot10^{-3}$ mmol	32.1 mg $3.9\cdot10^{-2}$ mmol	88.3 mg 0.47 mmol	0.08 mg $5\cdot10^{-4}$ mmol 0.12 equiv.	0.2 mL	92.0 mg 75%

Autoclave conditions:

25a: N_2 atmosphere, 24 h, 91 °C, 62.5 bar

25b: N_2 atmosphere, 24 h, 100 °C, 61.0 bar

25c: N_2 atmosphere, 24 h, 100 °C, 61.0 bar

25a: FT-IR (ATR, ν/cm^{-1}): 3063, 2962, 2022 (CO), 1919 (CO), 1547 (C-H), 1460 (imidazole ring), 1161,772

25b: FT-IR (ATR, ν/cm^{-1}): 3065, 2962, 2022 (CO), 1892 (CO), 1549 (C-H), 1460 (imidazole ring), 1163, 774

25c: FT-IR (ATR, ν/cm^{-1}): 3056, 2961, 2019 (CO), 1892 (CO), 1550 (C-H), 1466 (imidazole ring), 1162, 775

Die approbierte gedruckte Originalversion dieser Diplomarbeit ist an der TU Wien Bibliothek verfügbar
The approved original version of this thesis is available in print at TU Wien Bibliothek.
TU Bibliothek Your knowledge hub WIEN

7. Bibliography

[1] B. A. Rosen, A. Salehi-Khojin, M. R. Thorson, W. Zhu, D. T. Whipple, P. J. A. Kenis, R. I. Masel, *Science* **2011**, *334*, 643–644.

[2] K. M. K. Yu, I. Curcic, J. Gabriel, S. C. E. Tsang, *Chem. Sus. Chem.* **2008**, *1*, 893–899.

[3] Z. Yang, S. Kagawa, J. Li, *Urban Clim.* **2021**, *37*, 100812–100825.

[4] R. Betts, "Atmospheric carbon dioxide at record high levels despite reduced emissions in 2020," can be found under https://www.metoffice.gov.uk/research/news/2021/record-co2-levels-despite-lower-emissions-in-2020, **2021**.

[5] J. L. Sarmiento, N. Gruber, *Phys. Today* **2002**, *55*, 30–36.

[6] Intergovernmental Panel on Climate Change, "Climate Change 2022: Mitigation of Climate Change," can be found under https://www.ipcc.ch/report/ar6/wg3/, **2022**.

[7] R. A. Tufa, D. Chanda, M. Ma, D. Aili, T. B. Demissie, J. Vaes, Q. Li, S. Liu, D. Pant, *Appl. Energy* **2020**, *277*, 115557–115596.

[8] Umweltbundesamt, "Carbon Capture and Storage," can be found under https://www.umweltbundesamt.de/themen/wasser/gewaesser/grundwasser/nutzung-belastungen/carbon-capture-storage#grundlegende-informationen, **2022**.

[9] Umweltbundesamt, "Carbon Capture and Utilization (CCU)," can be found under https://www.umweltbundesamt.de/themen/klima-energie/klimaschutz-energiepolitik-in-deutschland/carbon-capture-utilization-ccu#Fazit, **2021**.

[10] N. Meunier, R. Chauvy, S. Mouhoubi, D. Thomas, G. de Weireld, *Renew. Energy* **2020**, *146*, 1192–1203.

[11] M. Bowker, *Chem. Cat. Chem.* **2019**, *11*, 4238–4246.

[12] M. Kauw, R. M. J. Benders, C. Visser, *Energy* **2015**, *90*, 208–217.

[13] Y. Amao, *J. CO2 Util.* **2018**, *26*, 623–641.

[14] P. Duarah, D. Haldar, V. S. K. Yadav, M. K. Purkait, *J. Environ. Chem. Eng.* **2021**, *9*, 106394–106409.

Die approbierte gedruckte Originalversion dieser Diplomarbeit ist an der TU Wien Bibliothek verfügbar
The approved original version of this thesis is available in print at TU Wien Bibliothek.
TU Bibliothek Your knowledge hub WIEN

[15] R. E. Owen, P. Plucinski, D. Mattia, L. Torrente-Murciano, V. P. Ting, M. D. Jones, *J. CO2 Util.* **2016**, *16*, 97–103.

[16] M. Gattrell, N. Gupta, A. Co, *J. Electroanal. Chem.* **2006**, *594*, 1–19.

[17] F. M. Baena-Moreno, M. Rodríguez-Galán, F. Vega, B. Alonso-Fariñas, L. F. Vilches Arenas, B. Navarrete, *Energy Sources, Part A* **2019**, *41*, 1403–1433.

[18] D. U. Nielsen, X. M. Hu, K. Daasbjerg, T. Skrydstrup, *Nat. Catal.* **2018**, *1*, 244–254.

[19] CORDIS, "Streamlined carbon dioxide conversion in ionic liquids – a platform strategy for modern carbonylation chemistry | CARBOFLOW Project," can be found under https://cordis.europa.eu/project/id/864991, **2022.**

[20] K. Schröder, "Carbon Dioxide Valorization," can be found under https://www.ias.tuwien.ac.at/ks/research-topics/carbon-dioxide-valorization, **2018.**

[21] J. L. Anthony, E. J. Maginn, J. F. Brennecke, *J. Phys. Chem. B* **2002**, *106*, 7315–7320.

[22] L. Wu, Q. Liu, I. Fleischer, R. Jackstell, M. Beller, *Nat. Commun.* **2014**, *5*, 1–6.

[23] J.-M. Lehn, R. Ziessel, *Proc. Natl. Acad. Sci.* **1982**, *79*, 701–704.

[24] H. Gruber-Woelfler, P. F. Radaschitz, P. W. Feenstra, W. Haas, J. G. Khinast, *J. Catal.* **2012**, *286*, 30–40.

[25] I. Chorkendorff, J. W. Niemantsverdriet, in *Concepts of Modern Catalysis and Kinetics*, John Wiley & Sons, Ltd, **2003**, pp. 1–21.

[26] M. Mikkelsen, M. Jørgensen, F. C. Krebs, *Energy Environ. Sci.* **2010**, *3*, 43–81.

[27] Z. Sun, J. Dong, C. Chen, S. Zhang, Y. Zhu, *J. Chem. Technol. Biotechnol.* **2021**, *96*, 1161–1175.

[28] Y. Kuramochi, O. Ishitani, H. Ishida, *Coord. Chem. Rev.* **2018**, *373*, 333–356.

[29] A. Z. Fadhel, P. Pollet, C. L. Liotta, C. A. Eckert, *Molecules* **2010**, *15*, 8400–8424.

[30] M. Zhu, Q. Ge, X. Zhu, *Trans. Tianjin Univ.* **2020**, *26*, 172–187.

[31] M. Cui, Q. Qian, J. Zhang, Y. Wang, B. B. Asare Bediako, H. Liu, B. Han, *Chem* **2021**, *7*, 726–737.

Die approbierte gedruckte Originalversion dieser Diplomarbeit ist an der TU Wien Bibliothek verfügbar
The approved original version of this thesis is available in print at TU Wien Bibliothek.
TU Bibliothek Your knowledge hub WIEN

[32] K. Tominaga, Y. Sasaki, K. Hagihara, T. Watanabe, M. Saito, *Chem. Lett.* **1994**, *23*, 1391–1394.

[33] S. Kattel, B. Yan, J. G. Chen, P. Liu, *J. Catal.* **2016**, *343*, 115–126.

[34] J. Ye, Q. Ge, C. J. Liu, *Chem. Eng. Sci.* **2015**, *135*, 193–201.

[35] X. Wang, C. Xia, L. Wu, *Green Chem.* **2018**, *20*, 5415–5426.

[36] K. Dong, R. Razzaq, Y. Hu, K. Ding, *Top. Curr. Chem.* **2017**, *375*, 1–26.

[37] P. G. Jessop, T. Ikariya, R. Noyori, *Nature* **1994**, *368*, 231–233.

[38] A. M. Appel, J. E. Bercaw, A. B. Bocarsly, H. Dobbek, D. L. Dubois, M. Dupuis, J. G. Ferry, E. Fujita, R. Hille, P. J. A. Kenis, C. A. Kerfeld, R. H. Morris, C. H. F. Peden, A. R. Portis, S. W. Ragsdale, T. B. Rauchfuss, J. N. H. Reek, L. C. Seefeldt, R. K. Thauer, G. L. Waldrop, *Chem. Rev.* **2013**, *113*, 6621–6658.

[39] T. Burgemeister, F. Kastner, W. Leitner, *Angew. Chem., Int. Ed. Engl.* **1993**, *32*, 739–741.

[40] F. J. Fernández-Alvarez, M. Iglesias, L. A. Oro, V. Polo, *Chem. Cat. Chem.* **2013**, *5*, 3481–3494.

[41] R. Tanaka, M. Yamashita, K. Nozaki, *J. Am. Chem. Soc.* **2009**, *131*, 14168–14169.

[42] C. G. Okoye-Chine, K. Otun, N. Shiba, C. Rashama, S. N. Ugwu, H. Onyeaka, C. T. Okeke, *J. CO2 Util.* **2022**, *62*, 102099–102128.

[43] L. G. Puppin, M. Khalid, G. T. T. da Silva, C. Ribeiro, H. Varela, O. F. Lopes, *J. Mater. Res.* **2020**, *35*, 272–280.

[44] M. Le, M. Ren, Z. Zhang, P. T. Sprunger, R. L. Kurtz, J. C. Flake, *J. Electrochem. Soc.* **2011**, *158*, E45–E49.

[45] S. Kaneco, H. Katsumata, T. Suzuki, K. Ohta, *Energy Fuels* **2006**, *20*, 409–414.

[46] D. Ren, Y. Deng, A. D. Handoko, C. S. Chen, S. Malkhandi, B. S. Yeo, *ACS Catal.* **2015**, *5*, 2814–2821.

[47] J. C. Kehr, D. G. Picchi, E. Dittmann, *Beilstein J. Org. Chem.* **2011**, *7*, 1622–1635.

Die approbierte gedruckte Originalversion dieser Diplomarbeit ist an der TU Wien Bibliothek verfügbar
The approved original version of this thesis is available in print at TU Wien Bibliothek.
TU Bibliothek Your knowledge hub WIEN

[48] F. R. Tabita, in *The Molecular Biology of Cyanobacteria* (Ed.: D.A. Bryant), Springer, Dordrecht, **1994**, pp. 437–467.

[49] P. R. Yaashikaa, P. Senthil Kumar, S. J. Varjani, A. Saravanan, *J. CO2 Util.* **2019**, *33*, 131–147.

[50] C. A. Kerfeld, S. Heinhorst, G. C. Cannon, *Annu. Rev. Microbiol.* **2010**, *64*, 391–408.

[51] M. B. Smith, J. March, *March's Advanced Organic Chemistry: Reactions, Mechanisms, and Structure*, Wiley, Hoboken, **2020**.

[52] C. K. Prier, D. A. Rankic, D. W. C. MacMillan, *Chem. Rev.* **2013**, *113*, 5322–5363.

[53] S. Zhu, D. Wang, *Adv. Energy Mater.* **2017**, *7*, 1700841–1700864.

[54] D. M. Arias-Rotondo, J. K. McCusker, *Chem. Soc. Rev.* **2016**, *45*, 5803–5820.

[55] G. Zhao, X. Huang, X. Wang, X. Wang, *J. Mater. Chem. A* **2017**, *5*, 21625–21649.

[56] E. E. Barton, D. M. Rampulla, A. B. Bocarsly, *J. Am. Chem. Soc.* **2008**, *130*, 6342–6344.

[57] J. Tae Song, H. Ryoo, M. Cho, J. Kim, J.-G. Kim, S.-Y. Chung, J. Oh, J. T. Song, H. Ryoo, M. Cho, J. Kim, S. Chung, J. Oh, J. Kim, *Adv. Energy Mater.* **2017**, *7*, 1601103–1601110.

[58] G. Sahara, R. Abe, M. Higashi, T. Morikawa, K. Maeda, Y. Ueda, O. Ishitani, *Chem. Commun.* **2015**, *51*, 10722–10725.

[59] H. Takeda, K. Koike, H. Inoue, O. Ishitani, *J. Am. Chem. Soc.* **2008**, *130*, 2023–2031.

[60] B. Gholamkhass, H. Mametsuka, K. Koike, T. Tanabe, M. Furue, O. Ishitani, *Inorg. Chem.* **2005**, *44*, 2326–2336.

[61] H. Kumagai, Y. Tamaki, O. Ishitani, *Acc. Chem. Res.* **2022**, *55*, 978–990.

[62] J. Hawecker, J. -M Lehn, R. Ziessel, *Helv. Chim. Acta* **1986**, *69*, 1990–2012.

[63] B. P. Sullivan, C. M. Bolinger, D. Conrad, W. J. Vining, T. J. Meyer, *J. Chem. Soc., Chem. Commun.* **1985**, 1414–1416.

[64] M. Freemantle, *An Introduction to Ionic Liquids*, RSC Publ., Cambridge, **2010**.

[65] L. A. Blanchard, J. F. Brennecke, *Ind. Eng. Chem. Res.* **2001**, *40*, 287–292.

Die approbierte gedruckte Originalversion dieser Diplomarbeit ist an der TU Wien Bibliothek verfügbar
The approved original version of this thesis is available in print at TU Wien Bibliothek.
TU Bibliothek Your knowledge hub WIEN

[66] Z. Z. Yang, Y. N. Zhao, L. N. He, *RSC Adv.* **2011**, *1*, 545–567.

[67] W. Keim, *Green Chem.* **2003**, *5*, 105–111.

[68] A. Kaftan, H. Klefer, M. Haumann, M. Laurin, P. Wasserscheid, J. Libuda, *Sep. Purif. Technol.* **2017**, *174*, 245–250.

[69] N. Noorani, A. Mehrdad, *J. Polym. Res.* **2021**, *28*, 1–12.

[70] Z.-H. Zhou, K.-H. Chen, S. Gao, Z.-W. Yang, L.-N. He, *Research* **2020**, *2020*, 1–11.

[71] W. Zhang, H. Shimakoshi, N. Houfuku, X. M. Song, Y. Hisaeda, *Dalton Trans.* **2014**, *43*, 13972–13978.

[72] S. N. V. K. Aki, B. R. Mellein, E. M. Saurer, J. F. Brennecke, *J. Phys. Chem. B* **2004**, *108*, 20355–20365.

[73] M. Ramdin, T. W. de Loos, T. J. H. Vlugt, *Ind. Eng. Chem. Res.* **2012**, *51*, 8149–8177.

[74] J. Lin, Z. Ding, Y. Hou, X. Wang, *Sci. Rep.* **2013**, *3*, 1–5.

[75] C. Cadena, J. L. Anthony, J. K. Shah, T. I. Morrow, J. F. Brennecke, E. J. Maginn, *J. Am. Chem. Soc.* **2004**, *126*, 5300–5308.

[76] S. Wang, X. Wang, *Angew. Chem., Int. Ed.* **2016**, *55*, 2308–2320.

[77] K. Qiao, F. Ono, Q. Bao, D. Tomida, C. Yokoyama, *J. Mol. Catal. A: Chem.* **2009**, *303*, 30–34.

[78] A. J. J. Lennox, G. C. Lloyd-Jones, *Chem. Soc. Rev.* **2014**, *43*, 412–443.

[79] P. Y. Bruice, O. Reiser, *Organische Chemie - Studieren kompakt*, Pearson Studium, München, **2011**.

[80] L. C. Chan, B. G. Cox, *J. Org. Chem.* **2007**, *72*, 8863–8869.

[81] C. R. J. Stephenson, T. P. Yoon, D. W. C. MacMillan, *Visible Light Photocatalysis in Organic Chemistry*, John Wiley & Sons, Incorporated, Newark, **2018**.

[82] Z. Fang, A. Ito, S. Keinan, Z. Chen, Z. Watson, J. Rochette, Y. Kanai, D. Taylor, K. S. Schanze, T. J. Meyer, *Inorg. Chem.* **2013**, *52*, 8511–8520.

[83] S. Sato, T. Morimoto, O. Ishitani, *Inorg. Chem.* **2007**, *46*, 9051–9053.

Die approbierte gedruckte Originalversion dieser Diplomarbeit ist an der TU Wien Bibliothek verfügbar
The approved original version of this thesis is available in print at TU Wien Bibliothek.
TU Bibliothek Your knowledge hub WIEN

[84] V. v. Chaban, O. v. Prezhdo, *J. Phys. Chem. Lett.* **2011**, *2*, 2499–2503.

[85] M. Uo, T. Wada, T. Sugiyama, *Jpn. Dent. Sci. Rev.* **2015**, *51*, 2–9.

[86] Y. S. Kim, A. Cha, J. Y. Shin, H. J. Jeon, J. H. Shim, C. Lee, S. Lee, *Chem. Commun.* **2012**, *48*, 8940–8942.

[87] L. Guo, Q. Deng, G. Fang, W. Gao, S. Wang, *J. Chromatogr. A* **2011**, *1218*, 6271–6277.

[88] H. J. Nie, J. Y. Shao, J. Wu, J. Yao, Y. W. Zhong, *Organometallics* **2012**, *31*, 6952–6959.

[89] T. Wang, N. Zabarska, Y. Wu, M. Lamla, S. Fischer, K. Monczak, D. Y. W. Ng, S. Rau, T. Weil, *Chem. Commun.* **2015**, *51*, 12552–12555.

[90] S. A. McFarland, F. S. Lee, K. A. W. Y. Cheng, F. L. Cozens, N. P. Schepp, *J. Am. Chem. Soc.* **2005**, *127*, 7065–7070.

[91] Y. Cheng, X. Zou, D. Zhu, T. Zhu, Y. Liu, S. Zhang, H. Huang, *J. Polym. Sci., Part A: Polym. Chem.* **2007**, *45*, 650–660.

[92] H. Shimakoshi, M. Nishi, A. Tanaka, K. Chikama, Y. Hisaeda, *Chem. Commun.* **2011**, *47*, 6548–6550.

[93] L. Wu, M. Kyle Brennaman, A. Nayak, M. Eberhart, A. J. M. Miller, T. J. Meyer, *ACS Cent. Sci.* **2019**, *5*, 506–514.

[94] B. D. Alexander, T. J. Dines, R. W. Longhurst, *Chem. Phys.* **2008**, *352*, 19–27.

[95] V. Bertini, S. Alfei, M. Pocci, F. Lucchesini, N. Picci, F. Iemma, *Tetrahedron* **2004**, *60*, 11407–11414.

[96] R. Marcilla, J. A. Blazquez, J. Rodriguez, J. A. Pomposo, D. Mecerreyes, *J. Polym. Sci., Part A: Polym. Chem.* **2004**, *42*, 208–212.

Die approbierte gedruckte Originalversion dieser Diplomarbeit ist an der TU Wien Bibliothek verfügbar
The approved original version of this thesis is available in print at TU Wien Bibliothek.
TU WIEN Bibliothek Your knowledge hub

8. List of figures

Figure 1: Atmospheric CO_2 concentrations from 1770 to 2021. Graphic taken from[4] 1
Figure 2: Closed CO_2 cycle. Graphic adapted from [7] 2
Figure 3: Pathways for the chemical utilization of CO_2. Graphic adapted from [7] 3
Figure 4: Process concept of CARBOFLOW. Graphic taken from [20] 5
Figure 5: CO_2 reduction with p-block element-containing reductants. Graphic taken from[35] . 9
Figure 6: Scheme of the electrochemical reduction of CO_2. Graphic adapted from [28] 11
Figure 7: Potential energy curves for diatomic molecules, E: electronic state, V: vibrational state, r: rotational state. Graphic adapted from [51] 14
Figure 8: Exemplary photoredox cycle, Pcat: photocatalyst, D: electron donor, A: acceptor. Graphic adapted from [53] 15
Figure 9: Chemical structures of $[Ru(bpy)_3]^{2+}$, $[Ru(dmb)_3]^{2+}$, $[Ir(bpy)_3]^{3+}$, fac- $Ir(ppy)_3$,and $ReCl(bpy)(CO)_3$. 16
Figure 10: Mechanisms of the Förster and the Dexter energy transfer. Graphic taken from[54] 16
Figure 11: Photocatalytic system for the reduction of CO_2, PS: photosensitizer, Cat: photocatalyst, D: electron donor. Graphic taken from [28] 17
Figure 12: Heterogeneous CO_2 reduction methods: (a) photocatalytic reduction, (b) electrochemical reduction. Graphics taken from[55] 18
Figure 13: Photoelectrochemical reduction of carbon dioxide. Graphics taken from [55] 19
Figure 14: Molecular orbitals of $[Ru(bpy)_3]^{2+}$ after photoexcitation. Graphic taken from[52] . 21
Figure 15: Proposed reaction mechanism for the reduction of CO_2 using fac-$Re(bpy)(CO)_3Cl$ from Hawecker et al. (process a)[62] and Sullivan et al. (process b)[63]. Graphic taken from [28] 22
Figure 16: Typical IL cations and anions. 23
Figure 17: The benefits of ILs in combination with CO2. Graphs taken or adapted from [1,21]23
Figure 18: Solubility of different gases in the IL $[bmim][PF_6]$ at 25°C. Graphic taken from[21] 24
Figure 19: Scheme of the change in free energy of the CO_2 reduction in water (solid line) or IL (dashed line). Graphic adapted from [1] 25
Figure 20: Schematic depictions of two heterogenous catalytic processes assisted by ionic liquids: (a) l-l-biphasic system, (b) SILP technology. Graphic (b) taken from [68] 25
Figure 21: Schematic concept for carbon dioxide valorization via photocatalytic reduction. . 27

Die approbierte gedruckte Originalversion dieser Diplomarbeit ist an der TU Wien Bibliothek verfügbar
The approved original version of this thesis is available in print at TU Wien Bibliothek.
TU Bibliothek Your knowledge hub WIEN

Figure 22: Schematic concept of the synthesis of a photocatalytically active cross-linked polymer, PS: photosensitizer, PC: photocatalyst, IL: ionic liquid. 28
Figure 23: Structures of the polymerizable photocatalytic monomers: CLP-PC, CLP-PS, SCP-PC, and SCP-PS. 29
Figure 24: Schematic structures of the CLP, and SCP. 29
Figure 25: Mechanism for the synthesis of 1-butyl-3-vinylimidazolium chloride. 31
Figure 26: Mechanism for the synthesis of 5,5'-divinyl-2,2'-bipyridine, RE: reductive elimination, OA: oxidative addition, TM: transmetalation. 32
Figure 27: Mechanism of the Gabriel synthesis 33
Figure 28: Mechanism for the amidation of 4-(aminomethyl)styrene and 4'-methyl-2,2'-bipyridine-4-carboxylic acid. 34
Figure 29: Ligand exchange of pentacarbonylchlororhenium(I) on the example of SCP-PC. 34
Figure 30: Ligand exchange of cis-bis(2,2′-bipyridine)dichlororuthenium(II) on the example of SCP-PS. 35
Figure 31: Mechanism of a radical polymerization 36
Figure 32: Polymerization reaction vessel, a: non-autoclave reaction, b: autoclave reaction. 38
Figure 33: ^{1}H NMR of 1-butyl-3-vinylimidazolium chloride and PIL. 40
Figure 34: FT-IR spectra of the IL, PIL, CLP-PC, and two CLPs. 41
Figure 35: Schematic depiction of a metal-to-ligand charge transfer state in $[Ru(bpy)_3]^{2+}$. Graphic redrawn from[82] 43
Figure 36: UV-Vis spectra of a CLP, SCP, $[Ru(bpy)_3][PF_6]_2$, and $Re(bpy)(CO)_3Cl$. 44
Figure 37: UV-Vis spectra of SCPs in different ratios. 45
Figure 38: TGA results of the PIL, two CLPs in different monomer ratios, and an SCP. 46
Figure 39: Schematic concept of characteristic X-ray generation for T-XRF spectroscopy. Graphic taken from [86] 47
Figure 40:T-XRF spectrum of a CLP. 48

Die approbierte gedruckte Originalversion dieser Diplomarbeit ist an der TU Wien Bibliothek verfügbar
The approved original version of this thesis is available in print at TU Wien Bibliothek.
TU Bibliothek Your knowledge hub WIEN

9. List of tables

Table 1: Selection of typical catalysts for homogeneous and heterogeneous RWGS reaction to CO. 8

Table 2: Selection of CO_2 hydrogenation reactions in $scCO_2$ to formates. Table adapted from [36] 10

Table 3: Selection of electrocatalytic CO_2 reduction reactions. 11

Table 4: Structural types of metal-CO_2 complexes. Table adapted from [26] 17

Table 5: Examples of semiconductor materials for photoelectrochemical CO_2 reduction..... 19

Table 6: Yields of the CLPs, Re: Re photocatalyst, Ru: Ru photosensitizer. 39

Table 7: Yields of the SCPs, Re: Re photocatalyst, Ru: Ru photosensitizer. 39

Table 8: T-XRF values of the CLPs, and SCPs. 48

Die approbierte gedruckte Originalversion dieser Diplomarbeit ist an der TU Wien Bibliothek verfügbar
The approved original version of this thesis is available in print at TU Wien Bibliothek.
TU WIEN Bibliothek Your knowledge hub